Variation in space and time of water flow and solute transport in heterogeneous soils and aquifers

A new multi-compartment percolation sampler and a new parameterization of the spatio-temporal solute distribution

Promotor:

Prof. em. dr. ir. R. A. Feddes   Hoogleraar Bodemnatuurkunde, Agrohydrologie en Grondwaterbeheer, Wageningen Universiteit

Copromotor:

Dr. ir. G. H. de Rooij   Universitair hoofddocent bij de leerstoelgroep Bodemnatuurkunde, Ecohydrologie en Grondwaterbeheer, Wageningen Universiteit

Promotiecommissie:

Prof. em. dr. H. Flühler	ETH Zürich, Zwitserland
Prof. dr. ir. J. Grasman	Wageningen Universiteit
Prof. dr. S. Uhlenbrook	UNESCO-IHE, Delft
Prof. dr. M. Vanclooster	Université Catholique de Louvain, België

Variation in space and time of water flow and solute transport in heterogeneous soils and aquifers

A new multi-compartment percolation sampler and a new parameterization of the spatio-temporal solute distribution

Esther Bloem

Abstract

Bloem, E. 2008. Variation in space and time of water flow and solute transport in heterogeneous soils and aquifers - A new multi-compartment percolation sampler and a new parameterization of the spatio-temporal solute distribution. Doctoral thesis, Wageningen University, The Netherlands. xii+153 pp.

The experimental and theoretical work reported in this thesis improves our ability to observe subsurface solute transport and increases the understanding of solute redistribution as it travels through the subsurface with flowing water.

A numerical study of solute movement in an aquifer highlighted the differences between resident and flux concentrations. Leaching surfaces at various aquifer cross-sections established the superiority of flux concentrations for quantifying solute movement. Flux concentrations can be approximated from resident concentrations with moment analysis. This works well if solute transport is analyzed over an entire cross-section of the aquifer, but performs poorly on the scale of individual numerical grid cells, mainly because it approximates local pore water velocities by averages over the entire trajectory upstream of the location of interest.

While flux concentration measurements will probably remain very difficult in aquifers, their observation in soils is difficult but possible. To do so, a new variable-suction multi-compartment percolation sampler was developed that can be buried below an undisturbed soil volume in the field. The instrument is capable of measuring downward water and solute fluxes at 100 locations within a 32.5 by 32.5 cm area with minimal disturbance of the local pressure head field. Samples can be extracted *in situ*, allowing the breakthrough curve of each cell to be measured under natural conditions. Three prototypes with different porous covers were tested in different laboratory and field experiments in Australia and the Netherlands. These involved uniform solute applications at the soil surface. Of the three covers, the membrane cover performed best, while the metal cover is also recommendable.

The measured breakthrough curves of the sampler cells were sorted in descending order of total solute amount, resulting into leaching surfaces. By fitting a mean pore water velocity and a dispersion coefficient for each breakthrough curve, these values could be expressed as a function of the ranking of the breakthrough curves. By combining the parameters of these functions with those of the spatial solute distribution curve that quantifies the spatial distribution of solutes, an entire leaching surface can be described by four to eight parameters. This facilitates a quantitative comparison of leaching surfaces for different soils and/or different circumstances.

Key words: Flux concentration, resident concentration, moment analysis, solute transport, spatial and temporal solute distribution, soil heterogeneity, multi-compartment sampler, unsaturated zone, saturated zone, tracer experiment, wastewater irrigation, leaching surface, breakthrough curve, parameterization

Voorwoord

Het voorliggende onderzoek ben ik in juli 2003 gestart aan de Universiteit van Wageningen bij de leerstoelgroep Bodemnatuurkunde, Agrohydrologie en Grondwaterbeheer. Het voorstel hiervoor was opgesteld door Ger de Rooij en werd financieel gesteund door de Nederlandse Organisatie voor Wetenschappelijk Onderzoek (NWO). Onderzoeksdoel was het opstellen van een parameterisatie van leaching surfaces: een spatiële en temporele beschrijving van het uitspoelingspatroon van opgeloste stoffen. Tijdens de beginfase van mijn onderzoek raakte ik tevens betrokken bij de ontwikkeling van een nieuwe 'multi-compartment sampler'.

Binnen dit onderzoek is op een positieve en constructieve wijze samengewerkt met een groot aantal mensen. In dit voorwoord wil ik graag de mensen bedanken die op enigerlei wijze hebben bijgedragen aan de voltooiing van mijn promotieonderzoek.

Allereerst wil ik mijn dagelijkse begeleider Ger de Rooij bedanken voor zijn begeleiding van mijn onderzoek. Samenwerken met Ger was een geheel nieuwe ervaring. Mijn werk is een vervolg op zijn promotieonderzoek, waardoor hij erg betrokken was. Door je kritische houding, hoge verwachtingen, en scherpe commentaren heb je duidelijk een kwaliteitsstempel op dit proefschrift gezet. Bedankt!

Daarnaast wil ik graag Reinder Feddes bedanken. Als promotor heeft Reinder vooral in de eindfase een duidelijke rol gehad. Kritisch en constructief werden al mijn hoofdstukken bekeken en werden de puntjes op de i gezet. Bedankt hiervoor!

Ook wil ik in het bijzonder Franck Hogervorst bedanken, met wie ik samen de multi-compartment sampler ontwikkeld heb en de werkkamer deelde. Bedankt voor je grote enthousiasme en inzet.

Het bouwen van een instrument gaat niet vanzelf. Een heel team heeft geholpen om dit instrument werkende te krijgen. Johan Römelingh en Herman Jansen van de werkplaats zeer bedankt voor het meedenken en de enorme hoe-

veelheid werk die jullie hebben verricht. De electronica van het instrument lag bij Pieter Hazenberg. Bedankt voor het helpen met het aansturingsprogramma van het instrument en het uitvoerig testen van de electronica.

Aan het einde van mijn eerste jaar als AIO kreeg ik de mogelijkheid om een bezoek te brengen aan het Forschungszentrum Jülich om daar samen te werken met Jan Vanderborght. Bedankt voor de plezierige discussies en de verfrissende kijk op transportprocessen.

In my second year I got the opportunity to work in Australia. Frank Stagnitti was the man behind the scene who made this possible. Thanks! I enjoyed this stay very much. I would like to thank Karen Hermon for our co-operation and all the time you have put into the project. It was hard work, resulting in the experiment discussed in Chapter 4. Also would I like to thank Peta Maher for all the nice discussions and staying at your place.

In mijn derde jaar als AIO ben ik het veld in getrokken, bij Proefboerderij Vredepeel. Hier zwaaide Marc Kroonen de scepter: bedankt voor de mogelijkheid om mijn experimenten op een goede wijze uit te voeren. Ook wil ik graag Harry Verstegen bedanken voor het verzamelen van neerslaggegevens, verwisselen van accu's, en kleine checks waardoor ik niet elke keer 150 km op een neer hoefde te rijden. Ook bedank ik Henny Gertsen voor alle hulp zowel tijdens mijn veldexperimenten als in het laboratorium.

Tijdens mijn onderzoek heb ik tweemaal versterking gekregen van afstudeerders. Henk Krajenbrink en Dieuwke Schotanus hebben allebei hun steentje bijgedragen. Voor mij een erg leerzame en leuke ervaring!

Gedurende mijn hele promotieonderzoek heb ik contact gehad met Maarten de Gee, het laatste jaar intensief. Hartelijk bedankt voor het helpen met de parameterisatie van de leaching surfaces. Het oorspronkelijke idee werkte niet, maar jouw commentaren stimuleerden mij om andere wegen in te slaan, uiteindelijk resulterend in twee hoofdstukken van dit proefschrift.

Vier jaar zijn zo voorbij, zeker als je een nieuw instrument ontwikkelt, nieuwe experimenten uitvoert, en vervolgens ook nog het een en ander wilt uitwerken. Ik bedank Sjoerd van der Zee voor de mogelijkheid die hij mij gaf om nog een half jaar extra aan de leerstoelgroep verbonden te blijven. Deels verlengde tijd voor mijn proefschrift, deels werk voor een interessant nieuw project.

Graag bedank ik alle fijne collega's van SEG en HWM voor de leuke tijd op de Nieuwlanden en later op Atlas. In het bijzonder Tineke van der Ploeg voor de vele sessies over de voortgang van onze onderzoeken en Hidde Leijnse voor alle hulp met Latex en Matlab gedurende de eindfase.

Verder mijn familie en vrienden: bedankt voor alle geïnteresseerde en motiverende back-office support!

Als laatste wil ik Berry bedanken voor zijn luisterend oor, zijn vrolijkheid, en zijn eeuwige optimisme. Je hebt me de afgelopen jaren enorm gesteund en daar ben ik je erg dankbaar voor.

Esther Bloem
Wageningen, april 2008

Contents

CHAPTER 1

Introduction

1.1 Background

Pollution of soils and groundwater is a widespread problem. During the last centuries, in vast areas of the world irrigation has lead to salinization, rendering large areas of agricultural land unfit for food production (e.g. *Hillel*, 1998). During the industrial age, also pollution of the subsurface environment in urban areas became prominent, particularly in delta areas. Here, a combination of factors increased both the risk and the impact of soil and groundwater pollution. The moderate climate and fertile soils of deltas, as well as the economical potential related to shipping (both overseas and upriver) made deltas attractive for trade and settlement. The concentration of human populations caused pollution problems, related to landfills for domestic waste, industrial waste deposits, accidental or illegal spills, and atmospheric deposition of various compounds. Agriculture also intensified in these areas, involving application of and pollution by fertilizers and pesticides.

The pollution risks were aggravated by the fact that groundwater levels in deltas are generally shallow, making them more vulnerable to contamination from surface applied substances, especially in climates with a precipitation surplus. Furthermore, the increasing demand on freshwater from the large population for domestic, agricultural, and industrial use ensures that any pollution of subsurface or surface freshwater reservoirs rapidly affects the water supply infrastructure, exposing the population to contaminated water.

In response to this pollution, soil physicists increasingly focused on solute transport in soils and its effect on groundwater (e.g. *Nielsen et al.*, 1986; *Germann*, 1988; *Leistra and Boesten*, 1994; *Wagenet*, 1990). The effects of soil

heterogeneity (*Biggar and Nielsen*, 1976; *Roth et al.*, 1991; *Jury and Flühler*, 1992; *Flühler et al.*, 1996; *Forrer et al.*, 1999; *Wendroth et al.*, 1999), macropore flow (*Beven and Germann*, 1982), and unstable flow (*Raats*, 1973; *DeBano*, 1981; *Hillel and Baker*, 1988; *Glass et al.*, 1989; *Ritsema et al.*, 1993; *Ritsema and Dekker*, 1994; *Wang et al.*, 1998a,b; *DeBano*, 2000; *de Rooij*, 2000; *Cho and de Rooij*, 2002) on the fate of solutes in soils were recognized. The flow features and soil water content variations associated with these phenomena typically occur within the square meter-scale, but their effects on solute leaching persist at much larger horizontal scales. This behavior is a consequence of the small scale in the main vertical flow direction, which in many deltas does not exceed a few meters (*Corwin et al.*, 2006).

Observing solute transport in the field is a challenge. Soil coring is laborious, destructive, and only provides resident concentrations (*Parker and van Genuchten*, 1984). Dye tracers (*Flury and Flühler*, 1994; *Flury and Wai*, 2003) and suction cups (*Corwin*, 2002) have been widely used, but a quantitative analysis of dye tracers (*Forrer et al.*, 1999; *Persson*, 2005) is not yet frequently applied and does not provide liquid concentrations (*Persson*, 2005). Suction cups do not sample the pore water uniformly, and give concentrations that are somewhere between resident and flux concentrations (*Parker and van Genuchten*, 1984). Moreover these cups also underestimate macropore flow (*Corwin*, 2002). To capture downward flow, various buried *in situ* samplers have been developed. Zero-tension samplers rely on gravity (*Brye et al.*, 1999), therefore a saturated column above the sampler is needed, which is not desirable in the unsaturated zone. Fixed-tension samplers perform much better (*Rimmer et al.*, 1995). In order to decrease the disturbing effects of samplers, present developments move towards variable suction samplers (e.g. *van Grinsven et al.*, 1988; *Brye et al.*, 1999; *Kosugi and Katsuyama*, 2004).

Some of the fixed-tension samplers consist of multiple compartments (e.g. *Quisenberry et al.*, 1994; *Poletika and Jury*, 1994; *Buchter et al.*, 1995; *Stagnitti et al.*, 1998; *de Rooij and Stagnitti*, 2000; *Strock et al.*, 2001), and thus provide information about the distribution of a leaching solute both in space and time. Multi-compartment samplers provide large amounts of temporal and spatial solute transport data. The temporal aspect of solute leaching is characterized by the breakthrough curve (BTC), which describes the travel time of solutes at a given depth (*Jury and Roth*, 1990). To describe the spatial data from such samplers, recently the spatial solute distribution curve (SSDC) (*Stagnitti et al.*, 1999; *de Rooij and Stagnitti*, 2000) was developed. This curve yields the total amount of leached solute as a function of the fraction of the total sampling area, with the sampling compartments sorted from high to low leaching. The leaching surface (*de Rooij and Stagnitti*, 2002a,b, 2004) results if the breakthrough curves of individual compartments are plotted next to one another in order of decreasing total leaching.

1.2   Research objectives

This study focuses on the spatial as well as on the temporal distribution of solute leaching, taking into account both theoretical and experimental aspects. The specific research objectives of this study are:

- To improve the capability to observe soil water and solute movement in space and time
    - By developing an advanced variable-suction multi-compartment sampler
    - By applying and testing this instrument in laboratory and field experiments
- To advance subsurface solute transport theory
    - By assessing the validity of resident concentrations for quantifying the movement of solutes
    - By evaluating temporal moment analysis as a tool to quantify solute movement and its spatial variation
    - By developing a method to quantitatively describe observed leaching surfaces with a limited number of parameters

1.3   Outline of this thesis

Chapter 2 discusses a numerical study of tracer movement in an aquifer. For the first time the leaching surface methodology is applied to a groundwater flow problem. Leaching surfaces at various distances from the solute application plane are constructed for flux concentrations, resident concentrations, and approximated flux concentrations. These approximated flux concentrations were derived from the resident concentrations with moment analysis. To investigate whether resident concentrations provide useful information to asses solute movement and to evaluate the potential of moment analysis to derive flux concentrations from resident concentrations the constructed leaching surfaces are compared.

Chapter 3 describes a newly developed subsurface variable-suction multi-compartment sampler, which has been constructed to directly observe downward fluxes of water and solutes in soils with a high spatial and temporal resolution in field and laboratory experiments. Particular attention is paid to the features that minimize the disturbance of the flow field by the instrument, the measurement of fluxes by counting the number of drops passing each compartment, and by collecting the drainage per compartment while leaving the sampler buried *in situ*. In order to allow sampling of reactive solutes a choice of the optimal porous cover for the sampling area is presented.

One prototype of the sampler described in Chapter 3 has been used in a project that investigates the effects of using wastewater for the irrigation of vineyards in Australia. To demonstrate the leaching risks in the vineyard clay loam soil, in Chapter 4 the experimental results of the performed tracer studies are discussed. The sampler was placed in a laboratory under a soil monolith from an Australian vineyard, which was subjected to an accelerated cycle of water applications that emulated one year of rainfall and irrigations with wastewater. One of the wastewater components was chloride. Due to the application regime the chloride can be regarded as a block application. In addition to this a bromide pulse has been applied and the results of this pulse will be compared with those of the chloride block application.

Two prototypes of the sampler described in Chapter 3 were installed in a Dutch field and for several months a solute transport experiment was conducted under a natural rainfall regime. Under harsh field conditions the instrument and the auxiliary equipments were tested and operating procedures were established. The solute transport experiment consisted of a chloride pulse followed by a Brilliant Blue dye tracing experiment. In Chapter 5 the results of the combined tracer tests to evaluate the spatial and temporal variation of solute leaching in the field are presented.

To show the temporal and spatial aspects of solute leaching, leaching surfaces were constructed. Chapter 6 presents a new parameterization that allows a leaching surface (typically consisting of $\sim 10^3$ data points) to be described by four to eight parameters. This is achieved by parameterizing the temporal and spatial aspects of solute leaching separately.

In Chapter 7 the fitting algorithm of Chapter 6 is made more efficient by fitting directly to solute flux densities, rather than first on observed flux concentrations.

The final Chapter (8) presents presents overall conclusions and recommendations for future research.

CHAPTER 2

Leaching surfaces to characterize transport in a heterogeneous aquifer: comparison between flux concentrations, resident concentrations, and flux concentrations estimated from temporal moment analysis

---

2.1 Introduction

Fresh groundwater is an important source of potable water. In order to preserve this valuable resource for future generations, it needs to be protected against contamination by point and diffuse pollution sources, and contaminated aquifers need to be cleaned up. Natural aquifer heterogeneity influences the transport and fate of contaminants (*Anderson*, 1987) and thus profoundly affects groundwater remediation projects, the effectiveness of natural attenuation, and risk assessments of a given contaminant plume contaminating drinking water wells or surface water. To improve treatment strategies, the predictability of natural attenuation, and risk assessments, we require a better understanding of the effect of heterogeneity on contaminant movement in aquifers.

Experiments involving the injection of solutes into an aquifer are difficult and can usually only be performed under legal restrictions. Consequently, ex-

---

This chapter is a slightly modified version of the manuscript: Bloem, E., J. Vanderborght, and G. H. de Rooij, Leaching surfaces to characterize transport in a heterogeneous aquifer: comparison between flux concentrations, resident concentrations, and flux concentrations estimated from temporal moment analysis.

perimental programs have been executed at a limited number of aquifers (the Borden aquifer (*Sudicky et al.*, 1983; *Mackay et al.*, 1986; *Freyberg*, 1986; *Sudicky*, 1986), Twin Lake site (*Killey and Moltyaner*, 1988; *Moltyaner and Killey*, 1988; *Dagan et al.*, 1997), Cape Cod field (*LeBlanc et al.*, 1991; *Garabedian et al.*, 1991; *Hess et al.*, 1992; *Rubin and Ezzedine*, 1997; *Woodbury and Rubin*, 2000), Columbus (*Boggs et al.*, 1992; *Adams and Gelhar*, 1992; *Rehfeldt et al.*, 1992), Horkheimer Insel (*Ptak and Teutsch*, 1994; *Ptak and Schmid*, 1996), and the Krauthausen site (*Vereecken et al.*, 2000; *Vanderborght and Vereecken*, 2001)). In order to investigate mixing and the spatial variability of the advection and mixing processes, in most tracer tests, local concentrations are measured using local groundwater samplers or multilevel samplers, which only minimally disturb the flow field.

Spatial or temporal moment analysis of resident concentration (*Parker and van Genuchten*, 1984) measurements in a tracer field experiment is often used to obtain parameters characterizing flow and transport in heterogeneous aquifers. Description of solute transport in terms of the positions of solute particles or the spatial distribution of solute concentrations at fixed times targets the spatial moments of a solute plume (*Aris*, 1956; *Freyberg*, 1986; *Garabedian et al.*, 1991; *Adams and Gelhar*, 1992; *Vereecken et al.*, 2000). Transport of solutes described in terms of the arrival times of solutes or temporal evolution of solute fluxes at fixed monitoring planes considers the temporal moments of solute breakthrough curves (BTCs) (*Kreft and Zuber*, 1978; *Ptak and Schmid*, 1996; *Dagan et al.*, 1997; *Rubin and Ezzedine*, 1997; *Vanderborght and Vereecken*, 2001).

Temporal moments analysis is considered more efficient than spatial moment analysis (*Rubin and Ezzedine*, 1997), because accurate estimates of spatial moments require a large number of samplers, distributed over a large area with a sufficiently high spatial resolution. Installing that many wells may not be allowed at some sites and will often be prohibitively expensive. The development of techniques to continuously monitor radioactive (*Killey and Moltyaner*, 1988; *Moltyaner and Killey*, 1988) or fluorescent (*Ptak and Teutsch*, 1994; *Ptak and Schmid*, 1996) tracer concentrations also stimulates the characterization of transport in aquifers using temporal moments (*Vanderborght and Vereecken*, 2001).

As illustrated by the experiments mentioned above, solute monitoring in the field is usually limited to observations of resident concentrations, whereas solute fluxes are relevant quantities for estimating solute travel times (e.g. *Dagan et al.*, 1992). Flux concentrations across a monitoring plane should be measured by collecting all the water flowing across the monitoring plane and measuring the concentration in the collected water. This strategy strongly reduces the spatial resolution and results in a massive disturbance of the flow field. More realistically, a limited number of pumping wells downstream from the injection can capture a portion of the water flowing through the monitoring plane. Using this approach, integrated measures of the transport process are obtained. The disturbance of the flow field by pumping, and mixing occurring close to and within the pumping well, change the tracer breakthrough as compared to the

natural flow conditions, which makes the interpretation of the measured tracer breakthrough more difficult.

Theoretically, the passage of a solute across the monitoring plane could be calculated from locally measured concentrations if it is assumed that the locally measured concentrations represent local flux concentrations and that local water fluxes are available. The first assumption is only valid if local concentration variations are sufficiently small. The latter criterion is also problematic since local water flow measurements are extremely difficult. *Vanderborght and Vereecken* (2001) discussed ways to approximate flux concentrations in a monitoring plane based on local resident concentration measurements. In one approach, they proposed to approximate the local water flux from the advection velocity of the tracer towards the observation point, which was derived from temporal moments of the locally measured time series of resident concentrations. To assess the merit of using resident concentrations to estimate solute fluxes, numerical simulations are at this time a more powerful tool than direct measurements. On the basis of numerical simulations of transport in a generated heterogeneous aquifer, *Vanderborght et al.* (2005) demonstrated that advection velocities estimated from local resident concentrations in time could be used as proxies for local water fluxes to calculate average solute fluxes across a reference surface.

One way of characterizing the heterogeneity of the transport process is to determine the variability and spatial correlation of locally observed peak arrival times. Since the peak concentration arrival time and the mean particle arrival time derived from a locally measured BTC are predominantly determined by the advection velocity of the tracer towards the observation point, the variability of peak or mean arrival times at several locations contains valuable information about the heterogeneity of the aquifer. Information about the spatial variability of peak or mean arrival times was used by e.g. *Rubin and Ezzedine* (1997), *Woodbury and Rubin* (2000), *Vanderborght and Vereecken* (2001), *Bellin and Rubin* (2004), and *Vanderborght et al.* (2005) to infer geostatistical parameters that characterize the aquifer heterogeneity. As an alternative measure to characterize transport heterogeneity, *de Rooij and Stagnitti* (2002a,b, 2004) recently presented the leaching surface as a tool to analyze the spatially and temporally non-uniform passage of solutes across a monitoring plane. The leaching surface is a curved surface constructed from a population of local-scale BTCs, thus preserving all information present in these BTCs. At present, the method has only been applied to unsaturated, macroscopically vertical solute transport in soils. For saturated, macroscopically unidirectional flows, the leaching surface method can be readily applied if a solute pulse is applied uniformly across a cross-section of the flow domain perpendicular to the macroscopic flow direction. The downstream monitoring plane(s) must be perpendicular to the main flow.

The objective of this paper is to characterize the effect of second-order stationary heterogeneity of the saturated hydraulic conductivity in an aquifer on solute transport in a flow field undisturbed by groundwater extractions (which otherwise would cause additional solute redistribution). In order to do

7

so, we apply the leaching surface methodology to a groundwater flow problem for the first time.

It is well established that flux concentrations should be used for quantifying solute movement, but these are often not available. Consequently, modelers and practitioners have to rely on resident concentrations. This introduces an unavoidable error, that can as yet not be quantified. A second objective is therefore to assess the validity of resident concentrations for quantifying solute migration. Leaching surfaces at various distances from the solute application plane were constructed for both resident concentrations and flux concentrations allowing investigation of their interchangeability. We also evaluated the potential of temporal moment analysis in solute movement problems by determining the first moments of local-scale time series of resident concentrations in order to derive flux concentrations from local resident concentrations. We constructed approximate leaching surfaces from those and compared these with the correct leaching surfaces.

2.2 Materials and methods

2.2.1 The aquifer

A steady-state saturated water flow in the 3D domain $0 \leq x_1 \leq 100$ m, $0 \leq x_2 \leq 100$ m, $0 \leq x_3 \leq 20$ m (x_1, x_2: horizontal coordinates [L], x_3: vertical coordinate [L]) was simulated using the finite element code TRACE (*Vereecken et al.*, 1994). The size of the grid blocks was 0.5 m in the horizontal directions (x_1 and x_2) and 0.1 m in the vertical direction (x_3). At the bottom and top boundaries ($x_3 = 0$ and $x_3 = L_3 = 20$ m) and at the two lateral boundaries ($x_1 = 0$ and $x_1 = L_1 = 100$ m), a zero flow or zero hydraulic head gradient boundary condition was implemented. At the front and back surfaces ($x_2 = 0$ and $x_2 = L_2 = 100$ m), a constant hydraulic head distribution was defined so that the general mean hydraulic head gradient $< \nabla \psi(\mathbf{x}) >= (0, -10^{-3}, 0)^T$ where ψ [L] denotes the hydraulic head, $\mathbf{x}$ [L] is the coordinate vector, superscript T denotes the transpose of the superscripted matrix, and $< a(\mathbf{x}) >$ is the arithmetic mean of function a over the flow domain. The porosity n [-] was uniform at 0.25, while g [-], the log-transformed scaled hydraulic conductivity,

$$g(\mathbf{x}) = \ln \left[\frac{K(\mathbf{x})}{K_0} \right] \tag{2.1}$$

had zero mean and unit variance. The geometric mean K_0 [LT^{-1}] of the hydraulic conductivity K [LT^{-1}] was set to 250 m d^{-1}, resulting in a mean pore water velocity $< \mathbf{v}(\mathbf{x}) >$ of 1 m d^{-1} in the direction of x_2, where $\mathbf{v}$ [LT^{-1}] is the pore water velocity vector. The random field $g(\mathbf{x})$ was second-order stationary with an exponential covariance structure

$$E[g(\mathbf{x})g(\mathbf{x} + \mathbf{h})] = \sigma_g^2 \exp \left[-\sqrt{\frac{h_1^2}{\gamma_1^2} + \frac{h_2^2}{\gamma_2^2} + \frac{h_3^2}{\gamma_3^2}} \right] \tag{2.2}$$

where $\mathbf{h}$ [L] denotes the separation vector with elements h_i [L] (with $i \in 1, 2, 3$ indicating the direction), γ_i [L] is the correlation length in direction i, and σ_g^2 is the variance of $g(\mathbf{x})$. In this model $\gamma_1 = \gamma_2 = 5$ m and $\gamma_3 = 1$ m. One realization of the heterogeneous field was generated using a Kraichnan generator (*Kraichnan*, 1970).

2.2.2 Numerical tracer experiment

Solute transport was described by the convection-dispersion equation

$$\frac{\partial C^r(\mathbf{x}, t)}{\partial t} = -\nabla[\mathbf{v}(\mathbf{x})C^r(\mathbf{x}, t)] + \nabla \cdot [\mathbf{D}(\mathbf{x})\nabla C^r(\mathbf{x}, t)] \qquad (2.3)$$

where t [T] denotes time, C^r is the solute resident concentration [ML^{-3}], and the elements D_{ij} [L^{2}T^{-1}] of the dispersion tensor $\mathbf{D}$ [L^{2}T^{-1}] are given, neglecting molecular diffusion, by *Bear* (1972)

$$D_{ij}(\mathbf{x}) = \lambda_T \mid \mathbf{v} \mid \delta_{ij} + (\lambda_L - \lambda_T)\frac{v_i v_j}{\mid \mathbf{v} \mid} \qquad (2.4)$$

where i and j denote coordinate directions, λ_L [L] and λ_T [L] denote the lateral and transversal dispersivity, respectively, and δ_{ij} is the Kronecker delta. In this study, $\lambda_L = 0.1$ m and $\lambda_T = 0.01$ m. *Vanderborght et al.* (2005) found macrodispersivities of about 4 m in this aquifer (their figure 9), which is consistent with field observations of aquifers with comparable dimensions reviewed by *Gelhar et al.* (1992) (their figures 2 and 3).

For the transport simulations, the particle tracking code PARTRACE (*Neuendorf*, 1997) was used. A uniform initial tracer concentration C_0 at time $t = 0$ was assumed of 0.5 m thickness in the x_2 direction at $x_2 = 20$ m in the region 25 m $< x_1 <$ 75 m and 5 m $< x_3 <$ 15 m. Outside the injection slab, the flow domain was initially solute-free. In total, 10^8 particles were injected at $t = 0$ in the injection slab and their displacement in the flow field was tracked. In the terminology proposed by *Jury and Scotter* (1994) this represents an initial value problem. The solute mass in each stream tube is proportional to its water content at the solute application plane (10^4 particles per grid block, $C_0 = 4 \times 10^5$ particles m^{-3}). Local-scale dispersion was modeled by adding a random displacement $Z\mathbf{B}\sqrt{\Delta t}$ to the advective displacement, where Δt is the time step, Z is a random variable drawn from Gaussian distribution with mean 0 and variance 1, and $\mathbf{B}$ a matrix that is related to the local scale dispersion tensor as: $\mathbf{B} \cdot \mathbf{B}^T = \mathbf{D}$. Concentration distributions were calculated until 150 days after tracer injection at daily intervals by counting the number of particles in the volumetric grid elements. The passage of the tracer was monitored at vertical monitoring planes downstream in the direction of increasing x_2 at Δx_2 = 10, 30, 50, and 70 m from the tracer injection plane, with 25 m $< x_1 <$ 75 m and 5 m $< x_3 <$ 15 m. Thus, the size of the monitoring planes equalled that of the solute injection plane. This helped to avoid having substantial areas in the domain without any solutes, which would have hampered the solute transport analysis.

2.2.3   Tracer plume analysis

Resident and flux concentrations and masses

We analyzed the properties of the tracer plume as it passed the monitoring planes, and the evolution of these properties as the travel distance increased. To do so, we calculated resident solute concentrations, and flow velocity components v_2 perpendicular to the monitoring planes, for all cubes for which the four downstream corner nodes were located in one of the monitoring planes. The values of v_2 were obtained from the average of the eight corner nodes, and the resident concentrations resulted from the number of particles in the cubes. For a solute plume passing a monitoring plane, the flux concentration is a more relevant parameter than the resident concentration (*Parker and van Genuchten*, 1984; *Jury and Roth*, 1990). The flux concentration C^f is defined as (*Jury and Roth*, 1990)

$$C^f(\mathbf{x}, t) = \frac{J_s(\mathbf{x}, t)}{J_w(\mathbf{x})} \tag{2.5}$$

where $J_s(\mathbf{x}, t)$ [ML^{-2}T^{-1}] the solute flux in the main flow direction and $J_w(\mathbf{x})$ [LT^{-1}] the water flux in the main flow direction.

A more formal definition is

$$C^f(x_1, x_3, t, x_2) =$$

$$\lim_{\substack{\Delta x_1^* \downarrow 0 \\ \Delta x_3^* \downarrow 0 \\ \Delta t \downarrow 0}} \frac{\displaystyle\int_{x_1-\frac{1}{2}\Delta x_1^*}^{x_1+\frac{1}{2}\Delta x_1^*} \int_{x_3-\frac{1}{2}\Delta x_3^*}^{x_3+\frac{1}{2}\Delta x_3^*} \int_{t-\frac{1}{2}\Delta t}^{t+\frac{1}{2}\Delta t} q_2(\xi_1, \xi_3, \chi, x_2) C(\xi_1, \xi_3, \chi, x_2) \mathrm{d}\chi \mathrm{d}\xi_3 \mathrm{d}\xi_1}{\displaystyle\int_{x_1-\frac{1}{2}\Delta x_1^*}^{x_1+\frac{1}{2}\Delta x_1^*} \int_{x_3-\frac{1}{2}\Delta x_3^*}^{x_3+\frac{1}{2}\Delta x_3^*} \int_{t-\frac{1}{2}\Delta t}^{t+\frac{1}{2}\Delta t} q_2(\xi_1, \xi_3, \chi, x_2) \mathrm{d}\chi \mathrm{d}\xi_3 \mathrm{d}\xi_1} \tag{2.6}$$

where C [ML^{-3}] is the point solute concentration, q_a [LT^{-1}] the flux density in principal direction a. The derivation of this equation is presented in Appendix A. Because the concentration and flow velocity within a cube and within a time interval are necessarily uniform in our numerical model, the resident and flux concentrations are equal at this smallest scale (see Appendix A) if the dispersive and diffusive fluxes are small compared to the advective solute flux. In our aquifer the Peclet number (Δx_2 / λ_L, with Δx_2 the lateral travel distance; (*Bolt*, 1982)) ≥ 100 for all monitoring planes, so in areas with appreciable solute transport this will generally be the case. In low flow areas this assumption may be invalid, but these regions only marginally affect solute movement. The mass that resides in a cube at a given time or the mass flux through its walls (neglecting molecular diffusion) during a time interval will generally be different

$$M_{p,b}^r = n \cdot \Delta x_1^* \cdot \Delta x_2^* \cdot \Delta x_3^* \cdot C_{p,b}^r \tag{2.7}$$

$$M_{p,b}^f = n \cdot v_{2,p,b} \cdot \Delta x_1^* \cdot \Delta x_3^* \cdot \Delta t_b \cdot C_{p,b}^r \tag{2.8}$$

where $M_{p,b}^r$ [M] is the mass residing in cube p with $\Delta x_1^* = 0.5$ m, $\Delta x_2^* = 0.5$ m, and $\Delta x_3^* = 0.1$ m at the end of the bth time interval (Δt_b [T]). The superscript * serves to distinguish the grid-scale length intervals from the larger scale travel distances elsewhere in this Chapter. $M_{p,b}^f$ [M] is the mass convectively moving in the x_2 direction through the downstream wall of cube p during Δt_b. Since the porosity n is uniform, weighting according to water content was not necessary. From Eqs. (2.7) and (2.8) we have

$$\frac{M_{p,b}^f}{M_{p,b}^r} = \frac{v_{2,p,b} \cdot \Delta t_b}{\Delta x_2^*} \tag{2.9}$$

At scales larger than that of individual cells, the variation of the flow field complicates the relationship between M^f and M^r. As a consequence, the resident and flux concentrations defined for volumes and planes larger than that of individual cells will no longer be identical.

Temporal moment analysis

In practice, resident rather than flux concentrations are measured in the field. We therefore attempted to derive mass fluxes from resident concentrations by using the temporal moment analysis as described by *Vanderborght and Vereecken* (2001). The zeroth moment of the travel time is a measure of the tracer mass recovered from the system and the first moment gives the mean travel time.

The first normalized temporal moment $\tau_1(\mathbf{x})$ [T] of a BTC at a node with location $\mathbf{x}$ is defined as

$$\tau_1(\mathbf{x}) = \int\limits_0^\infty t c^f(\mathbf{x}, t) \mathrm{d}t \tag{2.10}$$

where

$$c^f(\mathbf{x}, t) = \frac{C^f(\mathbf{x}, t)}{\int\limits_0^\infty C^f(\mathbf{x}, t) \mathrm{d}t} = \frac{C^f(\mathbf{x}, t)}{\tau_0(\mathbf{x})} \tag{2.11}$$

Here, $c^f(\mathbf{x}, t)$ [T^{-1}] is the normalized flux concentration at location $\mathbf{x}$ and time t, and τ_0 [ML^{-3}T] (the zeroth moment) is the area under the BTC measured at location $\mathbf{x}$.

The average solute travel time from the inlet surface to location $\mathbf{x}$, $\mu_t(\mathbf{x})$, is equal to $\tau_1(\mathbf{x})$. The average travel time of an inert solute is used to define the 'equivalent' solute particle velocity $v_{eq}(\mathbf{x})$ [L T^{-1}], which characterizes the BTC measured at location $\mathbf{x}$

$$v_{eq}(\mathbf{x}) = \frac{\Delta x_2}{\mu_t(\mathbf{x})} = \frac{\Delta x_2}{\tau_1(\mathbf{x})} \tag{2.12}$$

where Δx_2 [L] is the distance between the solute application plane and the monitoring plane. As mentioned above, in practice only resident concentrations are available. We therefore used $c^r(\mathbf{x}, t)$ instead of $c^f(\mathbf{x}, t)$ in Eq. (2.11) to arrive at a normalized resident concentration for use in Eq. (2.10). This allows us to investigate the suitability and accuracy of this frequently used approximation.

By approximating $v_{2,p,b}$ (the local advection velocity at observation point) in Eq. (2.8) by v_{eq} (the average velocity of the particle along its trajectory) for cube p, the solute mass moving in the direction of x_2 can be estimated from the resident concentration at any point using Eqs. (2.8) and (2.12).

Leaching surfaces

For each monitoring plane we prepared leaching surfaces (*de Rooij and Stagnitti*, 2002a,b, 2004) based on the scaled solute mass fluxes

$$m^f_{p,b} = \frac{M^f_{p,b}}{\int\limits_0^{150} \int\limits_5^{15} \int\limits_{25}^{75} M^f_{p,b} \, \mathrm{d}x_1 \mathrm{d}x_3 \mathrm{d}t} \tag{2.13}$$

Leaching surfaces leave the original data intact but represent them in a way that facilitates the analysis of the combined variation in space and time of the quantity under consideration.

The temporal aspect of solute transport can be expressed in the breakthrough curve (BTC), which describes the travel time distribution (*Jury and Roth*, 1990).

To calculate the leaching surface, the control plane perpendicular to the movement of the solutes needs to be subdivided into small equally-sized areas. If we record over time the amount of solute that passed through each area we can construct the BTC for each area. By sorting the areas in descending order of total solute amount passed through each of them we obtain the spatial solute distribution curve (SSDC) (*de Rooij and Stagnitti*, 2000). A plot of the fraction of the amount of captured solute versus the accumulated area produces the cumulative SSDC.

A leaching surface can be obtained by plotting the individual breakthrough curves (BTCs) of the different areas of the control plane adjacent to one another in order of descending cumulative leaching over the duration of the experiment (*de Rooij and Stagnitti*, 2002a). By sorting the individual areas, a spatial coordinate y is obtained with dimension L^2. The leaching surface thus has a horizontal time-axis and a second horizontal axis (y) that represents the cumulative area of the areas into which the control plane is divided. The vertical axis gives the solute amount, which can be scaled according to Eq. (2.13) to make the leaching surface integrate to unity.

12

Let $S(y,t)$ [$\mathrm{L^{-2}T^{-1}}$] be the resulting leaching surface: the scaled leached amount of solute per area per time. For any location y^*, the solute BTC at that location is the cross-section of S parallel to the t-axis at y^*.

$$\mathrm{BTC}(t)|_{y^*} = S(y^*, t), \qquad t \in [t_0, \infty) \tag{2.14}$$

The cross-section parallel to the y-axis at time t^* represents the spatial solute distribution curve (SSDC)

$$\mathrm{SSDC}(y)|_{t^*} = S(y, t^*), \qquad y \in [0, A] \tag{2.15}$$

where A [$\mathrm{L^2}$] is the combined area of all sampling compartments.

Suitable cross-sections of the leaching surface parallel to the time-axis or the spatial axis, or integrations along intervals of the space and the time coordinate, can yield a wealth of information about the distribution in space and time of solute movement. For instance, the integral of S over time $\int_0^\infty S(y,t)\mathrm{d}t$ gives the cumulative SSDC, and the integral over space $\int_0^A S(y,t)\mathrm{d}y$ gives the BTC of the entire monitoring plane.

For a given flow field, the amount of solute passing a given area depends in a straightforward way on M^f. The relationship between passing amount of solutes and M^r is less unambiguous. The formal definition of the scaled resident mass is

$$\mu_{p,b}^r = \frac{M_{p,b}^r}{\int\limits_0^{20} \int\limits_0^{100} \int\limits_0^{100} M_{p,b}^r \mathrm{d}x_1 \mathrm{d}x_2 \mathrm{d}x_3} \tag{2.16}$$

where the denominator is equal to the total injected mass for an inert solute that has not moved out of the flow domain. In our case, strict application of this definition would lead to leaching surfaces that do not integrate to unity, especially far away from the injection plane. We therefore replaced the total injected mass by the mass that resided in a particular monitoring plane during the simulation period. Similar to Eq. (2.13) we approximate $\mu_{p,b}^r$ by $m_{p,b}^r$ according to

$$m_{p,b}^r = \frac{M_{p,b}^r}{\int\limits_0^{150} \int\limits_5^{15} \int\limits_{25}^{75} M_{p,b}^r \mathrm{d}x_1 \mathrm{d}x_3 \mathrm{d}t} \tag{2.17}$$

We computed pseudo-leaching surfaces for the monitoring planes based on the $m_{p,b}^r$ and compared them to the leaching surfaces based on the scaled solute mass fluxes. Finally we constructed leaching surfaces based on approximate scaled solute mass fluxes derived from the temporal moment analysis. Thus,

$\Delta x_2 = 10$ m $\Delta x_2 = 30$ m

Flux
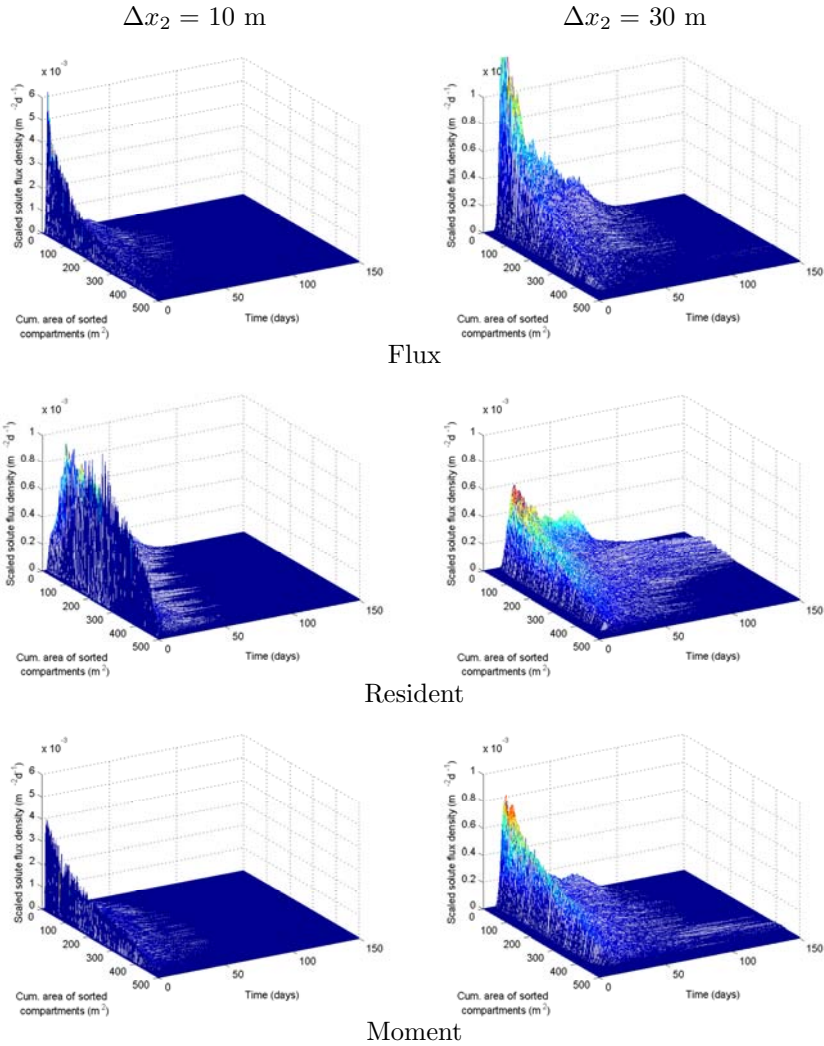
Resident

Moment

Figure 2.1: Scaled leaching surfaces of mass fluxes, resident masses and mass fluxes derived by moment analysis at monitoring planes at the indicated distances from the injection plane. A leaching surface consists of the sorted scaled breakthrough curves (BTCs) in descending order of total solute mass per cell of the analyzed monitoring plane (continued on p. 15).

the results of the various analyses are presented consistently, facilitating comparison.

In order to show the impact of high spatial resolution measurements, we also constructed the overall averaged BTCs for each monitoring plane. This is the BTC that would be obtained by adding the solute fluxes of all grid cells in a monitoring plane and dividing by the monitoring plane area.

$\Delta x_2 = 50$ m $\qquad\qquad\qquad \Delta x_2 = 70$ m

Flux

Resident

Moment
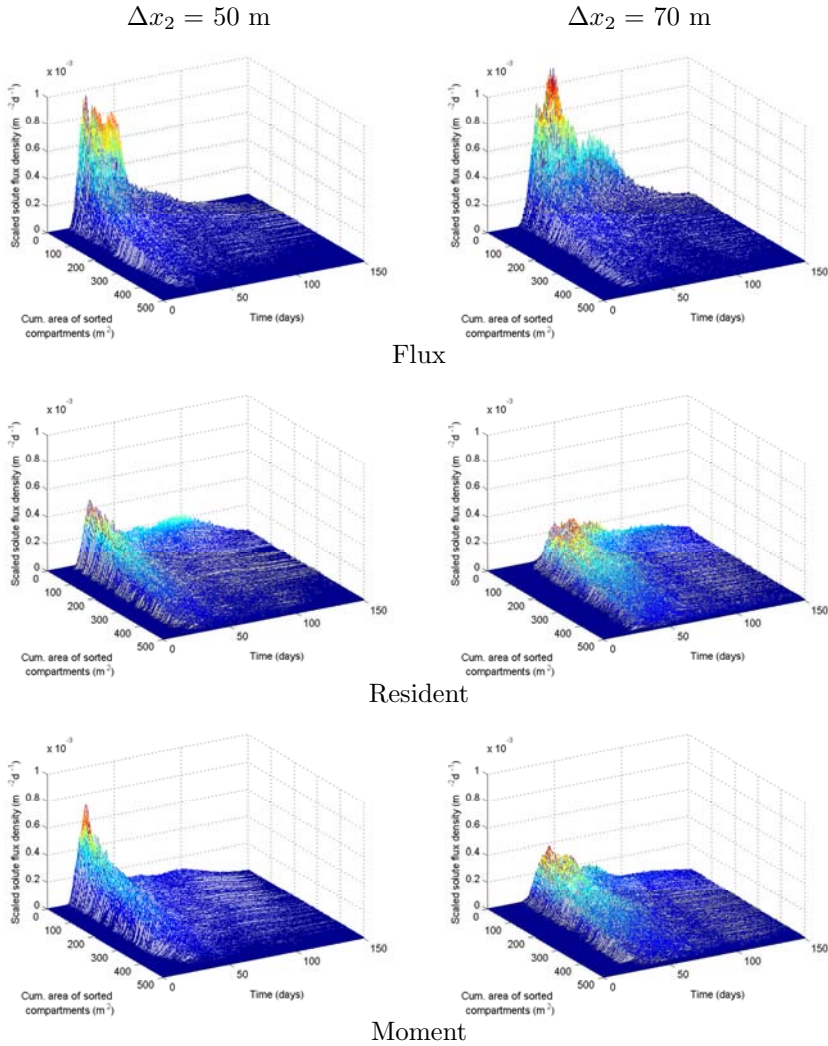
Figure 2.1: Continued from p. 14.

2.3 Results and discussion

2.3.1 Mass fluxes from the model output

Figure 2.1 presents the leaching surfaces at the monitoring planes, each constructed of 10000 individual BTCs. Moving downstream from the injection, the peaks descend (mainly between $\Delta x_2 = 10$ and 30 m) (Fig. 2.1 and Table 2.1). The maximum amount of solute passing through a single compartment changes only slightly (Table 2.2). Individual BTCs thus flatten and widen with increasing travel distance (Fig. 2.2). The overall averaged BTCs (for the

15

Table 2.1: Maximum peaks of the scaled leaching surfaces calculated from solute mass fluxes, resident solute masses, and the solute mass fluxes from the moment analysis, at various distances from the injection plane. These are the maximum peaks of individual breakthrough curves (BTCs), which are not necessarily from the first BTC in the scaled leaching surfaces. The last column gives the peak of the BTC for each entire monitoring plane, calculated from the mass fluxes.

| Distance | Maximimum peak ($m^{-2}d^{-1}$) | | | Overall peak |
Δx_2 (m)	Flux	Resident	Moment	($m^{-2}d^{-1}$)
10	6.2×10^{-3}	1.1×10^{-3}	4.0×10^{-3}	1.6×10^{-4}
30	1.6×10^{-3}	6.0×10^{-4}	8.1×10^{-4}	1.0×10^{-4}
50	9.7×10^{-4}	4.8×10^{-4}	7.2×10^{-4}	7.1×10^{-5}
70	1.1×10^{-3}	3.0×10^{-4}	3.8×10^{-4}	5.5×10^{-5}

entire monitoring plane) (Fig. 2.3) also flatten and widen with increasing travel distance.

At all distances a limited fraction of the cross-section carries most of the solutes: 25 % of the solutes is displaced by 4.5 to 5.9 % of the cells for the different monitoring planes (Table 2.3 and Fig. 2.4). The BTCs of these compartments vary considerably within one leaching surface (Fig. 2.5). This may reflect the limited role of dispersion in high velocity flow tubes versus a larger effect of dispersion in low velocity stream tubes.

Despite the fact that transport occurs by an imposed convective-dispersive transport regime at the local scale, solute transport at the aquifer scale is dominated by a few stream tubes in the total pore volume, as indicated by the fact the 50 % of the solute transport occurs through less than 16.7 % of the cross-section anywhere in all four monitoring planes (Table 2.3).

Table 2.2: Maximum fraction of the captured solute mass flowing through an individual cell at various distances from the injection plane, calculated from solute mass fluxes, resident solute masses, or moment analysis. This maximum fraction is the total amount of solute of the first BTCs in the scaled leaching surfaces.

| Distance | Largest amount of solute passing through an individual cell | | |
| | (Fraction of total mass captured at the monitoring plane) | | |
Δx_2 (m)	Flux	Resident	Moment
10	3.0×10^{-2}	1.1×10^{-2}	6.4×10^{-3}
30	2.1×10^{-2}	1.0×10^{-2}	7.6×10^{-3}
50	1.9×10^{-2}	1.2×10^{-2}	8.3×10^{-3}
70	2.7×10^{-2}	7.2×10^{-3}	5.8×10^{-3}
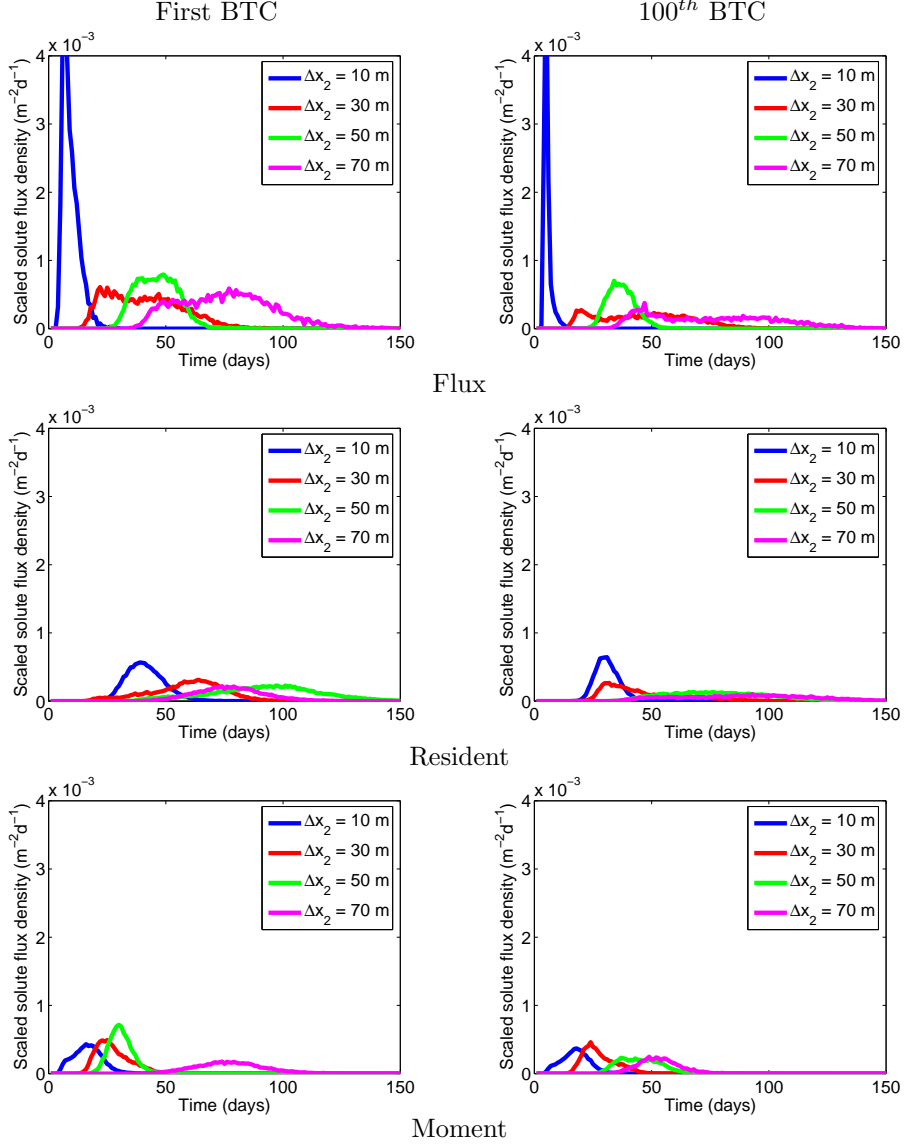
Figure 2.2: Breakthrough curves for the monitoring planes at the indicated distances (Δx_2) from the injection plane. The BTCs were obtained from mass fluxes, resident masses, and mass fluxes through moment analysis. The BTCs were determined for individual grid cell walls between four nodes. The first and 100th BTC are shown, as determined by the area under the curve. (The peak of the 1st flux BTC at $\Delta x_2 = 10$ m is 4.8×10^{-3} (m^{-2} d^{-1}), the peak of the 100th flux BTC at $\Delta x_2 = 10$ m is 5.4×10^{-3} (m^{-2} d^{-1})).
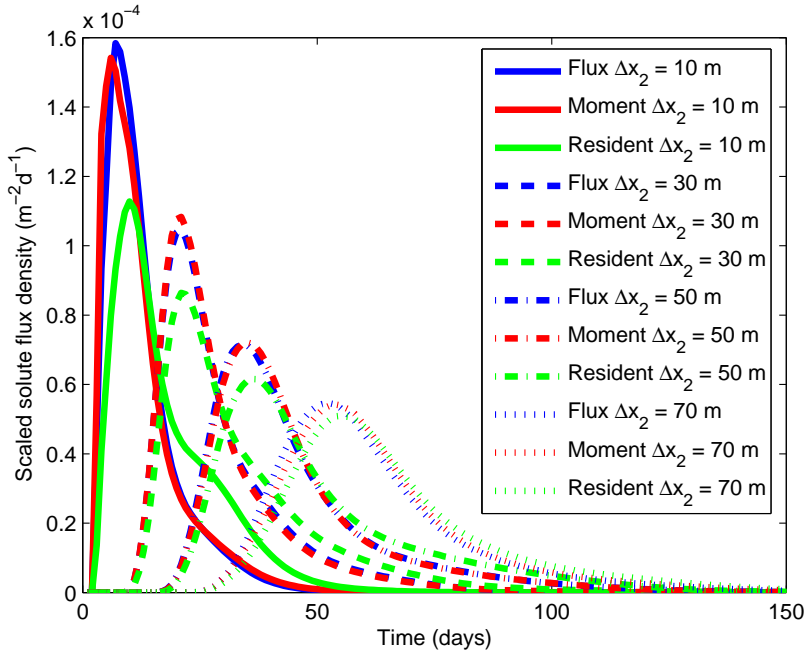
Figure 2.3: BTCs at the scale of the monitoring planes at the indicated downstream distances from the injection plane. The solute flux densities were derived from solute mass fluxes, resident solute mass, or through moment analysis.

The leaching surfaces indicate that 75% of the solute mass passed a vertical cross section through only 35% of its area. However, this does not imply that the fraction of the pore volume in which solutes are transported is only 35% of the total pore volume. If this were so, then the peak of the average solute fluxes should arrive already after 0.35 pore volumes, which was not the case. This indicates that the parts of the cross sectional area where most of the solute mass breakthrough occurs are not perfectly connected with areas of high solute flux in all other cross sectional areas. The lack of connection follows from the structure of the heterogeneity that we considered, i.e. Gaussian random fields in which high conductivity zones are not necessarily connected to each other. The poor connectivity of high-flow regions implies that each flow tube can have a wide range of flow velocities along its trajectory and the average velocity will vary among stream tubes, but will always be lower than the peak velocity. The variation in travel times expressed in the leaching surfaces, and the variation of flow velocities between and within stream tubes are consequential if kinetic processes (e.g. sorption) are important along the solute particle trajectories, for example with reactive barriers.

Figure 2.6 presents the actual amount of cells carrying solute per time step.

From Fig. 2.3 and Fig. 2.6 it is evident that that high flow cells carry most of the solute: the scaled solute flux density peaks are well ahead of the maximum cross-sectional extent of the solute plume for $\Delta x_2 = 30$ and 50 m. Also, the maximum percentage of active cells in Fig. 2.6 are consistently lower than the percentage of cells that carried most of the solute mass at some time during the simulated period (Table 2.3). This indicates that not all cells carried solutes at the same time, even when the bulk of the solutes passed a monitoring plane.

The injected mass at the injection surface is equal in each cell. After a short distance this mass is already redistributed towards zones with a higher water flux (Fig. 2.1). The crests of the leaching surfaces are similar to the observed trends in v_2 (Fig. 2.7). This also shows the importance of the velocity field.

Because the overall BTC is an average over the entire control area, the peak height of 1.6×10^{-4} m^{-2}d^{-1} is significantly lower than the maximum peak height of a single cell in the same area (Table 2.1). With the increase in spatial resolution it becomes obvious that overall BTCs underestimate the local concentration. A regulatory concentration limit can still be exceeded as the maximum peaks are not known with overall BTCs.

Table 2.3: Percentage of cells responsible for different fractions of displaced solute mass at the monitoring planes. The cells are sorted in descending order of cumulative transferred solute mass.

Distance Δx_2 (m)	Fraction of total mass	Percentage of cells (%)		
		Flux	Resident	Moment
10	0.25	5.3	7.7	11.9
	0.50	16.4	19.9	28.7
	0.75	35.9	40.7	51.7
	1.00	98.1	98.2	92.1
30	0.25	5.3	9.3	10.5
	0.50	15.0	23.6	25.4
	0.75	32.0	44.7	46.3
	1.00	98.5	98.7	90.2
50	0.25	5.9	9.1	11.6
	0.50	16.7	24.0	27.0
	0.75	35.6	46.3	47.7
	1.00	99.8	99.8	93.7
70	0.25	4.5	11.0	12.5
	0.50	15.7	27.4	29.2
	0.75	36.8	50.7	52.2
	1.00	99.2	99.4	97.0
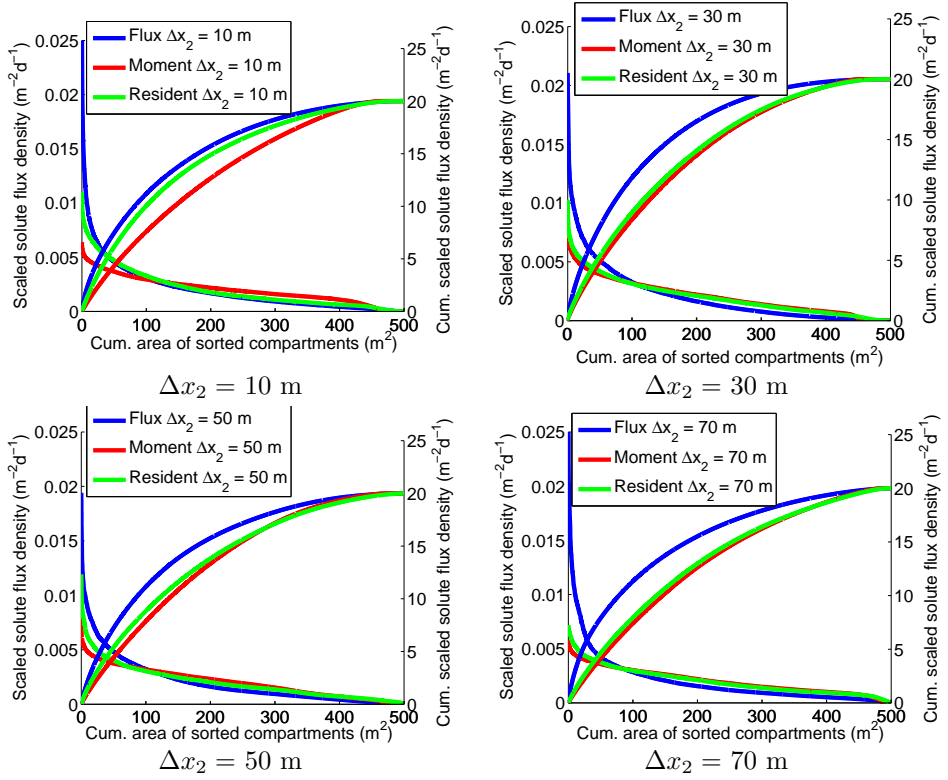
Figure 2.4: The spatial solute distribution curves (SSDC) and the cumulative SSDC for the monitoring planes.

2.3.2 Resident mass compared to mass fluxes

According to Table 2.3, slightly more cells contained mass (resident mass) than transported mass (mass fluxes) throughout the aquifer, indicating a small fraction of solute particles that hardly moved. Given the fact that these particles were not only found near the injection plane, they were not permanently stagnant, possibly owing to the random dispersive movement.

The effect of the inappropriate use of resident mass for solute transport is very detrimental to the leaching surfaces (Fig. 2.1), which become erratic and irregular. The noisy appearance of these pseudo-leaching surfaces reflects the random (dispersive) process that causes particles to arrive in low-flow regions of the aquifer. The difference between the leaching surfaces based on mass fluxes and resident masses is entirely caused by the different weighting factors assigned to the resident concentrations (Eqs. (2.7) and (2.8)). The conversion factor is given by Eq. (2.9), and in that equation, only $v_{2,p,b}$ varies between the cells that contributed to the leaching surface. The difference between the leaching surfaces in the first and second column of Fig. 2.1 suggest that dispersion was
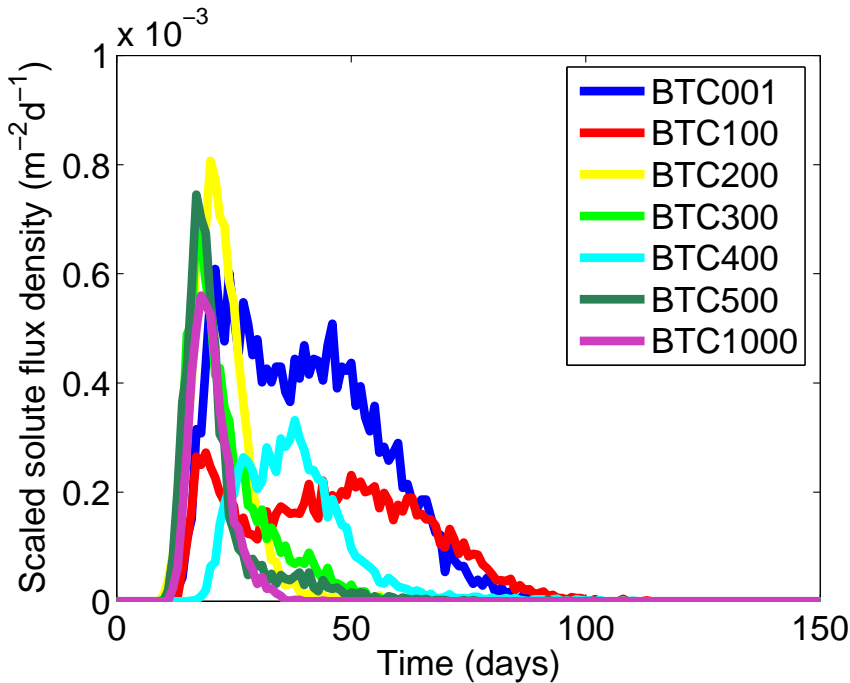
Figure 2.5: Individual BTCs of monitoring plane $\Delta x_2 = 30$ m based on mass fluxes. These BTCs show the differences of shape of the BTCs within a monitoring plane. The numbers in the legend indicate the rank number based on the area under the curve.

important in delivering solutes at various locations, but that the velocity field had a massive impact on the movement of these solutes.

The maximum solute flux density peak for the resident mass leaching surfaces is an order of magnitude too low (Table 2.1, and Fig. 2.2) and occurs much too late, because the resident mass underrepresents rapidly moving solutes in small portions of the flow domain. This leads to slightly delayed overall averaged BTCs with underestimated peaks (Fig. 2.3). The SSDCs for the resident mass (Fig. 2.4) underestimate the importance of the cells through which most of the solute passed. This effect is least pronounced at 10 m after the injection plane. This reflects the nature of the solute application in this study, which imposed an uniform resident concentration. In conclusion, the value of resident solute masses in describing solute movement hinges critically on the degree of detail and accuracy of the available information about the velocity field. For field studies, this poses a formidable observational challenge.

The coefficient of variation between the peak heights of the individual BTCs from which the leaching surfaces are constructed are between 113 and 130 % for the mass fluxes and between 55 and 65 % for the resident masses for the various monitoring planes. The difference stems from the additional variation
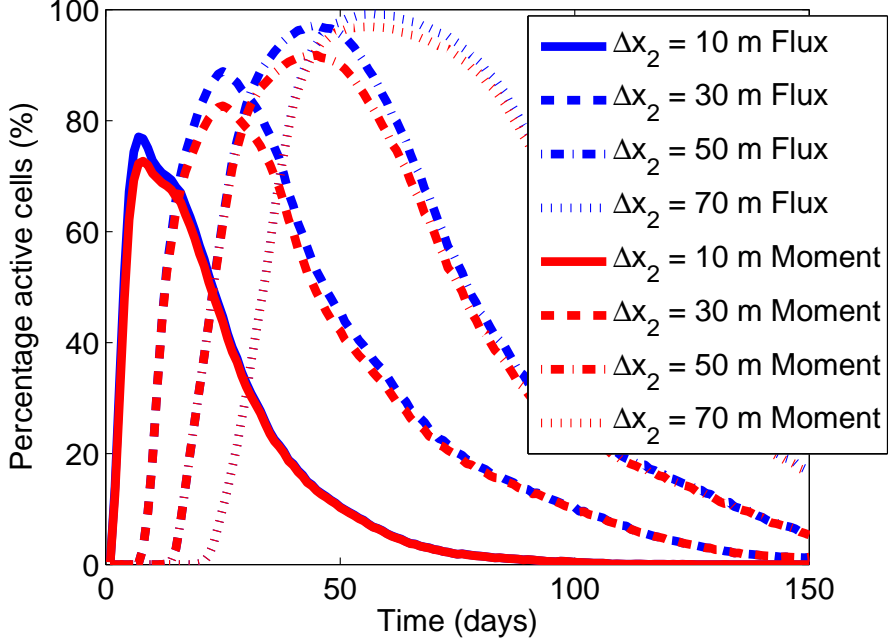
Figure 2.6: Number of active cells (cells containing solute particles) per time step based on flux masses and on estimated flux masses at the indicated monitoring planes.

of $v_{2,p,b}$ that adds to the variation of $C_{p,b}^r$ in Eq. (2.8) as compared to Eq. (2.7).

2.3.3 Measured and estimated mass fluxes compared

Estimating the conversion factor in Eq. (2.8) by using $v_{eq}(x)$, from Eq. (2.12), to approximate $v_{2,p,b}$ significantly improves the leaching surfaces (Fig. 2.1) and the overall averaged BTCs (Fig. 2.3) compared to the use of resident masses for solute transport problems. The effect on local BTCs (Fig. 2.2) and the SSDCs (Fig. 2.4) is considerably smaller. Temporal moment analysis improved the estimation of the time to peak (Fig. 2.2 and Fig. 2.3), while the amount of solutes passing a plane is still underestimated (Fig. 2.2 and Fig. 2.4). The degree of convergence of solute transport towards a limited portion of the cross-section is underestimated because of the averaging of the flow velocity over the trajectory (Tables 2.2 and 2.3 and Fig. 2.7). The approximate pore water velocities are significantly lower than the real ones for the high-flow cells, but higher for the low-flow cells (Fig. 2.7). The maximum peak at the monitoring planes of individual BTCs is consistently lower than those derived from the mass fluxes (Table 2.1). These findings corroborate the importance of the pore water velocity field evidenced by the poor results obtained when using only
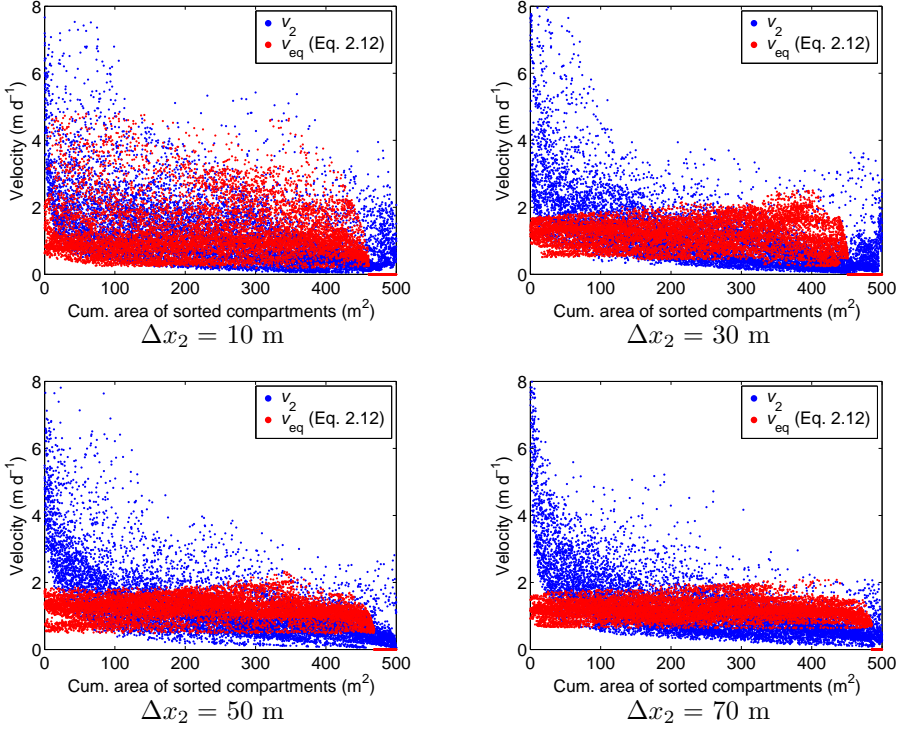
Figure 2.7: The pore water velocities in the main flow direction (x_2), v_2, of the individual cells in the monitoring planes at the indicated distance downstream of the solute injection plane. The cells are sorted in descending order of the total amount of solute that passed through them. In addition to the true water velocity, the trajectory-averaged pore water velocity (v_{eq}) according to Eq. (2.12) is also given.

resident solute mass.

To save computation time, we imposed a minimum number of particles present in a cube to produce non-zero concentration, this resulted in a non-continuous flow velocity distribution (Fig. 2.7) as calculated from the temporal moments. The effects of this manifest themselves in the crest of the leaching surfaces, at the sharp levelling of the SSDCs (Fig. 2.4), at the number of cells carrying solutes (Fig. 2.6 and Table 2.3), and by the number of cells with sub-threshold concentrations (Fig. 2.1).

The distribution of solute passage over the cells varies little with travel distance (Table 2.3). The use of resident concentrations in the moment analysis consistently leads to overestimation of the percentage of cells carrying a given fraction of the solute, particularly for the cells in the first quantile.

2.4   Conclusions

The leaching surfaces we constructed highlighted the dominating role of the spatial pore water velocity field. Lateral dispersion had very little effect on the spatio-temporal distribution of solutes at any cross-section perpendicular to the macroscopic flow direction. This illustrates the importance of the velocity field, even if dispersion is significant.

This study shows that assessing solute movement from resident concentrations should be done with care. Only if the local concentrations vary weakly with within the pore space, resident concentrations give reliable results. This implies that diffusion and dispersion must have had sufficient time to reduce local concentration gradients. This numerical study shows that for a realistic degree of heterogeneity, travel distances of 70 m are still insufficient to acquire the necessary degree of local mixing. In the range where resident and flux concentrations have not yet converged, moment analysis can help improve the results obtained from resident concentration observations.

Moment analysis performed adequately for evaluating solute movement over the entire cross-sections of the aquifer. Its approximation of the local velocity by averaging over the trajectory affected its performance at the scale of individual grid cells. Leaching surfaces proved to be an adequate tool to demonstrate, illustrate, and quantify the limitations of moment analysis.

It is likely that the difference between resident and flux masses increases with increasing aquifer heterogeneity and with increasing connectivity of conductive areas. The degree of heterogeneity in our study was by no means extreme. For aquifers with more pronounced variation and / or high flow regions, the conclusions above become even more pertinent. It is desirable to develop methodologies to measure flux concentrations or solute mass fluxes.

CHAPTER 3

Variable-suction multi-compartment samplers with
different porous covers to measure the spatial and
temporal distribution of unsaturated water and solute
movement

3.1   Introduction

Soil and groundwater contamination is a major concern in many densely popu-
lated areas. Solute movement in soils and its transfer through the unsaturated
zone to the groundwater is strongly affected by soil heterogeneity, which cre-
ates marked variations in soil water contents (e.g. *Wendroth et al.*, 1999) and
solute movement (e.g. *Butters et al.*, 1989; *van Wesenbeeck and Kachanoski*,
1991, 1994; *Forrer et al.*, 1999). These variations typically occur within the
square meter scale, but their effects on solute leaching persist at much larger
horizontal scales. This is a consequence of the small scale in the overall flow
direction i.e. vertical, which in many deltas does not exceed a few meters (*Cor-
win et al.*, 2006). Chapter 2 showed that fluxes instead of state variables should
be measured to correctly assess solute movement in soils. In order to be able
to measure both the spatial and temporal distribution of flow and transport
we need to measure water and solute fluxes at multiple locations with a high
temporal resolution.

This chapter is a slightly modified version of the manuscript: Bloem, E., F. A. N.
Hogervorst, G. H. de Rooij, and F. Stagnitti, Variable-suction multi-compartment
samplers with different porous covers to measure the spatial and temporal distribution
of unsaturated water and solute movement.

To do so in the field, one might install many samplers to capture the overall variation in the field, or install a Multi-Compartment Sampler (MCS) that divides a continuous sampling area into many adjacent sampling areas. In either approach, it is imperative that the sampler device minimizes the disturbance of the flow field. For this reason, suction cups are unattractive (e.g. *Corwin*, 2002).

Devices to capture infiltration mostly consist of a flat, horizontal sampling plate of porous material. As summarized by *Brye et al.* (1999), the collection of leachate in such lysimeter devices should generate minimal discontinuities in the flow path of moving water and a driving force for water movement. Maintaining a capillary connection between the soil column and the surface of the porous plate is essential to minimize ponding and preferential or bypass flow around the lysimeter (*Kung*, 1993; *Jemison and Fox*, 1994). Zero-tension lysimeters rely on gravity to cause water movement through the lysimeter's porous plate surface. They depend on the formation of a saturated soil zone above the porous plate before drainage can occur by gravitational flow. Fixed-tension lysimeters rely on both gravitational and matric potential gradients created by applying suction to the porous plate by means of pumps or capillary wicks (*Holder et al.*, 1991; *Boll et al.*, 1992; *Knutson and Selker*, 1994; *Rimmer et al.*, 1995). Fixed-tension lysimeters improve the flow patterns around and through the lysimeter's porous plate. Still, *Duke and Haise* (1973); *Dirksen* (1974); *Dagan* (1993); and *Flury et al.* (1999) showed that a near-constant pressure head can result in a biased sampling of a particular pore size. Therefore the applied suction should ideally follow the variable ambient matric potential in the soil.

Increasingly sophisticated percolate samplers were constructed by *Ivie and Richards* (1937); *Richards et al.* (1937); *Cole* (1958, 1968); *Duke and Haise* (1973); *Cary* (1968, 1970); *Dirksen* (1974). *van Grinsven et al.* (1988) developed a variable suction tensiometer that adapted the applied suction to the ambient matric potential i.e. an automatic equilibrium tension lysimeter. *Brye et al.* (1999) designed another variable suction sampler. *Kosugi and Katsuyama* (2004) constructed a controlled-suction period lysimeter, which controls the water extraction period instead of controlling the suction value.

Siemens and Kaupenjohann (2004) compared tensiometer-controlled suction plates, wick samplers, and ion-exchange resin boxes in a field solute leaching experiment in a sandy soil. They concluded that tensiometer-controlled suction plates allowed an overall satisfactory estimation of water and solute fluxes in the sandy soil.

All variable-suction instruments discussed above are single-cell instruments, incapable of observing heterogeneity effects. To quantify heterogeneity, multi-compartment samplers were developed for *in situ* installation (*Boll et al.*, 1992), but only with wicks. Most of these samplers have an area in the order of 10^{-1} to 10^0 m^2 divided into sampling compartments ranging between about 10^{-3} and 10^{-2} m^2. This scale envelopes a considerable portion of soil variability within a field (about 10^4 m^2) (*van Es*, 2002).

As *Siemens and Kaupenjohann* (2003) pointed out, porous cups and plates which are used to sample pore waters of soils may alter the sample composition due to filtration effects, precipitation of solid phases, gas exchange between sample and atmosphere, and sorption or release of chemical species (*Grossmann and Udluft*, 1991; *McGuire et al.*, 1992; *Krejsl et al.*, 1994; *Wessel-Bothe et al.*, 2000). Adsorption of NH_3, NH_4, P, K, Na, Ca, and Mg on ceramic sampler cups have been observed by *Wagner* (1962); *Grover and Lamborn* (1970); *Hansen and Harris* (1975); *Nagpal* (1982); *Bottcher et al.* (1984); and *Hughes and Reynolds* (1988). Therefore suction cups of more inert materials have been used, like nylon, polyethylene, poly(tetrafluorethene) (*Morrison*, 1982; *Beier et al.*, 1992), fritted glass (*Long*, 1978), and hollow fiber tubing (*Levin and Jackson*, 1977). Problems may still arise, for example, when low concentrations of heavy metal ions are sampled (*McGuire et al.*, 1992; *Wenzel and Wieshammer*, 1995; *Andersen et al.*, 2002).

We designed a new instrument that for the first time combines variable-suction and multi-compartment sampling. The instrument consists of 100 cells, each with a size of 31.5×31.5 mm. For each cell we can measure the amount of drops passing through each cell every 5 minutes. The percolate is retained for each cell, and can be repeatedly extracted for analysis while leaving the instrument buried *in situ*, facilitating prolonged operation times. Sub-atmospheric pressure is applied equally to all plates. As an additional advantage, the sampler has a limited height, allowing its deployment in areas with shallow groundwater. In order to make this instrument suitable for reactive solute transport we constructed three prototypes, in which the porous material covering each cell consisted of a polyamide fiber nylon mesh in the first sampler 'nylon sampler', sintered porous stainless steel 316 metal plates in the second sampler 'metal sampler', and a polyamide membrane in the third sampler 'membrane sampler'. We tested the nylon sampler in the laboratory, and the two other samplers in a field experiment. In this paper we discuss the construction, installation, operation, and performance of the multi-compartment sampler.

3.2   Materials and methods

3.2.1   Variable-suction multi-compartment sampler design

The three samplers (Figs. 3.1 and 3.2) consisted of a $325 \times 325 \times 20$ mm aluminum top plate. Square funnels were milled out in a 10×10 grid in the aluminium plate in such way that 0.4 mm wide, 6 mm high ridges blocked hydraulic contact between neighboring plates. The aluminium plate was then anodized. The size of each cell is 31.5 mm $\times$ 31.5 mm and the outer wall has a thickness of 3 mm.

Underneath the aluminum plate, a PVC sample collection chamber was placed. To retain the percolate for each cell one-hundred collection cells were
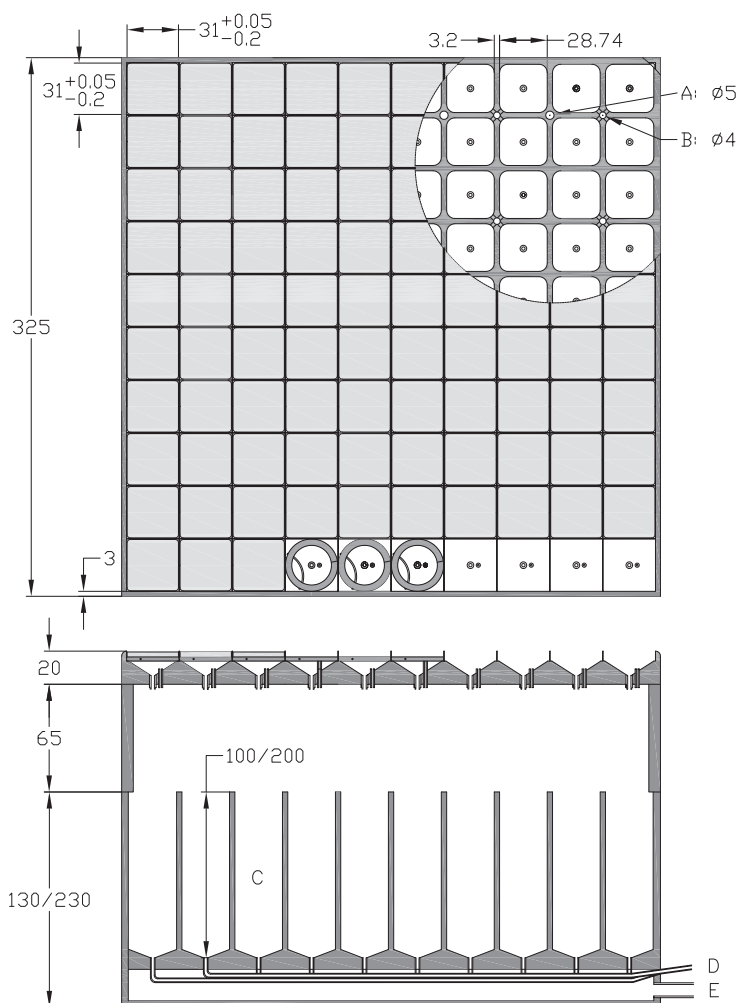
Figure 3.1: Top view and vertical cross section of the multi-compartment sampler. The top view shows metal plates, support rings, and funnel outlets at the center of each cell. In the circle the top plate has been removed. A bolting hole (A) as well as an overflow hole (B) are visible. The vertical cross section shows the sample collection chamber with sample collection cells (C), sample retrieval tubes (D), and the suction tube (E). Details are shown in Fig. 3.2.

made in a PVC block. Depending on the amount of percolate expected and the installation space for the samplers, the sample collection chamber could consist of several layers of PVC glued together. The bottom of the collection cells sloped towards the center, where a sample retrieval tube entered each collection cell (Fig. 3.1). Bundles of medical quality PVC tubes ran through
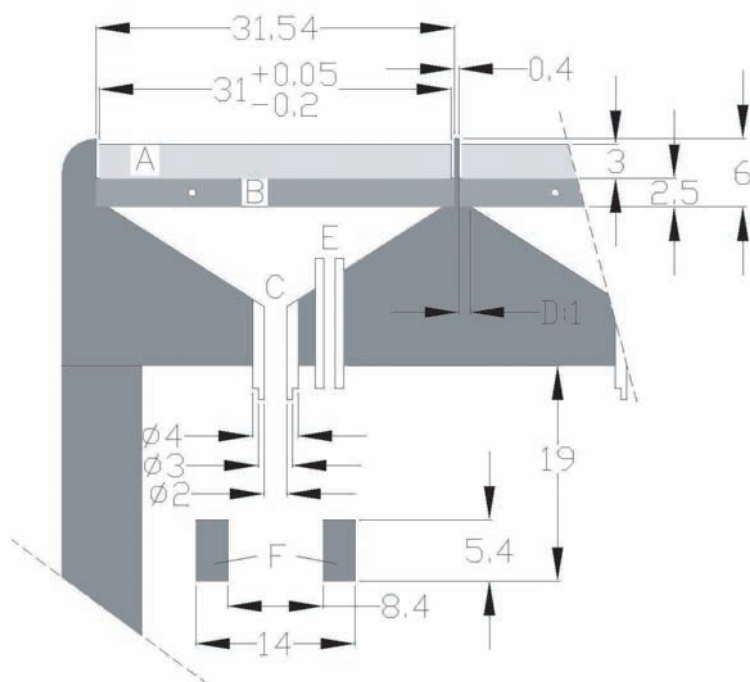
Figure 3.2: Vertical cross section of corner cell of Fig. 3.1, showing a metal plate (A), with support ring (B), a funnel milled in aluminum plate with dripper (C), the porous plate support rim (D), the aeration tube (E), an infrared drop counter unit (F) positioned below dripper.

grooves in the bottom plate through the outlet holes. PVC glue was used to seal the chink between the tubes and the exit holes in the wall. This construction made it possible to repeatedly sample the percolate of each individual cell for analysis while leaving the instrument buried *in situ*. The PVC block was bolted and glued to the aluminium plate.

In case of insufficient sample storage volume, the overflow was captured by vertical holes drilled at the corner of a cell in the separating wall. The excess water was deposited at the bottom of the chamber where it flowed into the direction of the vacuum line. This excess water was transported horizontally towards the vacuum Erlenmeyer flask buried next to the sampler, without disturbing pressure regulation.

The funnel outlets of the aluminium plate were outfitted with PVC tubes (3 mm o.d., 2 mm i.d.) to guide water droplets through the infrared beam of drop counters installed in the chamber below each funnel (Fig. 3.2). The electronic parts of these counters were waterproofed by 5 dip treatments in resin. Their power supply and data cables were guided through air- and water-tight outlet ports in the chamber wall. Air flow through electrical cables was blocked by
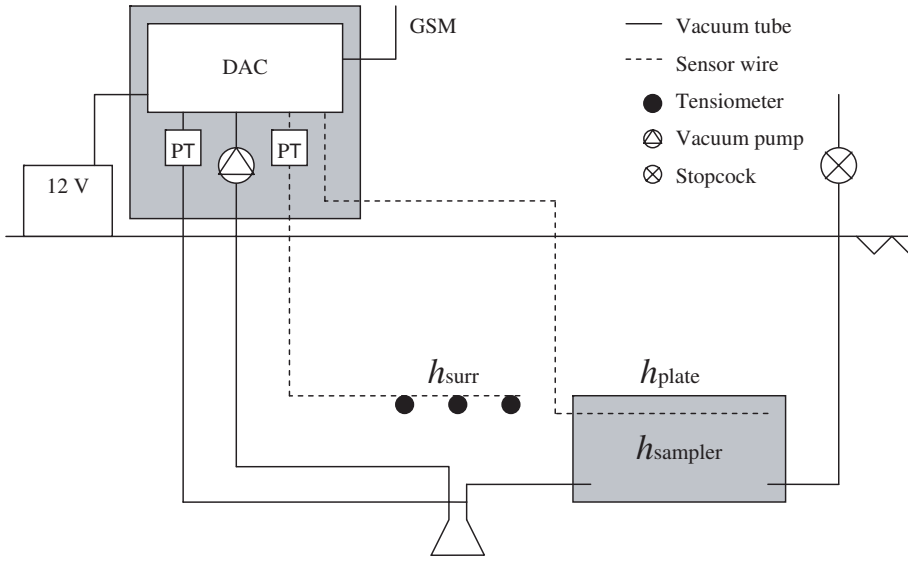
Figure 3.3: Vertical cross section of above- and below ground components connected by vacuum tubes and sensor wiring. Two parallel rain gauges (not in drawing) are placed within 5 meters from the instrument. The Data Acquisition and Control unit (DAC), Pressure Transducers (PT), and the vacuum pump operate on 12 V battery power.

soaking both ends in resin. After passing the drop counters, the droplets were retained in the sample collection cells.

3.2.2 Variable-suction multi-compartment sampler suction control in the field

For field use, the sampler was installed horizontally below an undisturbed soil volume. The sampler was connected to a power supply, data logger (CR10X, Campbell Scientific Instruments) with a GSM data transmitter, and pressure control equipment (Fig. 3.3). The latter consisted of pressure transducers, a vacuum pump, and a suction release valve, all operated by the data logger. The suction level was set in real time by the data logger from tensiometer readings recorded by the same data logger. The tensiometers were installed at the same depth as the top of the samplers. Ideally, the matric head immediately above the porous plate (h_{plate} [L]) is equal to the matric head at the same depth in the vicinity of the sampler (h_{surr} [L]), so as to minimize the sampler's effect on the matric pressure field, and hence on the flux field *Kosugi and Katsuyama* (2004)

$$h_{\text{plate}}(t) = h_{\text{surr}}(t) \tag{3.1}$$

The air pressure applied to the porous plates must account for the pressure head loss (Δh [L]) over the plates, leading to a target pressure head (h_{target} [L]) according to

$$h_{\text{target}}(t) = h_{\text{surr}}(t) - \Delta h \tag{3.2}$$

where Δh [L] is positive and varies with the flux density.

3.2.3   The porous materials covering the sampler funnels

Polyamide fiber nylon mesh

The nylon mesh supplied by Merrem & la Porte B.V. was made of a polyamide fiber, woven into a cloth with a mesh size of 7 μm and an open area of 2 %. Due to its relatively high air entry value ($\approx$ -70 cm for two layers of mesh) the nylon mesh is not suitable for field experiments in which the soil dries out quickly.

To support the mesh, perforated PVC plates were placed on the porous plate support rims (Fig. 3.2). Two layers of nylon mesh were placed on top of the aluminum top plate and glued (one after the other) to the ridges between the funnels. The glue prevented lateral flow through the mesh. After hardening, we tested the sampler to find leaks by wetting the mesh with de-aerated filtered water until saturation, and then applied water to an individual cell to see if there was no drainage to neighboring cells. The area of the nylon mesh including the separating glue was 1015 cm^2. Including half the area of the outer rim of the sampler gave a sampling area of 1035 cm^2.

Porous stainless steel 316 metal

The sintered stainless steel 316 metal filters were manufactured by GKN Sinter Metals Filters GmbH (material: AISI 316L with GKN Quality SIKA R1 AX and size: 31.0 $\times$ 31.0 $\times$ 3 mm with 4$\times$R2.0). The plates had a porosity of 21 %, with pores ranging from 1.4 to 8 μm diameter.

To mount the plates we applied non-foaming poly-urethane glue over the full height of the vertical sides of the metal porous plates and placed them in their slots, on the support rims of the funnels in the aluminum plate. After hardening, we tested the sampler to find leaks by slowly wetting the plates with de-aerated filtered water until saturation, and then increased the air pressure inside the sample collection chamber while the plates were covered by a thin layer of water. The remaining leaks were filled with glue that was applied by a syringe, again followed by a test. Some excess glue that extended upwards from the intercept surface was carefully cut away with a scalpel. The area of the plates plus the separating rims was 1015 cm^2. Including half the area of the outer rim of the sampler gave a sampling area of 1035 cm^2.

Polyamide membrane

The membrane filter is a polyamide suction membrane (pore size 0.45 μm and air entry value of 1000 cm H_2O supplied by EcoTech Umweltsysteme GmbH. Because the membrane was only available in a 300 mm width, the outer rows of the 10×10 cells of the sampler were only partially covered with the porous membrane. This required the other half of these cells to be sealed as the membrane and its support were glued and clamped on top of the original grid. The membrane required a separate nylon support to mount it on the top plate, which left 30×30 mm porous areas between the separating rims. To prevent lateral flow in the membrane, the grid pattern of the sampling cells was imprinted by narrow lines of glue that locally closed the pores of the membrane. The total porous surface plus the glue separation lines between the cells was 913 cm^2. Including half of the sealed area and the outer rim gave a sampling area of 1057 cm^2. The need for a separate nylon support led to a large outer rim of this sampler.

During one laboratory experiment fungal growth was observed, which clogged the membrane and significantly reduced the membrane's hydraulic conductivity. Microscopic analysis of the particulate matter on the membrane revealed the presence of both bacteria and ciliate organisms, consistent with the membrane pore size. This could be a risk during any experiment involving nonsterilized soil. However, we only observed this during a laboratory experiment, and not during later field trial.

When wetted the nylon support for the membrane was found to expand by a few percents. Since the rest of the sampler did not expand, the membrane deformed, and was not level anymore. This volume and shape change may cause poor contact between the soil and the sampler. We removed the sampler, completely wetted the nylon components to let them expand prior to assembly, and then reassembled and installed the sampler.

3.2.4 Laboratory experiment with the nylon sampler

For the laboratory experiment, we excavated an undisturbed soil monolith (43 $\times$ 43 $\times$ 29 cm, L $\times$ W $\times$ H) from a vineyard soil between Stawell and Ararat in Victoria, Australia. Details of the soil (a yellow duplex soil, of a clay loam texture) are given by *Badawy* (1982). The monolith was excavated by carving out its shape, fitting a plywood frame around it and carefully digging underneath it from the surrounding trench. The monolith was placed upside down and its base levelled with spatulas in the laboratory. One stone was removed and its cavity refilled with soil material. We wetted the monolith base to ensure good contact with the MCS and then placed the sampler (with nylon mesh) on top, firmly connecting it to the frame containing the monolith and placed the set-up upright (Fig. 3.4).

The nylon mesh that covered the MCS funnels had been soaked in 2 mg l^{-1} $CuSO_4$ (*Flemming and Trevors*, 1989; *Khan and Jury*, 1990; *Epstein and Bassein*, 2001; *Binnie et al.*, 2002) and allowed to dry before it was glued in place.

Figure 3.4: The laboratory set-up with the nylon sampler. The multi-compartment sampler is placed on the table, under the soil column in its plywood casing. Above the soil column the rainfall simulator is installed.

To prevent fungi, bacteria, and algae growth, the rainfall simulator of the type described by *de Rooij* (1996) and *de Rooij and Stagnitti* (2000) was regularly flushed with 2 mg l^{-1} $CuSO_4$ during preparations. No biological activity was observed in the rainfall simulator or the mesh during and after the experiment. Copper sulfate was not added to the irrigation water to avoid interference with naturally occurring soil biological activity (*Coleman and Crossley*, 1996; *Nannipieri and Badalucco*, 2003).

In the field, winter rainfall (May - October) is 373 mm on average, and summer rainfall (November - April) averages 216 mm. In the summer the vineyard is irrigated with 637 mm on average. We simulated this by representing each

month by two water applications within 3.5 days (2 × approximately 31 mm for winter and 2 × approximately 71 mm for summer) to deliver the amount of water corresponding to winter or summer months. In total we had 32 water applications: first 8 winter applications (4 months), then 12 summer applications (6 months), and finally 12 winter applications (6 months). To mimic the patchy irrigation pattern produced by the drip irrigations installed on-site and reduce boundary effects we applied water to the inner 35 × 35 cm of the monolith's surface only. The equivalent water layers above relate to this monolith area.

We maintained a constant pressure head of -50 cm (monitored every 15 minutes) to the bottom of the soil and kept the ambient temperature at 20 °C. Droplets per cell were counted and recorded in 5-minute intervals. The collected percolate was weighed after each water application, and during water applications as often as required to prevent individual sample collection cells from overflowing.

3.2.5 Field experiment with the metal and membrane samplers

We installed the metal and membrane samplers in an agricultural field in Vreedepeel in the south-eastern part of The Netherlands. To install the metal and membrane samplers at the field site, we excavated a trench 1.30 m long and 1.0 m deep. On either side of this trench we dug a tunnel (ceiling at 0.31 m depth for the metal sampler and 0.25 m depth for the membrane sampler) in which we installed the two samplers. The tunnel ceiling was levelled with a scraper. The scraper was constructed by gluing PVC rings in a triangular grid. This stiff grid was then milled flat (tolerance 0.05 mm). The instruments were then pressed against the ceiling with a jack. After installation we lowered the instruments once (the tunnel ceilings did not collapse) to check the contact by visually inspecting at the imprint of the samplers in the ceilings. The distance between the trench wall and the samplers was 0.18 m in both cases, and the horizontal center-to-center distance between the instruments was 2.00 m. The tubing and wiring from the samplers were led horizontally away from the sampler bottom for about 0.2 m and then to the soil surface.

To provide ambient matric potential readings to help adjust the suction in the sampler chambers we installed self de-aerating tensiometers (*Miller and Salehzadeh*, 1993); manufacturer: Rhizosphere Research Products, Wageningen, The Netherlands) by carefully pre-drilling installation holes. The tensiometers were placed near the membrane sampler at depths of 0.24 m, 0.25 m, and 0.26 m. One tensiometer was 0.12 m away from the membrane sampler and 2.00 m from the metal sampler. The other two were installed 0.08 m apart at 0.45 and 0.46 m distance from the membrane sampler. The distances towards the metal sampler of these tensiometers were 1.22 and 1.29 m.

To double-check the contact between sampler and soil we applied 19 mm demineralized water at the soil surface over an area of 0.70 × 0.70 m above either sampler in no more than 5 minutes. All cells intercepted percolate, indicating good contact, and the amounts were such that boundary effects

appeared negligible (no significantly larger or smaller amount of percolate at the perimeter). We then backfilled the cavities around the samplers with local material and backfilled the trench.

Two tipping-bucket rainfall gauges were installed in the field to measure the rainfall rates (logged every minute during rainfall) and amounts (cumulative rainfall logged every hour). After each rainfall event (usually a cluster of small rain showers (Table 3.1)), water samples were collected from the individual cells. In the membrane sampler, drop counters in all 100 sampling cells recorded in 5-minute intervals the number of droplets falling into the sample collection cells. After sampling the percolate, we computed every 5 minutes the average drop volume to arrive at flux-density values.

We used the lowest reading of three tensiometers to determine $h_{\mathrm{surr}}(t)$ every three seconds. We also determined the pressure inside the sampler and converted this to a pressure head h_{sampler} [L]. Ideally h_{sampler} should be equal to h_{target} (Eq. (3.2)). When $h_{sampler}(t) < h_{\mathrm{surr}}(t) - \Delta h$, the vacuum pump was thus switched off. When $h_{\mathrm{sampler}}(t) > h_{\mathrm{surr}}(t) - \Delta h$, the vacuum pump was switched on. This decision routine was run every three seconds, if it was activated. Tensiometer readings and chamber pressure were logged every 15 minutes. For the metal sampler Δh was set to +5.8 cm, which gave adequate results. For the membrane sampler we calculated a negligible pressure drop and owing to the thin, conductive membrane therefore Δh was set to zero. The pump overshot the target pressure for the membrane sampler, and we found that setting Δh to -6.0 cm remedied the problem.

The activation or deactivation of the pressure regulation routine was deter-

Table 3.1: Percolate sampling dates and rainfall and evapotranspiration characteristics for each sample collection period. Day = Day of sampling, Rain = Rainfall measured over sampling interval, RI = Rainfall Intensity, ET_{pot} = Evapotranspiration, I = Infiltration.

Date	Day nr	Rain (mm)	Nr. rain	RI_{min} (mm h^{-1})	RI_{max} (mm h^{-1})	ET_{pot} (mm)	I (mm)
20-12-05	6	17.6	13	0.1	2.0	1.3	16.4
03-01-06	20	12.4	16	0.1	1.4	3.0	9.4
25-01-06	42	20.1	19	0.1	2.2	6.7	13.5
10-02-06	58	15.4	15	0.1	3.2	5.2	10.2
17-02-06	65	26.7	13	0.1	3.0	2.6	24.1
22-02-06	70	30.4	17	0.1	2.9	1.6	28.9
07-03-06	83	11.6	16	0.1	1.0	10.6	1.0
11-03-06	86	24.4	8	0.1	2.5	1.0	23.5
28-03-06	104	22.5	22	0.1	3.3	22.1	0.4
05-04-06	112	23.8	22	0.1	3.0	11.7	12.1
08-05-06	145	27.9	27	0.1	4.0	48.7	-20.8

mined by rainfall (measured by tipping bucket gauges), tensiometer readings, and number of droplets counted. If rainfall was monitored according to Table 3.2 the vacuum pump and thus the suction control, was switched on. The vacuum pump was also switched on if $h_{\mathrm{surr}}(t) \geq -40$ cm. The vacuum pump was switched off if there was no drainage (i.e. zero drops counted for one hour), and besides this there occurred no rainfall according to Table 3.2.

Table 3.2: The pump was switched on if rainfall was monitored. The pump was switched off if there was no drainage and besides this no rainfall.

	Interval (minutes)	Switch on Rainfall (mm)	Switch off Rainfall (mm)
Rainfall	15	≥ 0.4	
Rainfall	60	≥ 0.6	< 0.6
Rainfall	180	≥ 3.0	< 2.0
Rainfall	720	≥ 8.0	

3.3   Results and discussion

3.3.1   Laboratory experiment with the nylon sampler

During the entire experiment the vacuum pump was working constantly, indicating that the nylon sampler was not capable of maintaining vacuum for a long period. On day 14 the instrument reached its desired pressure head of -50 cm (Fig. 3.5). From day 14 onwards the pressure head in the tank stayed between -42 and -52 cm. Once the nylon mesh was saturated, the pressure head retained stable. During half an hour on day 40 the pump was switched off. During this period the pressure head in the sample collection chamber approached zero. After switching the vacuum pump back on, the target pressure head was reached within seconds, indicating that a saturated mesh effectively blocks air flow. After the end of the irrigation period (day 46) we kept the pump running. The nylon mesh gradually dried out and became permeable to air. Consequently, the pressure head started to increase at day 65.

Figure 3.6 presents the water application regime and the resulting drainage (over the entire sample collection area). From four cells with a consistent drop volume of 0.05 ml as determined from collected volumes and drop counts, we present the response to an individual summer water application event (event on day 22, Figs. 3.6 and 3.7) with an irrigation flux of 8.0 mm h^{-1}. Drainage starts within 80 - 100 minutes after the start of the rainfall, and the drainage flux decreases rapidly when irrigation ceases (within 25 - 45 min after ceasing
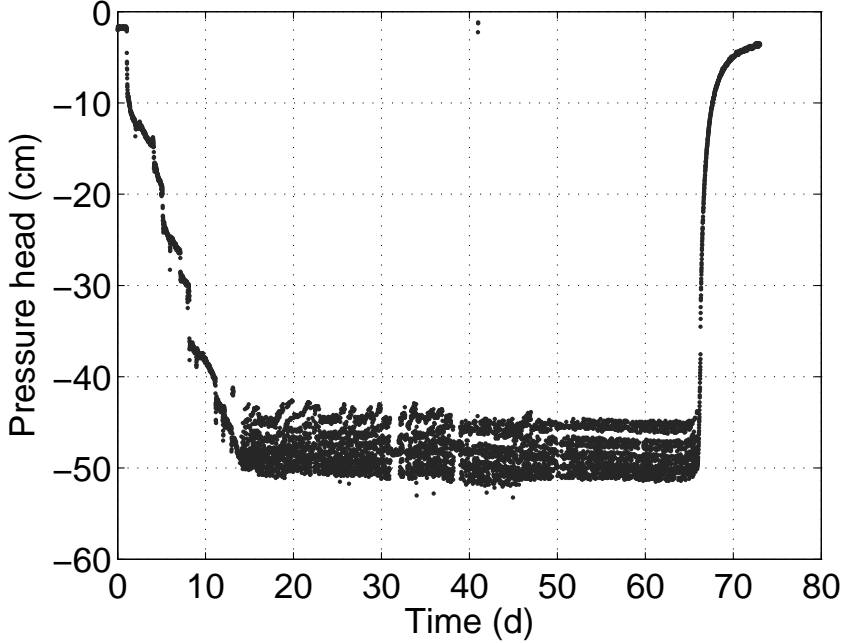
Figure 3.5: Observed pressure head in the sample collection chamber of the nylon sampler during a laboratory experiment with irrigations according to Fig. 3.6a and with a target pressure head of -50 cm. The measurement interval was 15 minutes. At t = 0 days the first water application started.

of the irrigation). The stable drainage flux densities of cells 21, 80, and 40 are 4.3 mm h^{-1}, 4.7 mm h^{-1}, and 5.4 mm h^{-1} respectively, resulting in a total drainage during that event of 33.7 mm for cell 21, 40.6 mm for cell 80, and 42.4 mm for cell 40. The drainage flux for cell 76 is stable around 16.8 mm h^{-1} resulting in a drainage of 156.8 mm. On average the drainage is 75.1 mm during this event.

During one event (day 25, Fig. 3.6) the rainfall simulator malfunctioned, resulting in a very high rainfall rate. The spatial distribution did not differ significantly from other events, indicating no artificial lateral distribution caused by lateral flow above the mesh at this higher flux density (Fig. 3.8).

We studied the spatial distribution of drainage by ranking the sampling cells in descending order of total captured percolate, and plotted the spatially accumulated fraction of total captured percolate with cumulative fraction of sampling area. The resulting spatial drainage distribution curves (SDDCs) are given in Fig. 3.8. The SDDCs are nearly similar. The contrast between cells with high and low flow sharpens in time, and the later SDDCs consequently have a more pronounced curvature. Neither the SDDCs (Fig. 3.8) nor the
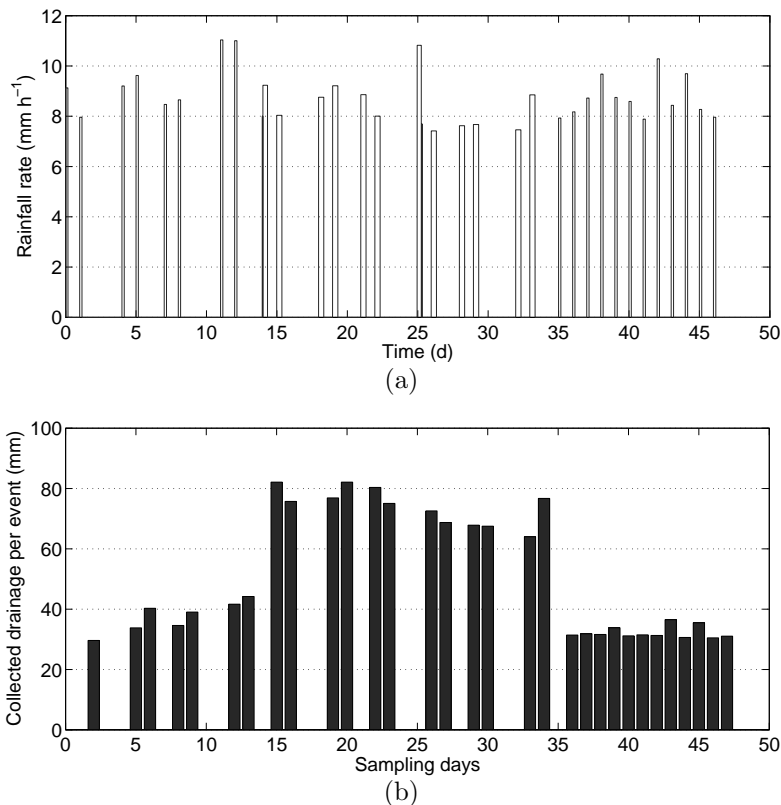
Figure 3.6: Observed rainfall rate in the laboratory per water application event (a) and collected total drainage per event (b). There were 32 water application events in total: 8 winter events (from day 0 to day 12), 12 summer events (from day 14 to day 33), and 12 winter events (from day 35 to day 46). The drainage was collected 23 hours after the start of each water application.

spatial pattern of drainage (Fig. 3.9) show a significant effect of the factor two difference between summer and winter water application other than a different pattern in the early stages of wetting (Fig. 3.9a). The fact that pressure head could not be maintained early on did not affect the drainage patterns.

Four cells dominate the spatial percolation pattern (Fig. 3.9). There is no indication of lateral flow above the sampler, which would have caused smoother peaks. Such lateral redistribution can occur if the applied suction is too small (with water piling up), or if the porous cover is insufficiently conductive.

We conclude that the nylon mesh cover needs to be fully saturated to function properly. Its high permeability makes maintaining even a low vacuum difficult when it dries out. It is most suitable under relatively wet conditions. Its high conductivity makes it suitable for detecting preferential flow paths.
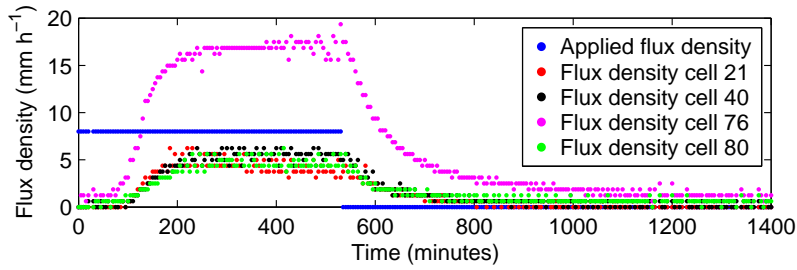
Figure 3.7: The measured drainage fluxes for four individual cells, during a summer water application event on day 22 (Fig. 3.6a).
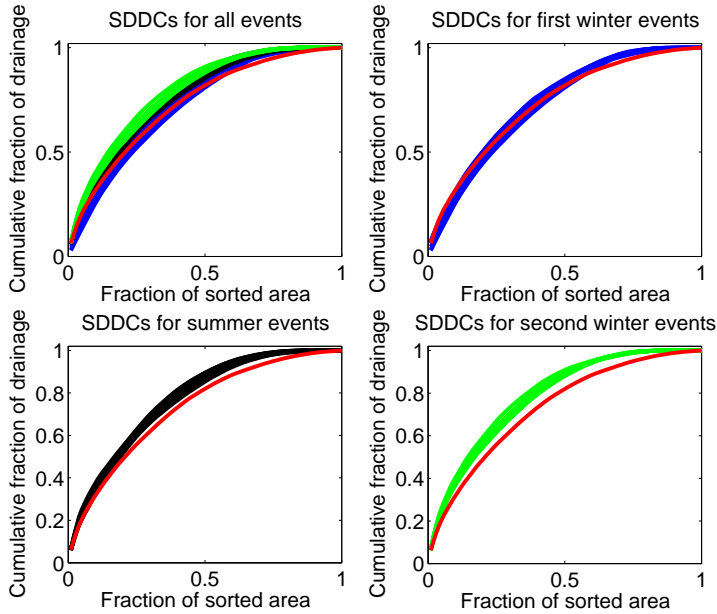
Figure 3.8: Spatial drainage distribution curves (SDDC) for each irrigation event (Fig. 3.6) for the nylon sampler. The individual compartments are ranked in descending order of captured drainage. The blue lines are the SDDCs for the first winter events, the black lines are the SDDCs for the summer events, the green lines are the SDDCs for the second winter events, and the red line is the overall SDDC.

(a) (b)

(c) (d)
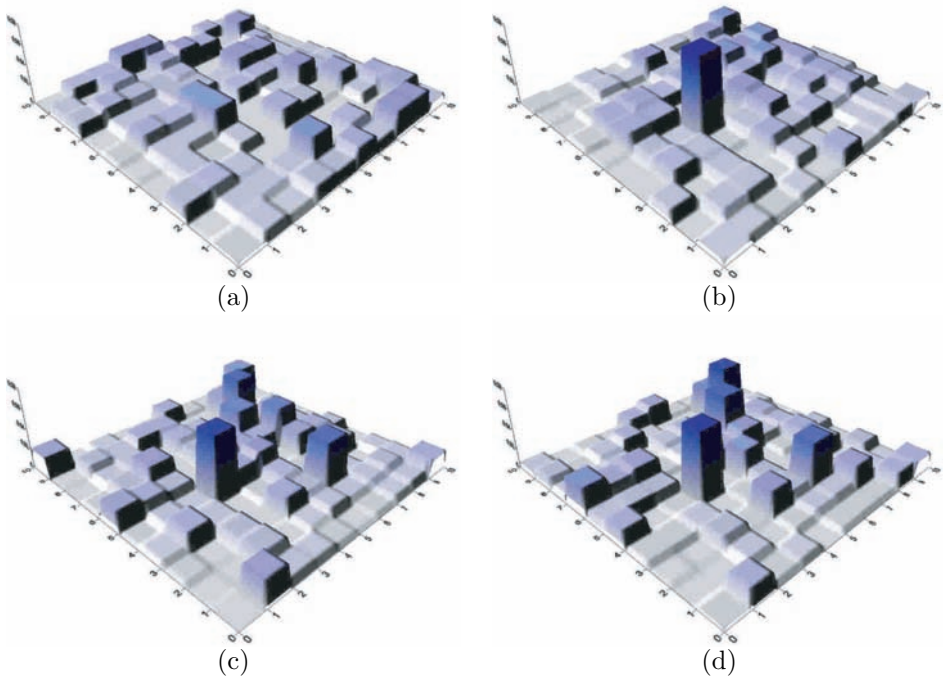
Figure 3.9: Drainage pattern for the nylon sampler after water application on day 2 (a), on day 7 (b), on day 22 (c), and on day 35 (d) (Fig. 3.6). For comparison the drainage patterns are scaled to add up to 1. The water applications on day 2, 7, and 35 are winter events, the water application on day 22 is a summer event. On the x-axis the columns and on the y-axis the rows of the sampler are indicated. The z-axes indicate the fraction of drainage (0 - 0.08).

3.3.2 Field experiment with the metal and membrane samplers

Both samplers easily achieved and maintained the desired (variable) vacuum levels (Fig. 3.10). Only during the final rainfall event which started on day 146 did the metal sampler not completely reach the required vacuum immediately. A dry period of 22 days (with only 7.3 mm of rain) before the final rainfall led to an ambient pressure head of -144 cm. The sample collection chamber could be maintained only at -32 cm. After the rainfall, the sintered metal plates wetted up slowly (36 hours to reach the target pressure head of -144 cm), and the ability to maintain the ambient pressure head inside the sampler collection chamber was restored. Probably, the metal plates and the soil had dried out, opening an air conduit through the soil between the sampler and the atmosphere. When the soil wetted up the sampler functioned properly, indicating that the air conduit had closed. Although the membrane reached the required vacuum immediately after this dry period, the membrane porous plate was deformed again, indicating that the plate was not fully saturated anymore.

Figure 3.11 shows the rainfall and the percolation for the membrane sampler and pressure head response at 0.25 m depth. The percolation response is remarkably peaked, and clear dry periods occur between drainage episodes. During percolation the pressure head was mostly above -70 cm. Both samplers recovered amounts of percolation between the amount of cumulative rainfall and cumulative net infiltration when the actual evapotranspiration was assumed to be equal to the potential evapotranspiration at all times (Fig. 3.12).

The spatial distribution of drainage for both samplers (Fig. 3.13) varies considerably within the monitoring area. Clusters of compartments with high or low drainage are small compared to the sampling area, and directional trends are not visually apparent. For recording variability within this scale, the samplers appear adequate. Heterogeneities with larger length may manifest themselves if samplers are installed further apart. The percolation of the bottom right row of cells of the membrane sampler appears to have been affected by the trench. Possibly, the backfilling was not entirely adequate. The metal sampler shows no boundary effects, except for slightly enhanced drainage in the upper left row of cells.

Although the metal and membrane sampler showed a different percolation pattern (Fig. 3.13), the SDDCs for both samplers are nearly identical (Fig. 3.14). The identical SDDCs suggest that the MCS size was adequate for capturing the effect of plot scale soil heterogeneity on percolation in this soil.
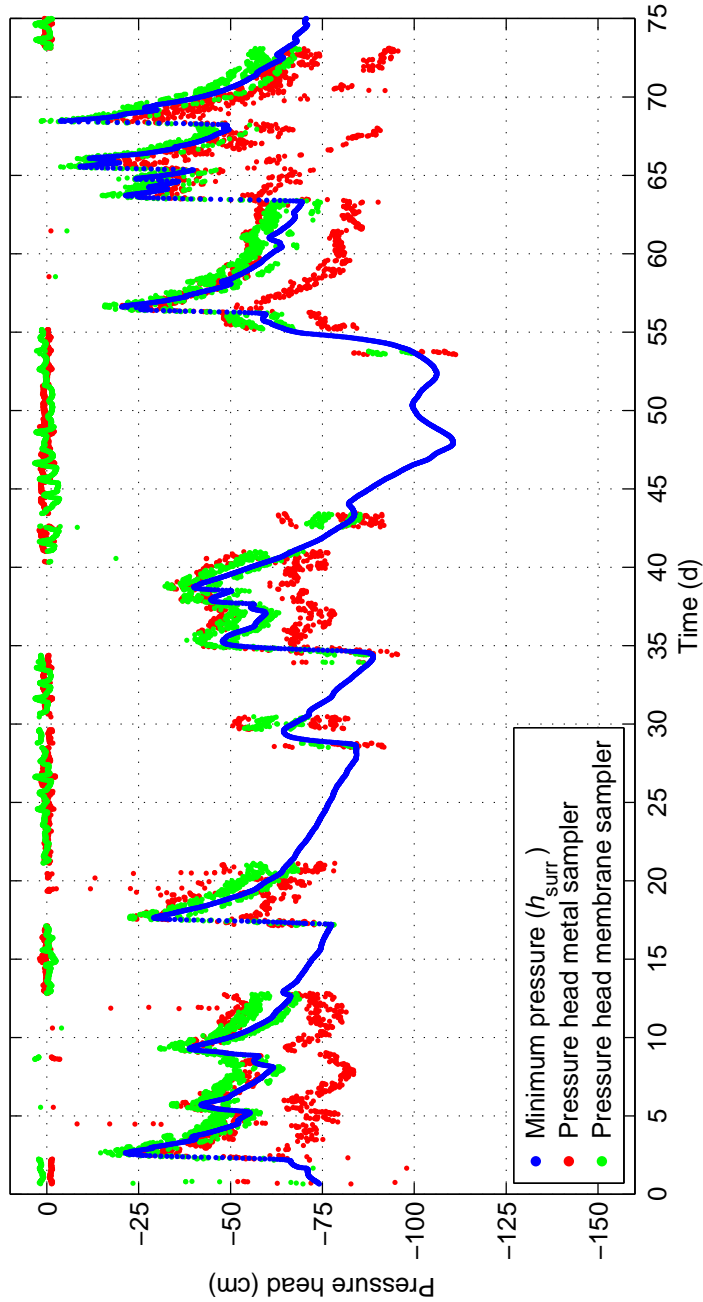
Figure 3.10: Observed pressure head $(h_{sampler}(t))$ for the metal sampler and membrane sampler and the matric pressure head in the surrounding soil $(h_{surr}(t))$ at the sampler depth (continued on p. 43).
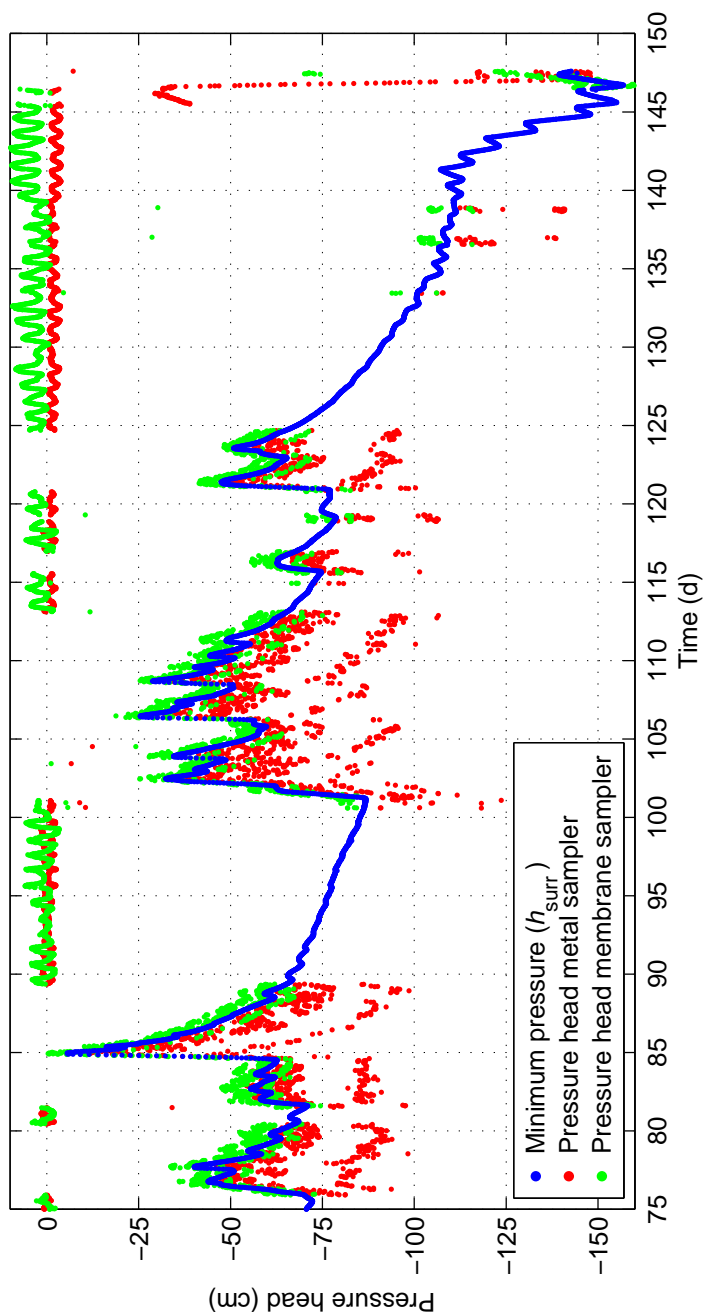
Figure 3.10: Continued from p. 42.
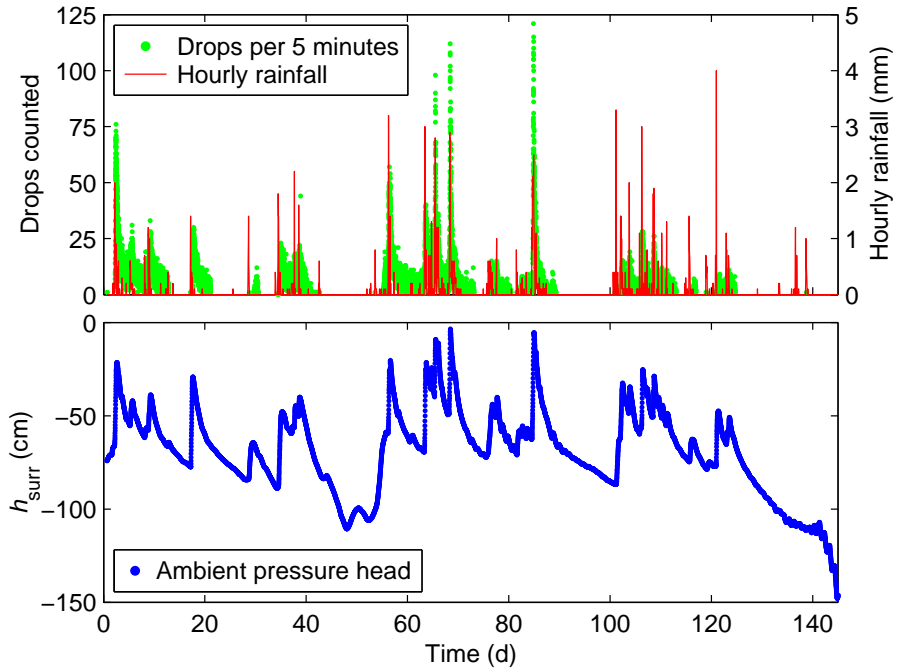
Figure 3.11: Observed accumulated rainfall for 1-hour intervals (right axis) at the field site, pressure head at 0.25 m depth (negative left axis), and number of drops counted in the membrane sampler in 5-minute intervals (positive left axis). Time is zero on 14-12-2007, 0:00.
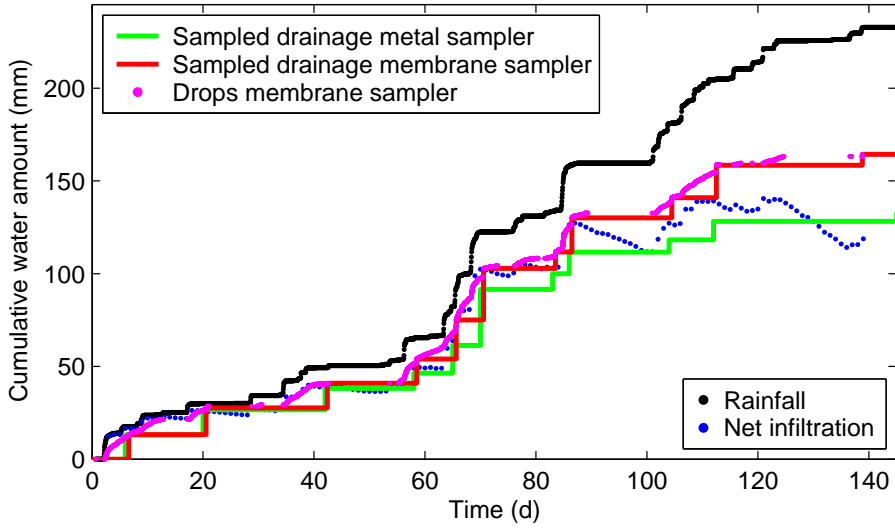
Figure 3.12: Cumulative rainfall and captured percolate during the experimental period for both samplers. For the membrane sampler, percolation between sampling times was derived from 5-minute interval drop counts. Potential evapotranspiration is accounted for to provide the envelope for net infiltration.
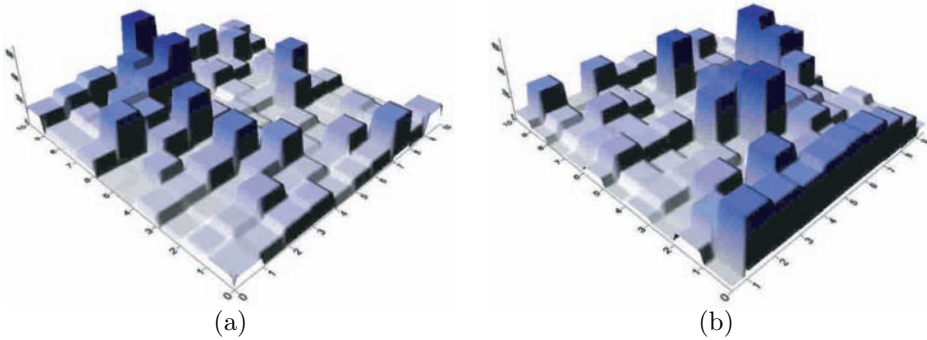
Figure 3.13: Total drainage captured per cell for the metal (a) and membrane (b) sampler. The side facing the trench is at the bottom right. On the x-axis the columns and on the y-axis the rows of the sampler are indicated. The z-axes indicate the total drainage (0 - 700 mm).
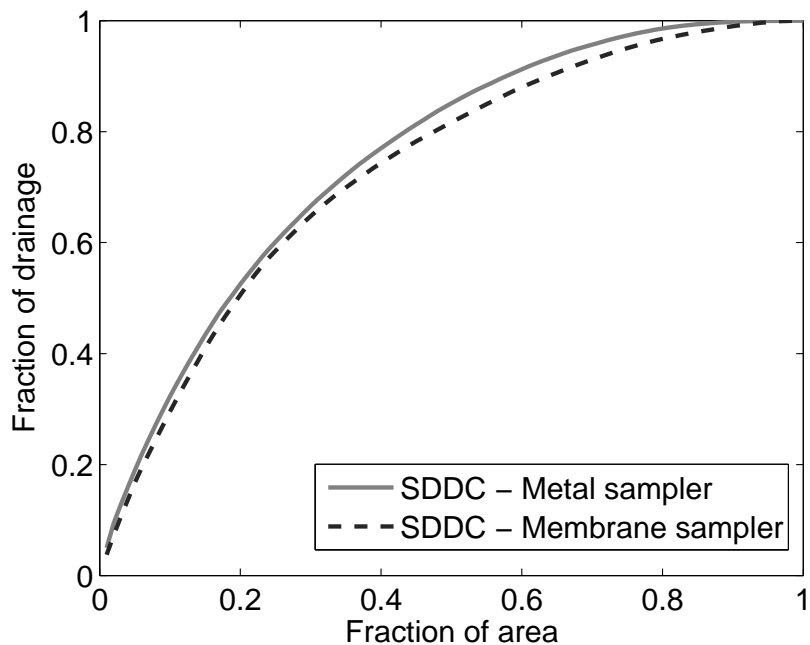
Figure 3.14: Cumulative spatial drainage distribution curves (SDDCs) for both samplers for the entire field experiment. To facilitate comparison, the curves were scaled to make the total captured drainage equal to one.

3.4 Conclusions

Various prototypes of the variable-suction MCS functioned well. Both in the laboratory and the field the MCS was a valuable instrument to measure the spatial and temporal leaching of the drainage. The suction control capability depended strongly on the type of porous cover. Once the porous covers were saturated, suction control could be readily achieved, even under transient field conditions.

During flow the suction control ideally should take into account the pressure drop over the porous cover. This was only an issue for the metal sampler though; the two other samplers had such thin porous covers that the pressure drop over them was negligible.

The newly developed drop counters gave valuable detailed information about the response time and drainage flux per cell. We could observe the differences per cell, and per event. Several of the data interpretations discussed above could not have been made without this detailed information.

Of the three porous covers we tested, we do not recommend to use the nylon cloth in field studies, because of its high air-entry value. The vacuum pump would be pumping most of the time (if not constantly), creating artificial air flows, and rapidly draining batteries.

The metal sampler worked fine in the field. The membrane sampler had some disadvantages. Caution should be taken during long dry periods. The sintered metal may dry (not necessarily detrimental to the experiment), but the nylon support plate of the membrane sampler can deform. Another problem of the membrane sampler is the large outer rim, which can probably be reduced in follow-up designs. In the field both metal and membrane samplers gave good results, which makes those instruments also suitable for reactive transport.

CHAPTER 4

Spatial and temporal distribution of a pulse and block
tracer from an irrigated monolith of a loamy vineyard
soil

4.1 Introduction

Fresh water scarcity is an increasing problem world-wide, with 40 % of the
world's population currently experiencing severe water shortages (*Pimentel
et al.*, 1999; *Bennett*, 2000). Agriculture is the largest single freshwater user.
About 75 % of the freshwater consumption is used for irrigation (*Bennett*,
2000). Sustainable agricultural water use is therefore critical to alleviate water
scarcity. *Qadir et al.* (2003) identified various strategies to that end, among
which irrigating with drainage water. Alternatively, treated sewage-water can
also be used for irrigation. Both involve using low-quality water for irrigation,
thus allowing high-quality waters to be used for domestic supply (*Hespanhol*,
1997).

Effluent from sewage water treatment plants generally contains suspended
and dissolved inorganic and organic substances. The inorganic compounds
usually include nutrients, chloride, sodium, and heavy metals. The organic
substances may include pesticides, pharmaceuticals, and pathogens such as
bacteria, viruses, protozoa, but also may include biologically active molecules
such as hormones (e.g. *Tarchitzky et al.*, 1999; *Hamilton et al.*, 2007). Many
of these may be harmful to the environment of human health (*Hamilton et al.*,

---

This chapter is a slightly modified version of the manuscript: Bloem, E., K. M.
Hermon, G. H. de Rooij, and F. Stagnitti, Spatial and temporal distribution of a
pulse and block tracer from an irrigated monolith of a loamy vineyard soil.

2007). As *Candela et al.* (2007) pointed out water quality criteria related to agricultural re-use of wastewater mainly focus on the presence of pathogens (*WHO*, 1989), total dissolved solids, and salinity aspects (*Ayers and Westcot*, 1994; *Martínez-Beltrán*, 1999).

The effects of wastewater irrigation on soil properties have also received attention. Wastewater irrigation affects soil hydraulic conductivity as well as porosity. *Vinten et al.* (1983), *Vandevivere and Baveye* (1992), and *Tarchitzky et al.* (1999) observed reductions of the soil hydraulic conductivity. *Coppola et al.* (2004) reported a reduced porosity and a shift towards smaller pores in the pore size distribution, accompanied by a corresponding reduction in water storage capacity, hydraulic conductivity, and dispersivity in an increasingly disturbed layer immediately below the soil surface. They showed that the chemical and microbiological composition of the wastewater does not provide sufficient information to evaluate its suitability for irrigation.

In addition to the soil properties, wastewater can also adversely impact the soil water in the vadose zone and in deeper groundwater. For example, irrigation excess is often required to leach salts from the root zone, resulting in groundwater quality deterioration (*Stevens*, 2006). *Candela et al.* (2007) found increased electrical conductivity (EC) and chloride concentration in the underlying aquifer when a golf course was irrigated with treated sewage water.

Acceptance by farmers of irrigation with wastewater is hampered by concerns over long-term effects on soil quality (e.g. *Keremane and McKay*, 2007). Nevertheless, in response to a serious shortage of water during the summer some Australian vineyards have started to irrigate with treated sewage water (*Maher et al.*, 2005). This offers the opportunity to investigate the effects on soil physical properties and the risks of polluting the deeper subsoil and the groundwater. As part of a large project targeting the groundwater contamination risks associated with wastewater irrigation in Australian vineyards (*Maher et al.*, 2005), we developed a novel laboratory experiment that applied a water regime representing a combination of rain water and wastewater inputs to an undistributed soil monolith collected from a vineyard in Australia. We used a unique 100-cell Multi-Compartment Sampler (MCS) (Chapter 3) and separated the leaching of rainfall and wastewater irrigation water by using different inert tracers.

Since soil water and solute heterogeneity is expected to be important in the Australian vineyard study (*Maher et al.*, 2005), we placed the undisturbed soil monolith on the 100-cell MCS. Such samplers produce detailed information about the spatial and temporal variations of water and solute movement in a soil (Chapter 3). Multi-compartment samplers have been used successfully in the laboratory to study macropore flow by *Wildenschild et al.* (1994) and *Quisenberry et al.* (1994), and to study heterogeneous flow and solute transport by *Poletika and Jury* (1994); *Buchter et al.* (1995); *Stagnitti et al.* (1998); *de Rooij and Stagnitti* (2000); and *Strock et al.* (2001). These tracer studies used pulse applications of conservative tracers. In our study however the wastewater applications in the vineyards are not a pulse but last over a long period and can therefore be regarded as a block applications.

The main objective in this study is to quantitatively characterize the leaching risk in the vineyard soil under an irrigation regime that augments rainfall with applications of treated sewage water during the summer while relying on rainfall only in winter. Besides the summer wastewater applications that contained chloride we also applied a bromide tracer pulse. We compared the chloride leaching from the wastewater (block) applications to the bromide (pulse) leaching.

4.2   Materials and methods

4.2.1   Field site, climate, and irrigation

The experiments were carried out on a vineyard soil in Great Western, between Stawell and Ararat in Victoria, South-East Australia (*Maher et al.*, 2005). The soils for the experiment were excavated from pasture adjacent to vine plantings. The vineyard soils were surveyed in 1982, with soils near to the collection site described as sandy loams, sandy clay loams, and clay loams with mottled yellow upper subsoils. A strong texture contrast exists between the hard setting surface soil horizon and the moderate to strongly pedal clayey subsoil (*Badawy*, 1982). The profile nearest to the core collection site was described as a yellow duplex (texture contrast) soil, of a clay loam texture, with topsoil extending to 60 cm (Table 4.1).

Chemical analysis performed on soils from the study site indicate that topsoils were acidic (pH(CaCl$_2$) ranging from 4.6 to 5.3), non-saline (EC 1:5 water) from 0.02 to 0.2 mS cm^{-1}), and sodic or marginally sodic (ESP ranging from 4.2 to 8.2 in 50 cm). Note that a soil is classified as sodic according to Australian definitions if the ESP is greater than 6 (*Isbell et al.*, 1997). The upper B horizon is sodic (ESP averaging 6.6) and has an average pH(CaCl$_2$) of 5.7. According to the Australian Soil Classification (*Isbell et al.*, 1997), this soil would be classified as a Sodosol.

A reconnaissance soil survey conducted in 1996 identified the soils as being suitable for vineyard development with some limitations requiring management. Limitations identified were: low pH and associated nutrient deficiency problems; reduced infiltration of the surface layer; localized ponding and run-off; and subsurface water accumulation and lateral flows (*IMT*, 1996).

We used the average annual rainfall and temperature data from the weather stations at Ararat (data record 1969-2004) and Stawell (1969-1998), as Great Western lies between these two locations. Average annual temperature is 19.7 °C in Stawell and 18.8 °C in Ararat. At the vineyard field site, the winter rainfall (May - October) is 373 mm on average, and the summer rainfall (November - April) averages 216 mm.

In the summer, the vineyard is irrigated with 637 mm on average by drip irrigation, with drippers spaced at 0.6 m intervals along the vine row. The distances between vine rows are 3 m. One dripper supplies an area with diameter 0.6 m (0.28 m^2). The flow rate of one dripper is 2.3 l h^{-1}, which is equivalent

Table 4.1: Clay loam profile nearest the column collection site, as adapted from data collected by *Badawy* (1982).

Property	Soil
Depth (cm)	40-60
Color	dark brown,
	dark red brown
Texture	Clay Loam
Inclusions	Quartz, ferruginous, and shale,
	most common just
	above subsoil
Occurrence	Gullies and shallow depressions
Bulk density (g cm^{-3})	
total soil material	1.44
Total porosity (%)	46.9
Void ration	0.89
Particle size distribution (%)	
Stone (> 2 mm)	15
Sand (fine / coarse)	39
Silt	27
Clay	17

to 8.13 mm h^{-1} over the wetted area.

4.2.2   Collection and preparation of soil column

We excavated an undisturbed soil monolith ($43 \times 43 \times 29$ cm, L $\times$ W $\times$ H) from the vineyard soil site. The monolith was excavated by carving out its shape, fitting a plywood frame around it and carefully digging underneath it from a surrounding trench. The monolith was placed upside down and its base leveled with spatulas in the laboratory. One stone was removed and its cavity refilled with soil material. We wetted the monolith base to ensure good contact with the MCS and then placed the sampler (with nylon mesh (Chapter 3)) on top, firmly connected the sampler to the frame containing the monolith and placed the set-up upright (Fig. 3.4).

4.2.3   Multi-compartment sampler

Drainage was captured by a variable-suction MCS of the type discussed in Chapter 3. The sampler consisted of a top plate with supports for 10×10 porous plates (31×31 mm) and separate funnels below these plates (Figs. 3.1 and 3.2). The top plate was mounted on a pressurized chamber with individual

sample collection cells. A vacuum tube and sampling tubes ran from the sampler to the datalogger, pressure control equipment, and sampling equipment. The MCS we developed can specify any desired pressure inside the chamber and percolation samples could be repeatedly collected without having to disconnect the sampler. We used a nylon cloth cover described in Chapter 3. The cloth was made of a polyamide fiber, woven with a mesh size of 7 μm, and had an air entry value of $\approx$ -70 cm for two layers of mesh.

To support the mesh, perforated PVC plates were placed on the funnel rims designed to support porous plates. Two layers of nylon mesh were placed on top of the aluminum top plate and glued (one after the other) to the narrow walls between the funnels. The glue prevented lateral flow through the mesh. The area of the nylon mesh including the separating glue was 1015 cm^2. Including half the area of the outer rim of the sampler gave a sampling area of 1035 cm^2.

To prevent bioclogging, the nylon mesh had been soaked in 2 mg l^{-1} CuSO$_4$ biocide (*Flemming and Trevors*, 1989; *Khan and Jury*, 1990; *Epstein and Bassein*, 2001; *Binnie et al.*, 2002) and allowed to dry before it was glued in place. The rainfall simulator of the type described by de *de Rooij* (1996) and *de Rooij and Stagnitti* (2000) was regularly flushed with 2 mg l^{-1} CuSO$_4$ during preparations to prevent fungi, bacteria, and algae growth. During and after the experiment no biological activity was observed in the rainfall simulator or the mesh . To avoid interference with naturally occurring soil biological activity, copper sulfate was not applied in irrigation water directly to the soil column (*Coleman and Crossley*, 1996; *Nannipieri and Badalucco*, 2003).

4.2.4 Experimental laboratory setup

We simulated winter and summer rain and summer wastewater irrigations by representing each month by two water applications within 3.5 days (2 $\times$ approximately 31 mm for winter and 2 $\times$ approximately 71 mm for summer) to deliver the amount of water corresponding to winter or summer months. The tracer experiment involved 12 summer applications (6 months), followed by 12 winter applications (6 months). To mimic the patchy irrigation pattern produced by the drip irrigations installed on-site and to reduce boundary effects we applied water to the inner 35 $\times$ 35 cm of the monolith's surface only, with a flux rate according to Fig. 4.1. This was also the closest approximation of the MCS area that was feasible with the 5 cm spacing of the rainfall simulator's drip emitters. In the laboratory we measured on average 3.1 mm per day of evaporation from an open water surface. The mean daily evaporation measured at the nearby Stawell weather station is 4 mm.

We maintained a constant pressure head of -50 cm to the bottom of the soil and kept the ambient temperature at 20 °C. The suction inside of the MCS was recorded every 15 minutes. Effluent droplets per cell were counted and recorded in 5-minute intervals. After each water application the collected percolate was weighed. To prevent individual sample collection cells from overflowing we also took samples during water applications as often as required.
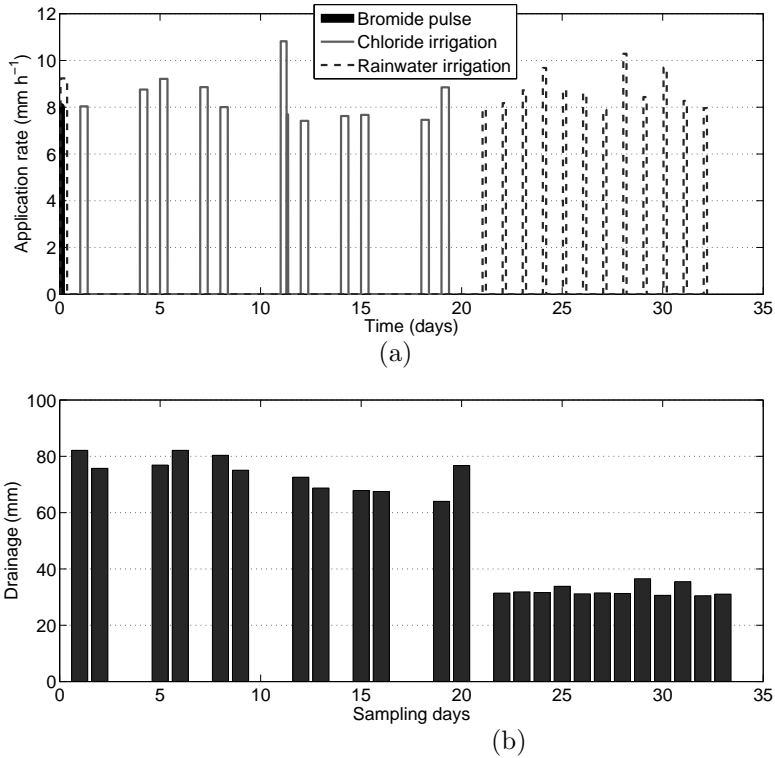
Figure 4.1: Irrigation scheme of the tracer experiment (a) and the resulting drainage over the entire sampler after each water application (b). Water applications between day 0 and day 20 reflect summer applications, applications from day 21 onwards represent winter rainfall. During the first 8 mm of the first summer water application a bromide pulse was applied (application time of 1 hour). During the summer water applications from day 1 to day 20 the water contained chloride. Time was set zero at the start of the first summer application.

4.2.5 Bromide and chloride tracer experiments

Samples of the wastewater irrigation were collected on five occasion between October 2003 and April 2004. Samples were collected from operating drip irrigation systems within the vineyard during an irrigation event. Sample collection and analysis protocols, including collection, sample container type, preservation requirements, and maximum holding periods, followed EPA recommendations (*EPA*, 2000). In short, samples were collected into clean 1 l HDPE containers and stored on ice until transfer to the laboratory, where analysis were then completed with specified time periods. Physical and chemical analysis of irrigation waters was conducted by the Water Quality Laboratory at Deakin University, Warrnambool (NATA Accredited Laboratory No. 2457)

54

using standard methods (*APHA*, 1999) or NATA accredited laboratory methods. We reproduced the wastewater composition according to Table 4.2 for our laboratory experiments. To approximate a pulse application we spiked the first 8 mm of the first summer application of the reproduced sewage water with 3.699 g l^{-1} NaBr, (2.87 g l^{-1} Br^{-}). We also applied all other solutes in this batch of water, and therefore used 8.7 times concentrated sewage water, without the NaCl to correct for the added bromide. The remainder of the first irrigation application was completed with deionised water with 0.68 g l^{-1} CaSO$_4$.

Because the sewage water contained significant amounts of chloride (Table 4.2) we considered the combined applications of reproduced sewage water a block application of chloride. To increase solubility HCl was added. The concentrations of bromide and chloride in the water applications are presented in Table 4.3.

Table 4.2: Composition of the wastewater used as irrigation water during summer in the vineyard in Great Western. This irrigation water is an addition to the rain water.

Compound	Concentration (g l^{-1})
NaCl	0.569
NaHCO$_3$	0.169
CaCO$_3$	0.068
KNO$_3$	0.0061
KH$_2$PO$_4$	0.0314
MgSO$_4$	0.087

Table 4.3: Concentrations of two anions in the water applications for the soil monolith. The bromide was applied in a single pulse.

Anion	Pulse (day 0)	Wastewater (day 1 to day 20)	Rainwater (day 21 onwards)
		Concentration (g l^{-1})	
Bromide	2.87	0	0
Chloride (before day 2)	0	0.26	0
Chloride (after day 2)	0	0.32	0
		Summer applications	Winter applications

4.2.6   Sample analysis

We collected the leachate from the individual sample collection cells 23 hours after the start of each water application. For the cells with large drainage volumes we also collected additional water as necessary during the water application. The volume was determined by weighing. After that the individual samples were transferred to 100 flasks, each corresponding to a collection cell of the sampler. If the accumulated volume in any flask exceeded 50 ml, the composition of its content was determined by ion chromatography (US EPA Method 300.0 (*USEPA*, 1993)). The solution was then discarded and the flask rinsed and dried for further sample storage.

4.2.7   Data analysis

We constructed Spatial Drainage Distribution Curves (SDDC) in analogy with the Spatial Solute Distribution Curve (SSDC) (*Stagnitti et al.*, 1999; *de Rooij and Stagnitti*, 2000) for both tracer experiments. The cells were sorted in descending order of total drainage per cell. We also described the spatial distribution of cumulative leaching by the SSDC.

Furthermore, we determined the breakthrough curve (BTC) from each sample collection cell. From these we constructed the leaching surfaces for both the bromide and chloride tracer experiment by sorting them in descending order of total amount of solute leached and then plotting them adjacent to each other (*de Rooij and Stagnitti*, 2002a,b, 2004). Leaching surfaces facilitates the analysis of the combined variation in space and time of the plotted quantity. In addition, we constructed leaching surfaces based on flux concentrations instead of solute amounts. We also determined the relationship between amount of drainage and amount of solute per sample collection cell. Finally we determined the BTC for the sampler as a whole for both bromide and chloride experiments. The signatures of the pulsed bromide and the continuously applied chloride in the BTCs, SDDCs, SSDCs, and leaching surfaces were compared and contrasted.

4.3   Results and discussion

4.3.1   Drainage measurements

To verify the suitability of the rainfall regime, we analyzed the drainage response to the water applications of day 2 through 8. The drop counter data indicated that percolation typically started 1.6 hours after the start of the water application, increased for 2.3 hours to its steady value, and then started dropping 0.2 hours after the water application ended, with prolonged tailing. By the start of the next application, percolation was negligible (12 drops per 5 minutes over the entire sampler). We therefore concluded that the timing of the water applications was adequate.
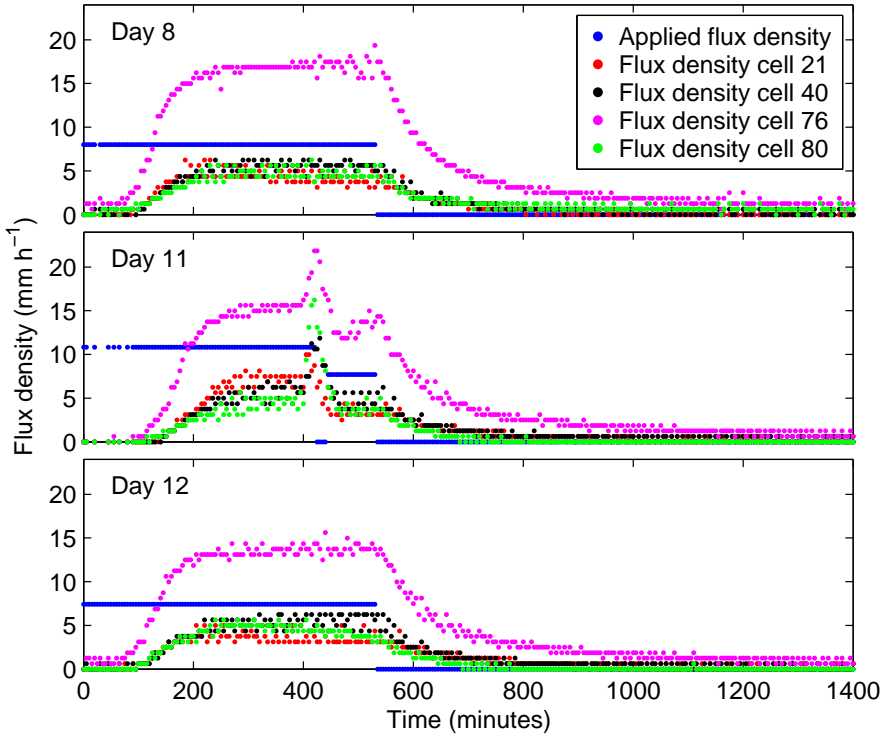
Figure 4.2: Water application and the response of four collection cells during days 8, 11, and 12. Time is zero at the start of the water application of interest. During day 11 the rainfall simulator broke down resulting in an excessive water application of an unknown duration. The water application rate in the figure was calculated from the total amount applied and the total duration from the start of the water application until we shut down the rainfall simulator. Therefore the application rate for day 11 does not correctly reflect the application rate with time.

Four of the cells with approximately almost uniform drop sizes allowed a more detailed study of the behavior of the percolation (Fig. 4.2). We focused on three summer water applications (days 8, 11, and 12) (Fig. 4.1). For the monitored water applications the flux density between the cells varied considerably but consistently (Table 4.4). During the water application on day 11, equipment failure caused an excessive water application of an unknown duration. The response of the collection cells was consistent with their behavior during the regular applications of approximately 8 mm h^{-1}. While cell 76 clearly reflected preferential flow, it responded only marginally faster to the onset of the water application. Its tailing was more prolonged than that of the other cells, possibly reflecting more extensive lateral flow towards the prefer-

ential flow path and slower emptying of a larger volume of a wetter pore space in the flow tube feeding into the cell.

During the entire experiment the spatial percolation pattern was stable (Fig. 4.3). The increased flux application during day 11 did not influence the percolation pattern. Also the difference in duration between summer and winter events did not change the overall pattern of the percolation.

The spatial pattern of total percolation, with 4 out of 100 cells clearly peaking, but without structure or boundary effect is shown in Figure 4.4. The cumulative SDDC corresponding to the percolation pattern is smooth (Fig. 4.5), indicating a gradual transition of the degree of convergence / divergence of flow paths, and suggesting that macropore flow was of little importance for the imposed water application rates. Nevertheless, the degree of flow heterogeneity was considerable: 25 % of the percolation occurred through 6 % of the sampling area (Table 4.5), with the most productive cell (1 % of the sampling area) collected 7 % of the percolation. In total 94 % of the applied water was recovered.

Table 4.4: Key features of the percolation fluxes of four selected multi-compartment sampler compartments during three summer water application events (day 8, 11, and 12). For comparison also the average total percolation per event for the entire sampling area are given (under applied). The steady flux density refers to the observed drainage rate after the initial increase caused by the arrival of the wetting front at the bottom of the monolith. TP = Total percolation, SFD = Steady flux density.

Day		Applied	Cell 21	Cell 40	Cell 76	Cell 80
8	TP (mm)	75.1	33.7	42.4	156.8	40.6
	SFD (mm h^{-1})	8.0	4.3	5.4	16.8	4.7
11	TP (mm)	72.6	37.7	40.7	139.1	36.6
	SFD (mm h^{-1})	10.8	6.9	5.4	15.2	4.4
	SFD (mm h^{-1})	10.8	10.0	11.9	21.9	16.2
	SFD (mm h^{-1})	7.7	3.3	4.6	13.5	3.7
12	TP (mm)	68.7	31.3	41.2	128.6	29.2
	SFD (mm h^{-1})	7.4	3.7	5.3	13.5	4.7

Table 4.5: The distribution of the total captured percolate, bromide, and chloride over the porous percolate interception area of the multi-compartment sampler. The fractions of the porous area that intercepted the indicated fractions of the percolate or solute are calculated by considering the cells in descending order of amount of the indicated substance captured.

Fraction of captured fluid or ion	Fraction of the porous interception area capturing the indicated fluid or ion fraction		
	Drainage	Bromide	Chloride
0.25	0.06	0.07	0.06
0.50	0.19	0.19	0.19
0.75	0.39	0.39	0.39
1.00	0.96	0.94	0.96

Day 0

Day 8

Day 11
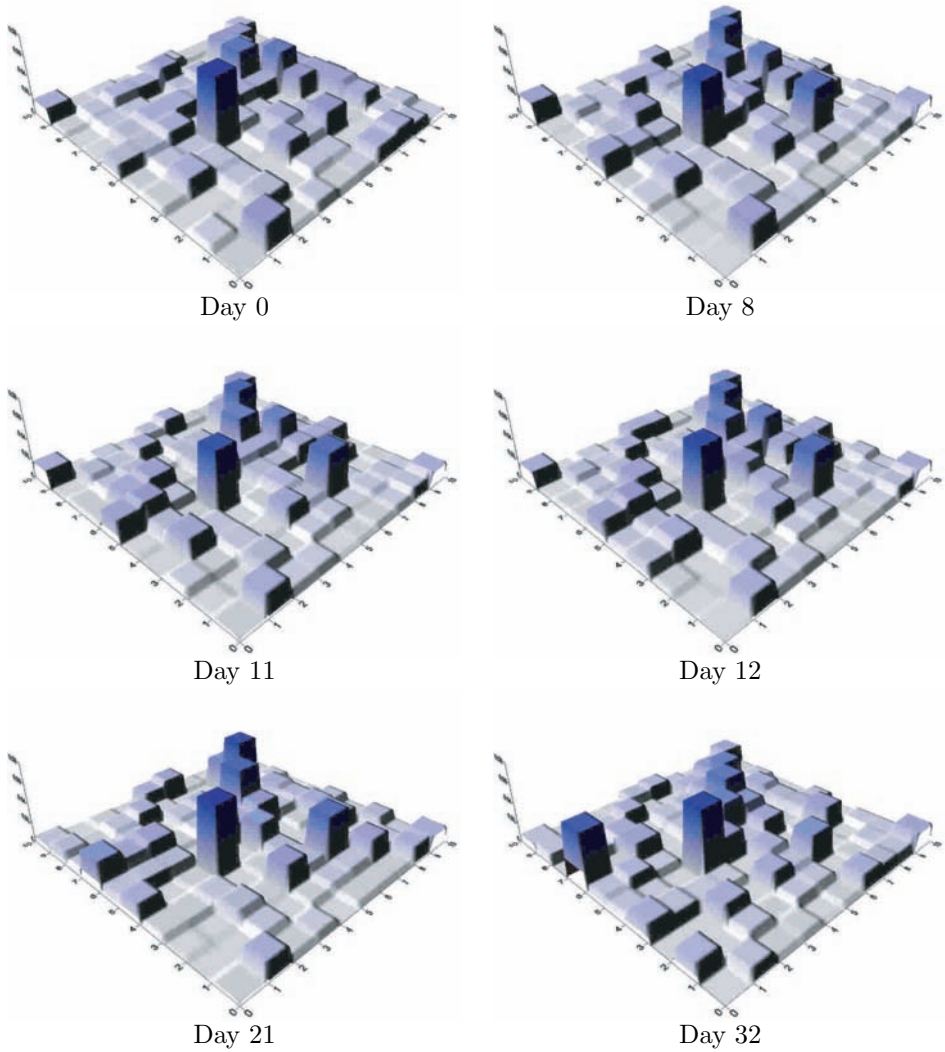
Day 12

Day 21

Day 32

Figure 4.3: Drainage pattern after the first water application at day 0, and after the water applications at day 8, day 11, day 12, day 21, and the final water application at day 32. For comparison the drainage patterns are scaled to 1. The water applications at day 0, 8, 11, and 12 are summer events, the water applications at day 21 and 32 are winter events. During day 11 the rainfall simulator failed, resulting in a high rainfall rate. On the x-axis the columns and on the y-axis the rows of the sampler are indicated. The z-axis indicate the fraction of drainage (0 - 0.08).

Bromide (pulse)　　　　　　　Chloride (block)

Total drainage (mm)

Maximum concentration (mg l^{-1})

Total mass (mg)
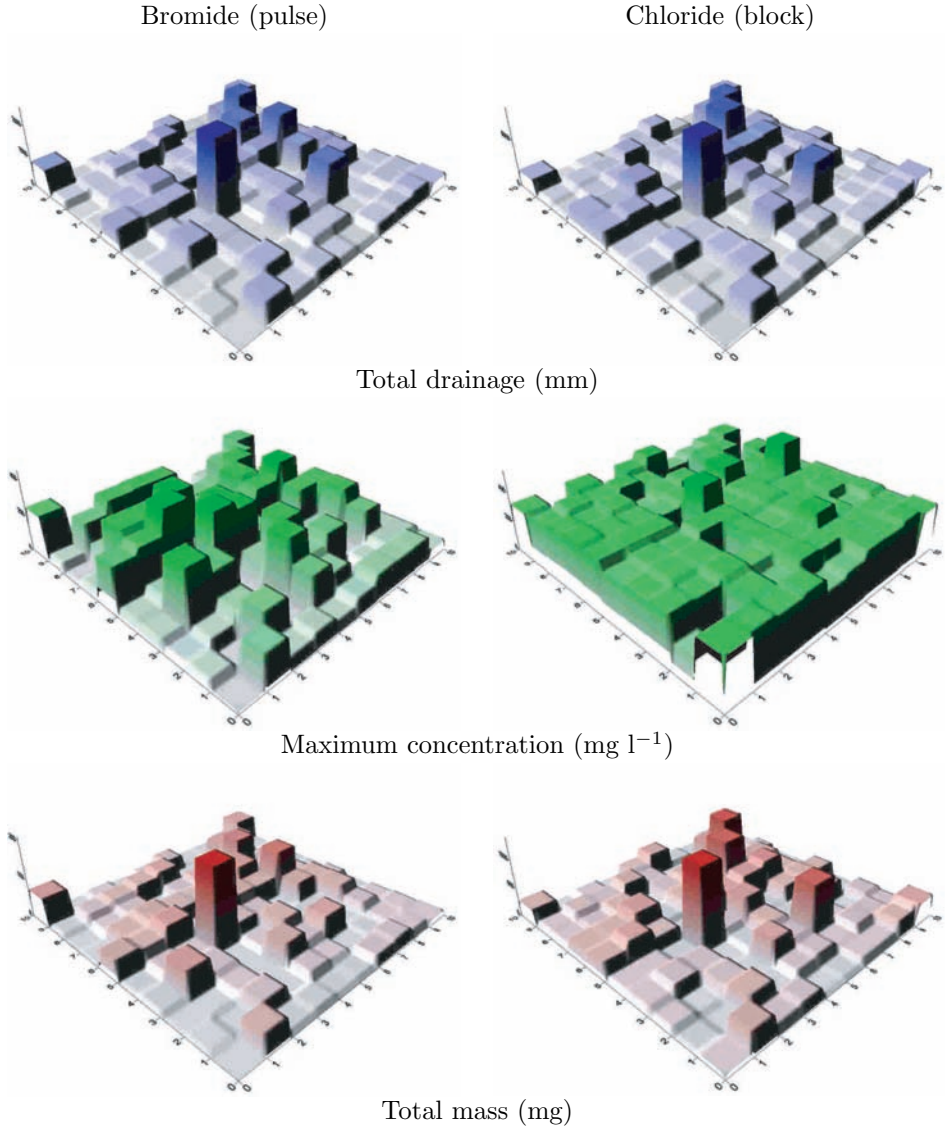
Figure 4.4: Total drainage, maximum measured concentration, and total captured chloride per cell for the bromide (left) and chloride (right) tracer. On the x-axis the columns and on the y-axis the rows of the sampler are indicated. The z-axis indicate the total drainage for the bromide (0 - 2600 mm) and for the chloride (0 - 8500 mm) experiment, the maximum bromide concentration (0-450 mg l^{-1}) and the maximum chloride concentration (0 - 540 mg l^{-1}), and the total bromide mass (0 - 210 mg) and chloride mass (0 - 1400 mg).
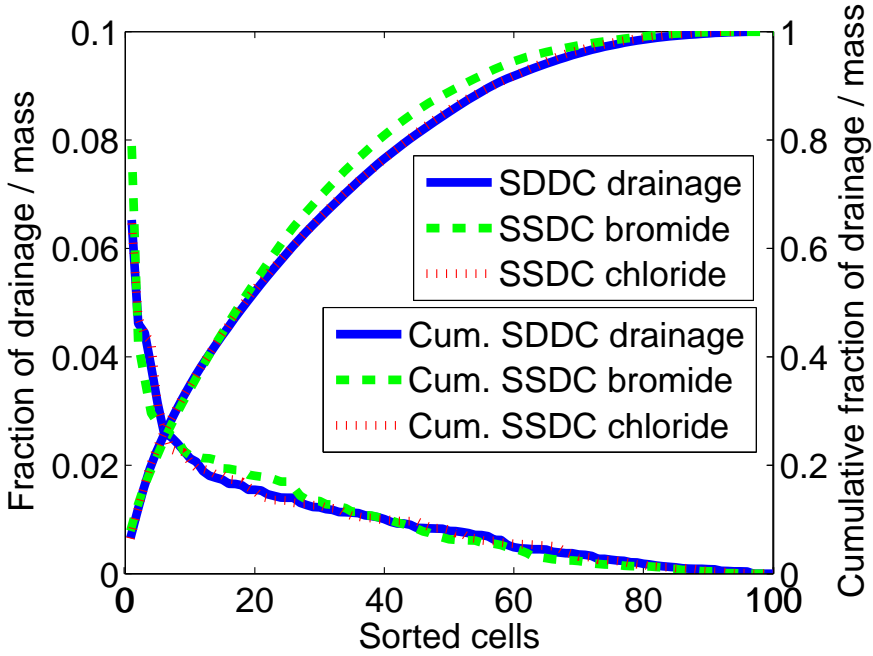
Figure 4.5: Cumulative Spatial Solute and Drainage Distribution Curves (SSDC and SDDC) for both tracers for the entire experiment. The individual compartments are ranked in descending order of captured solutes. To facilitate comparison, the curves were scaled to make the total captured solutes and drainage equal to one.

4.3.2 Bromide and chloride tracers

As evidenced by the spatial variation (CV = 0.78) of the maximum concentration, the bromide pulse travelled through the soil with relatively little transfer of bromide between highly mobile and less mobile water (Fig. 4.4). Strongly contrasting peak concentrations occurred frequently in adjacent cells. Note that the chloride mass peak somewhat to the right of the middle in Figure 4.4 is much less pronounced for bromide. The drainage flux in this cell increased as the experiment progressed and was smaller when the bromide was applied.

The prolonged chloride application allowed a near-complete exchange between pore waters of different mobility, leading to a spatially much more uniform distribution of the peak concentration than the distribution of the bromide peak concentration (Fig. 4.4). As a consequence of the effective chloride exchange and the similar application periods of water and chloride, the spatial distribution of chloride more closely resembled that of the drainage than the bromide distribution did (Fig. 4.5).

The more detailed information in the leaching surfaces (Fig. 4.6) is con-

sistent with the spatial patterns. The combination of higher concentrations of bromide in cells with large amounts of drainage gave a very sharp bromide mass peak in the space-time domain. The leaching surface based on flux concentration rather than bromide amounts demonstrates that, while the concentrations are far from spatially uniform, they explain only part of the peaked nature of the spatio-temporal distribution. Note the importance of a high spatial resolution to detect the peaks in Fig. 4.6a.

For the chloride tracer, the results are similar. Note that the lateral redistribution was driven by relatively slow dispersion and diffusion, and that it became more effective as time progressed: the flux concentration was much more spatially variable in the first 200 mm of the drainage than later on. The effective lateral distribution of chloride and the match between chloride and water application resulted in a less noisy relationship between total captured drainage and chloride as compared to the drainage-bromide relationship (Fig. 4.6). Consistent with this, the SDDC and SSDC for chloride are nearly equal, while the SSDC for bromide differs (Fig. 4.5).

Figure 4.5 and Table 4.5 quantify the degree of flow heterogeneity within the monolith. Despite the differences in spatial patterns and leaching surfaces, the results for drainage and the tracers are remarkably similar and document significant convergence of the dominant stream tubes.

The overall bromide BTC is sharp with a pronounced tail (Fig. 4.7). The overall chloride BTC rised more slowly, reflecting the lower input concentration. Note that the bromide application preceded the chloride application. In relative terms, the elevation in tracer concentrations had risen to comparable levels (as fractions of the input concentration). This was observed after 60 mm of drainage since their first application. The chloride concentration drop after application ceased, is comparable to that of bromide, with some erratic tailing, possibly caused by chloride release from regions with immobile water.

After 160 mm of drainage the chloride concentration reached an equilibrium and approximately equal to the applied chloride concentration. From that time on, the amount of chloride in the soil water remained almost uniform. This result implies that the vines in the vineyard will be exposed to elevated levels of chloride and other non-sorbing solutes in the irrigation water during most of the growing season. The decrease of chloride concentration started immediately after the chloride application had stopped. At the end of the winter irrigation the relative chloride concentration was 0.03 of the applied concentration (for the high drainage compartments the chloride concentration was less than 0.01 of the applied concentration).

The chloride application mimics the chloride load in the vineyard. While the chloride concentration in the percolate is only 3% of the applied concentration at the end of the simulated winter rainfall, the recovery was only 68 % (compared to 93 % for the bromide), possibly because chloride could move out of the irrigated area through diffusion and slow lateral flow. Since the vineyard is drip-irrigated this suggest a potential mechanism for relatively rapid salinisation of the soil which might require adequate leaching with uniformly applied high-quality water. This would limit the desired conservation of fresh
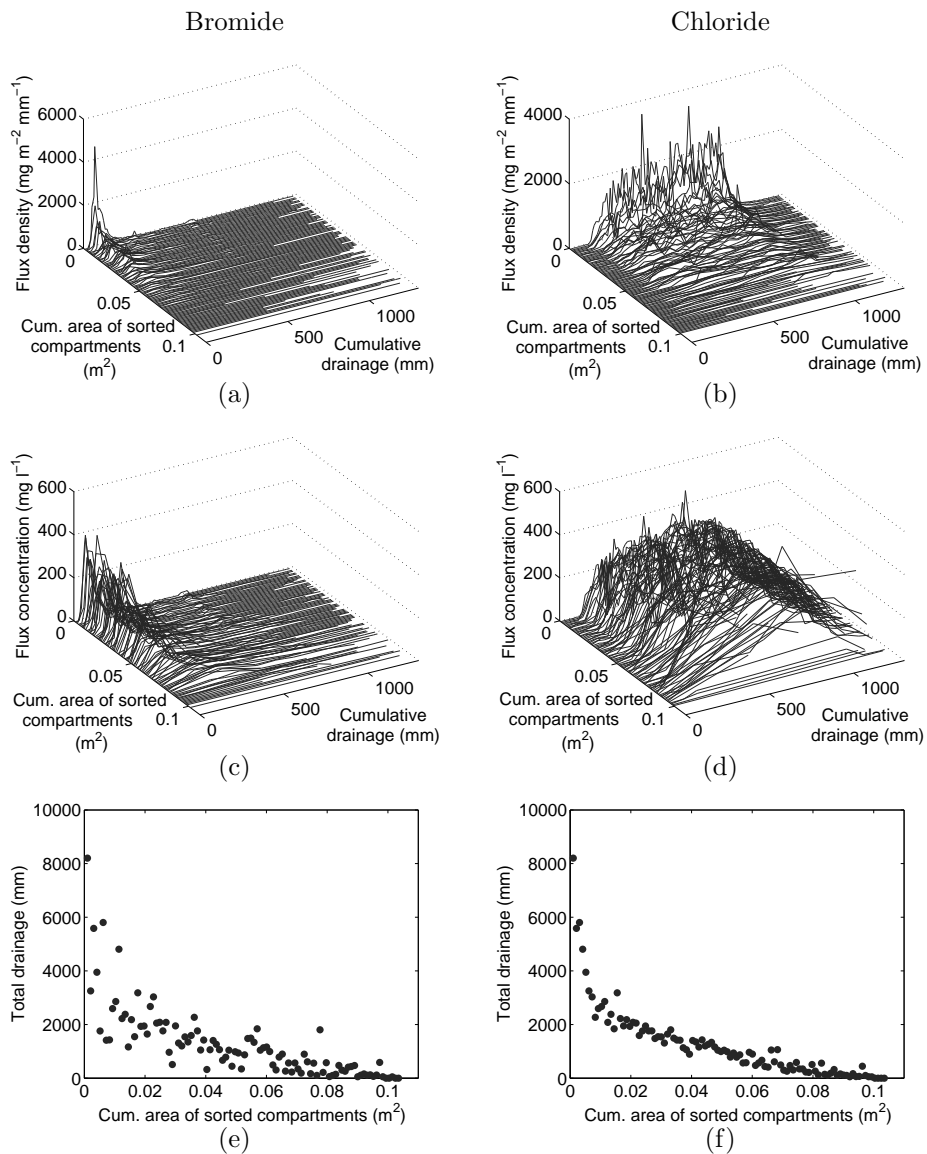
Bromide   Chloride

Figure 4.6: Leaching surfaces based on leached amount for the bromide
(a) and chloride (b) experiment, and leaching surfaces based on flux con-
centrations for the bromide (c) and chloride (d) experiment, and rela-
tionship between ranking based on total leached amount and amount of
captured percolate per cell for the bromide (e) and chloride (f) experiment.

64
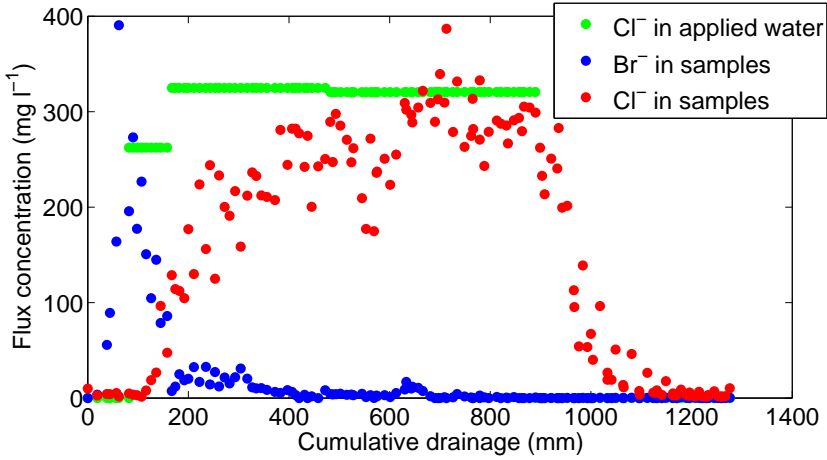
Figure 4.7: Breakthrough Curves (BTCs) of the entire sampling area based on flux concentrations for the bromide (Br^-) and chloride (Cl^-) tracers. The bromide was applied as a pulse with a concentration of 2870 mg l^{-1}.

water reserves and merits further study.

4.4 Conclusions

We quantitatively characterized the leaching risk of a chloride tracer under continuous application under an irrigation regime that augments rainfall with applications of wastewater during summer while relying on rainfall only in winter. The winter rains are just sufficient to reduce the outflow concentration to 3 % of the applied concentration. At that time, some chloride still remains in areas with less mobile water within the soil.

During the entire simulated year, leaching of solutes towards the groundwater have been measured. The results indicate a high risk for the fresh groundwater reserves.

The mass flux density pattern of bromide (applied as a pulse) is comparable to that of the chloride. Therefore a pulse application is adequate to assess conservative solute transport. The main difference between the pulse and block application is the duration, which makes it possible for the chloride to spread through the entire soil, including the less mobile domains. One should realize that during the growing season the EC level within the soil is high if wastewater is applied.

CHAPTER 5

A field experiment with variable-suction
multi-compartment samplers to measure the
spatio-temporal distribution of solute leaching in an
agricultural soil

5.1 Introduction

Water and solutes redistribute in space and time as they move through the
soil as a result of atmospheric forcing, root water uptake, and water transfer
between the vadose zone and the groundwater. In order to understand this
redistribution and gain quantitative understanding of its role in delivering wa-
ter and nutrients to plants, retarding and degrading potentially harmful com-
pounds, and recharging the groundwater, several experimental methodologies
have emerged.

Of these, dye tracing is the oldest. In order to properly and safely trace
the pathways of infiltrating water, dyes should be mobile, distinctly visible,
and non-toxic (*Flury and Wai*, 2003). Brilliant Blue has been frequently used
(e.g. *Flury et al.*, 1994), even though it is adsorbent (*Flury and Flühler*, 1994;
Kasteel et al., 2002). Due to its adsorbent character Brilliant Blue is not ideal
for tracing the travel times of water itself. For detecting flow patterns in soils,
Flury and Flühler (1995) recommended to use Brilliant Blue in combination

with a non-sorbing conservative tracer like chloride. The disadvantages of dye experiments are the fact that they allow only a single observation time on a given location, and that their concentrations as determined by image analysis are expressed per volume of soil, which makes separate soil water content data necessary (*Persson*, 2005).

Sampling percolating water and measuring the concentration of solutes gives flux concentration of solutes, which are more relevant for solute transport. Inert, non-adsorbing solutes such as chloride and bromide reflect the travel time of water quite accurately, even though anion exclusion may lead to underestimation in clayey soils. If both the spatial and temporal properties of the flow are of interest, samples need to be repeatedly collected at numerous locations. For this purpose, various types of multi-compartment samplers were developed to sample downward fluxes in soils. Multi-compartment samplers have been used in the laboratory to study macropore flow by *Wildenschild et al.* (1994) under free drainage and by *Quisenberry et al.* (1994) using a pressure head of -2.0 kPa at the outflow base. *Poletika and Jury* (1994), *Buchter et al.* (1995), *de Rooij and Stagnitti* (2000) and *Strock et al.* (2001) used multi-compartment samplers in the laboratory to study heterogeneous flow and transport at pressure heads of -5 kPa, -2.0 to -2.2 kPa, -3.5 kPa and -2.5 kPa, respectively. *Boll et al.* (1997) used multi-compartment samplers in which hanging wicks provided suction to the outflow surface. They buried their samplers in the field by tunneling below an undisturbed soil volume. *Weihermüller et al.* (2007) give details about other soil solution samplers and the intricacies of sampling under suction.

While laboratory experiments have the advantage of controlled conditions, *in situ* observations are required for a truthful representation of the behavior of water and solutes under natural conditions. One aspect is the transient nature of the matric potential field in the soil. While the multi-compartment sampler experiments listed above all applied (nearly) constant suctions to the soil water extraction area of the samplers, the matric potential in the field soil varies considerably.

To minimize flow disturbance caused by the applied suction of a buried multi-compartment sampler under transient field conditions, we recently developed a new instrument, capable of modifying the applied suction to correspond to the ambient pressure head, as measured by tensiometers installed at the same depth as the instrument (Chapter 3). The instrument consists of 100 cells, each 31.5 x 31.5 mm. Water fluxes are measured with drop counters over the individual cells with a high temporal resolution. The percolate is retained for each cell, and can be repeatedly extracted for analysis while leaving the instrument buried *in situ*. In order to make this instrument suitable for reactive solute transport we constructed two prototypes, in which the porous plates covering each cell consisted of sintered porous metal plates in one type, and an inert membrane in the other (Chapter 3).

With this novel technology available field experiments with multi-compartment samplers over prolonged periods of time become feasible. As an advantage over excavating soil monoliths or installing monolith lysimeters on

site, there are no artificial flow barriers in the soil above the sampler. Such barriers can constrict lateral flow (*de Rooij et al.*, 2006). Installing samplers *in situ* limit the disturbance of the naturally occurring variations in the pressure head field and flow patterns, that eventually affect the soil's leaching behavior.

Multi-compartment samplers provide large amounts of solute transport data. The quantitative analysis of these data in terms of spatial and temporal distribution of solutes is considerably facilitated by a set of analytical tools: breakthrough curves, spatial distribution curves, and leaching surfaces. The breakthrough curves (BTCs) give information about the temporal aspect of solute leaching. Breakthrough curves can be constructed for each cell of a multi-compartment sampler. The spatial aspect can be described by the spatial solute distribution curve (SSDC) (*Stagnitti et al.*, 1999; *de Rooij and Stagnitti*, 2002a, 2004). *de Rooij and Stagnitti* (2002a,b) proposed the leaching surface as a tool to efficiently organize, present and analyze these data, while preserving all individual observations. Leaching surfaces combine the BTCs and the SSDCs.

The objective of this paper is to quantify the spatial and temporal variation of solute leaching below the root zone in an agricultural field under natural rainfall in winter and spring. To do so, we installed two multi-compartment samplers with adaptive suction as described above. Following the recommendation of *Flury and Flühler* (1995), we first applied a chloride pulse, followed by a Brilliant Blue dye tracing experiment. The quantitative analysis of both water quality and quantity fully utilized the newly developed analytical tools discussed above.

5.2   Materials and Methods

5.2.1   Field site

The field site was situated in the southern part of the Netherlands. The sandy soil was classified as Typic Haplohumod (*Soil Survey Staff*, 1988). It developed in wind-deposited Pleistocene fine sand without visible textural layering (narrow grain size distribution M50 $\sim$ 120 μm). The soil has a historic use as arable land and was under grass for 4 years before installation of the field equipment. The management history resulted in a compacted topsoil and shows signs of repeated shallow plowing and treatment with a "deep tooth" for breaking the weakly developed Spodic horizon. The groundwater level is maintained between 1 and 1.5 m below the soil surface by a subsurface drainage/infiltration network with a drain tube distance of 6 m at a depth of 1.40 m connected to a weir-controlled ditch. Average rainfall is 712 mm yr^{-1}, and average potential evapotranspiration for a reference crop of short grass is 542.7 mm yr^{-1}. Daily rainfall was measured by two tipping-bucket rainfall gauges installed on site. Daily potential evapotranspiration data for a reference crop of short grass were obtained from two weather stations.

5.2.2 Instrumentation

During this experiment we used two variable-suction multi-compartment samplers of the type described in Chapter 3. Each sampler consisted of a top plate with supports for 10×10 porous plates (31×31 mm) and separate funnels below these plates (Figs. 3.1 and 3.2). The top plate was mounted on a pressurized chamber with individual sample collection cells. The pressure in this chamber could be regulated to apply a variable suction to the porous top cover in contact with the soil. Sampling tubes and a vacuum tube ran from the buried sampler to the soil surface to allow the establishment inside the chamber of any desired sub-atmospheric pressure above the air-entry value of the cover while percolation samples could be repeatedly collected without having to excavate the sampler. We used sintered porous stainless steel (metal sampler) and membrane (membrane sampler) covers described in Chapter 3. The sintered metal filters were manufactured by GKN Sinter Metals Filters GmbH (material: AISI 316L with GKN Quality SIKA R1 AX and size: 31.0 $\times$ 31.0 $\times$ 3 mm with 4$\times$R2.0). The membrane filter is a polyamide suction membrane (pore size 0.45 μ m and bubbling pressure of 1000 hPa) supplied by EcoTech Umweltsysteme GmbH (Bonn, Germany). Because the membrane was only available in a 300 mm width, the outer rows of the 10×10 cells of the sampler were only partially covered with the porous membrane. This required the other half of these cells to be sealed as the membrane and its support was glued and clamped on top of the original grid.

The metal filter plates were glued into their slots in the top plate of the sampler, directly above the individual sample collection cells. Solid vertical rims between the plates prevented lateral flow between the plates. The area of the plates including the separating rims was 1015 cm^2. Including half the area of the outer rim of the sampler gives a sampling area of 1035 cm^2.

The membrane required a separate nylon support to mount it on the top plate, which left 30×30 mm porous areas between the separating rims. The outer halves of the cells that could not be covered by the membrane were sealed. To prevent lateral flow in the membrane, the grid pattern of the sampling cells was imprinted by narrow lines of glue that locally closed the pores of the membrane. Here too, the MCS surface was smooth. The total porous surface plus the glue separation lines between the cells was 913 cm^2. Including half of the sealed area and the outer rim gives a sampling area of 1057 cm^2.

To install the samplers at the field site, we excavated a trench 1.30 m long and 1.0 m deep. At either side of this trench we dug a tunnel (ceiling at 0.31 m depth for the metal sampler and 0.25 m depth for the membrane sampler) in which we installed the two samplers. The instruments were pressed against the ceiling with a jack. After installation we lowered the instruments once (the tunnel ceilings did not collapse) to check the contact by visually inspecting at the imprint of the samplers in the ceilings. The distances between the trench wall and the samplers was 0.18 m in both cases, and the horizontal center-to-center distance between the instruments was 2.00 m.

To provide ambient matric pressure readings to help adjust the suction in

the sampler chambers we installed four tensiometers by carefully pre-drilling installation holes. The tensiometers were placed near the membrane sampler at depths of 0.24 m, 0.25 m, and 0.26 m. The fourth tensiometer was installed at 0.31 m depth, but failed to operate properly. One tensiometer was 0.12 m away from the membrane sampler and 2.00 m from the metal sampler. The other two were installed 0.08 m apart at 0.45 and 0.46 m distance from the membrane sampler. The distance towards the metal sampler of these tensiometers were 1.22 and 1.29 m.

To double check the contact between sampler and soil we applied 19 mm demineralized water at the soil surface over an area of 0.70×0.70 m above either sampler in no more than 5 minutes. All cells intercepted percolate, indicating good contact, and the amounts were such that boundary effects appeared negligible (no significantly higher or lower amounts of percolate in the outer compartments). We then backfilled the cavities around the samplers with local material and backfilled the trench.

The pressure in the sample collection chamber was adjusted according to the lowest of the three tensiometer readings every three seconds. Tensiometer readings and chamber pressure were logged every 15 minutes. The saturated hydraulic conductivity of the metal plates created a pressure head gradient over the plates. To compensate for this we off set the target pressure head inside the chamber by -5.8 cm compared to the ambient pressure head, which appeared to be adequate. The membrane was so thin that the pressure head drop was negligible. The pump overshot the target pressure however, and therefore we off set the target pressure by 6.0 cm compared to the ambient pressure had, which remedied the problem.

Two tipping-bucket rainfall gauges were installed in the field to measure the rainfall rates (during rainfall logged every minute) and amounts (cumulative rainfall logged every hour). After each rainfall event, i.e. usually a cluster of small rain showers (Table 5.1), water samples were collected from the individual cells while leaving the instrument buried in-situ. In the membrane sampler, drop counters in all 100 sampling cells recorded the number of droplets falling into the sample collection cells for 5-minute intervals. After sampling the percolate, we computed the average drop volume to arrive at flux-density values every 5 minutes.

5.2.3 Chloride experiment

At the 14th of December 2005 we cut the grass in the 0.70×0.70 m area above each sampler to 3 cm and applied 4.5 mm of a 1 M $CaCl_2$*$2H_2O$ solution. This concentration was low enough to prevent density-driven flow in the unsaturated zone (*Simmons et al.*, 2002), but could also produce a breakthrough curve (BTC) well above the background electrical conductivity (EC) of the percolate of maximum 426 μS cm^{-1} (target: peaks of BTCs ten times above background readings and with an assumed dilution factor of 0.05 for the peak concentration).

To eliminate side effects on the instrument of both converging and diverging

Table 5.1: Percolate sampling dates and rainfall and evapotranspiration characteristics for each sample collection period. Day = Day of sampling, Rain = rainfall measured over sampling interval, RI = Rainfall Intensity, ET_{pot} = Evapotranspiration, I = Infiltration.

Date	Day nr	Rain (mm)	Nr. rain	RI_{min} (mm h^{-1})	RI_{max} (mm h^{-1})	ET_{pot} (mm)	I (mm)
20-12-05	6	17.6	13	0.1	2.0	1.3	16.4
03-01-06	20	12.4	16	0.1	1.4	3.0	9.4
25-01-06	42	20.1	19	0.1	2.2	6.7	13.5
10-02-06	58	15.4	15	0.1	3.2	5.2	10.2
17-02-06	65	26.7	13	0.1	3.0	2.6	24.1
22-02-06	70	30.4	17	0.1	2.9	1.6	28.9
07-03-06	83	11.6	16	0.1	1.0	10.6	1.0
11-03-06	86	24.4	8	0.1	2.5	1.0	23.5
28-03-06	104	22.5	22	0.1	3.3	22.1	0.4
05-04-06	112	23.8	22	0.1	3.0	11.7	12.1
08-05-06	145	27.9	27	0.1	4.0	48.7	-20.8

streamlines of the chloride concentration applied the tracer solution on 0.70 × 0.70 m plots. We covered each application area by a 21 × 21 cell PVC grid, with a syringe holder in the center of each cell. We filled 441 medical 10 ml syringes with 5 ml tracer solution (CV = 0.7 %), and placed these in the syringe holders. To achieve a spatially uniform tracer pulse application we then emptied all syringes within two minutes. The soil surface directly above the sampling areas of the two samplers received 33.0 g Cl$^-$ (metal sampler) and 33.7 g Cl$^-$ (membrane sampler).

After each rainfall event (Table 5.1) the collected leachate was extracted from the sampling cells of both samplers. The collected volumes were determined and the solute concentration was derived from the EC as measured with an EC meter (Cond 315i and TetraCon325 from WTW; individually calibrated).

After 145 days, virtually all tracer had passed the sampling depth. The mass collected during the final sampling round was less than 0.01 % for the metal sampler and 0.06 % for the membrane sampler of the applied mass over the sampling area.

5.2.4 Brilliant Blue experiment

After the chloride had leached, we manually applied 44.1 mm of a 5 g l^{-1} Brilliant Blue solution on 0.70 × 0.70 m area above the metal sampler in four doses (Table 5.2). Before each application, ten cups of 6 cm diameter were placed in the application area to calculate the coefficient of variation of the applied volume. The captured volumes in the cups were measured immediately

after application and the cups were then emptied at the areas they covered.

A dry period before the dye application led to an ambient pressure head of -144 cm H_2O. The porous plates of the metal sampler had dried out, and as a consequence the pressure head inside the sample collection chamber could be maintained at only -28 cm. After the dye application, the sintered metal plates wetted up slowly (36 hours to reach a pressure head of -142 cm), and the ability to maintain the ambient pressure head inside the sampler collection chamber was restored. We sampled leachate from the metal sampler and estimated the dye concentration by visual comparison with an array of 16 calibration samples with dye concentrations ranging from 5.00×10^{-5} g l^{-1} through 5.00 g l^{-1}.

On the third and fourth day after the first application, the application area was excavated in vertical profiles spaced 0.05 m apart outside the sampler area and at 0.02 m spacing within the sampler area. The exposed profiles were photographed.

5.2.5   Data analysis

For each sampler we constructed spatial drainage distribution curves per sampling round (SDDC) in analogy with the spatial solute distribution curve (SSDC), with the cells sorted in descending order of total drainage per cell. We also determined the BTC of the sampler as a whole and the cumulative BTC.

Furthermore, we determined the BTC from each sample collection cell of each sampler. From these we constructed the leaching surfaces of both samplers by sorting them in descending order of total amount of solute leached and then plotting them adjacent to one other (*de Rooij and Stagnitti*, 2002a,b, 2004). Leaching surfaces leave the original data in tact but represent them in a way that facilitates the analysis of the combined variation in space and time of the plotted quantity. In addition, we constructed leaching surfaces based on flux concentrations instead of solute amounts. We also determined per sample collection cell the relationship between amount of solute and amount of drainage. We also determined spatial solute distribution curve (SSDC) (*Stagnitti et al.*, 1999; *de Rooij and Stagnitti*, 2000) to describe the spatial distribution of cumulative leaching.

Table 5.2: Details of the application of a Brilliant Blue solution to the soil surface above the buried metal multi-compartment sampler.

Date (dd-mm-yy)	Application time	Applied (mm)	CV (%)
08-05-06	12:02 - 12:09	9.1	8.7
09-05-06	11:01 - 11:03	11.4	15.5
09-05-06	12:19 - 12:21	12.9	9.9
09-05-06	14:43 - 14:46	10.7	10.0

5.3 Results and discussion

5.3.1 Water flux measurements

Figure 5.1 shows the rainfall, the percolation, and pressure head response at 0.25 m depth. The percolation response is remarkably peaked, and clear dry periods occur between drainage episodes. Figure 5.2 shows a very noisy relationship between the downward flux density and the pressure head at the sampling depth, but there appears to be a threshold pressure head: 99.4 % of all 17010 five-minute intervals during which the drop counters registered percolation occurred when the pressure head was higher than -70 cm. Rainfall rates and amounts were generally low, and the pressure head was well above -100 cm at the start of most showers (Fig. 5.1).

We selected ten rain showers that represented a broad range in amount, intensity, and duration of rainfall to investigate the various ways in which rainfall was transformed into percolation (Table 5.3 and Fig. 5.1). The wetter the soil, the shorter the time lag between the first rainfall and the first percolation. 14 hours or more for pressure heads below -80 cm; around 9 - 9.5 hours for pressure heads around -75 cm (and one outlier of -86.6 cm); and around 3 hours for pressure heads above -65 cm. The largest response time (shower: C) resulted from a modest shower (4.3 mm in 7 hours). Showers D and H (Table 5.3) had comparable amount of rain and initial pressure heads, but the higher average rainfall rate (not the maximum) of shower D apparently reduced the time lag for percolation from 14.5 to 9 hours. The showers that occurred when percolation was occurring (E, F, G, and I) increased percolation rates after 2.5 to 3.5 hours.

We collected the percolate from both samplers 11 times (Fig. 5.1 and Table 5.4). Since conditions were fairly wet throughout the experimental period, net infiltration can probably be estimated reasonably well from rainfall and potential evapotranspiration data. The cumulative results of Table 5.4, as well as the continuously measured cumulative drainage values derived from the drop counters have been summarized in Fig. 5.3. Evapotranspiration rose after day 60 (Feb 22). After day 86 (March 11), the absolute rainfall generated little percolation, reflecting the increased transpiration. Given the fairly uniform distribution of rainfall over the year and the rainfall deficit in summer this helps explain why the winter is very important for solute leaching and groundwater recharge.

Note that Figure 5.3 shows periods with negative net infiltration (caused by evapotranspiration) that correlate with marked drops in the ambient pressure head and zero or limited downward flux at the sampler depth (Fig. 5.1). We conclude that the net flux of water from the soil to the atmosphere dried out the root zone and consequently was not compensated by a comparable flux at the bottom of the root zone caused by capillary rise. Upward flow can only occur when the pressure heads are lower than their value at hydrostatic equilibrium. For the membrane sampler (25 cm depth), the ambient pressure head at hydrostatic equilibrium is between -75 and -125 cm for the groundwater

74

Table 5.3: Details of the rain showers that were used to analyze the response of the soil to infiltration. The final column does not contain any value if drainage from a previous shower did not cease before the rain shower of interest started to produce drainage. December 14th, 2005 is day 0. The showers are sorted by response time between first rainfall and first drainage at 0.25 m depth. R_{total} = Total rainfall, RI_{max} = maximum rainfall intensity, h_{surr} R = Pressure head at 0.25 m depth at the time rainfall started, Δ t = Time between first rainfall and first drainage at 0.25 m depth, h_{surr} D = Pressure head at 0.25 m depth at the time drainage started.

Label	Day	R_{total} (mm)	Duration (h)	RI_{max} (mm hr^{-1})	h_{surr} R (cm)	Δ t (h)	h_{surr} D (cm)
A	2	11.4	13	2	-63.1	3	-61.1
D	34	6.2	6	1.8	-86.6	9	-72.1
J	120	6.9	8	4	-74.9	9	-59.1
B	17	3.5	5	1.4	-75.1	9.5	-31.3
H	101	6.6	8	3.3	-84.7	14.5	-66.3
C	28	4.2	7	1.4	-82.2	28.5	-62.3
E	39	7.5	5	3.2	-57.5	2.5	
F	76	3	9	0.6	-60.1	3	
I	106	7.8	5	3	-55.2	3	
G	84/85	20.1	17	2.5	-60.9	3.5	

Table 5.4: Percolation sampling dates, and rainfall, potential evapotranspiration, and captured percolation (for both samplers) for each sample collection period.

Day	Rainfall (mm)	Potential evapotranspiration (mm)	Net infiltration (mm)	Drainage Metal (mm)	Drainage Membrane (mm)
6	17.60	1.25	16.35	13.14	13.27
20	12.40	3.00	9.40	13.46	14.37
42	20.10	6.65	13.45	11.57	13.33
58	15.40	5.20	10.20	8.22	13.07
65	26.70	2.60	24.10	14.96	21.04
70	30.40	1.55	28.85	30.22	27.72
83	11.60	10.60	1.00	8.44	8.93
86	24.40	0.95	23.45	11.61	18.36
104	22.50	22.10	0.40	6.59	10.79
112	23.80	11.70	12.10	10.05	17.59
145	27.90	48.70	-20.80	5.08	5.88
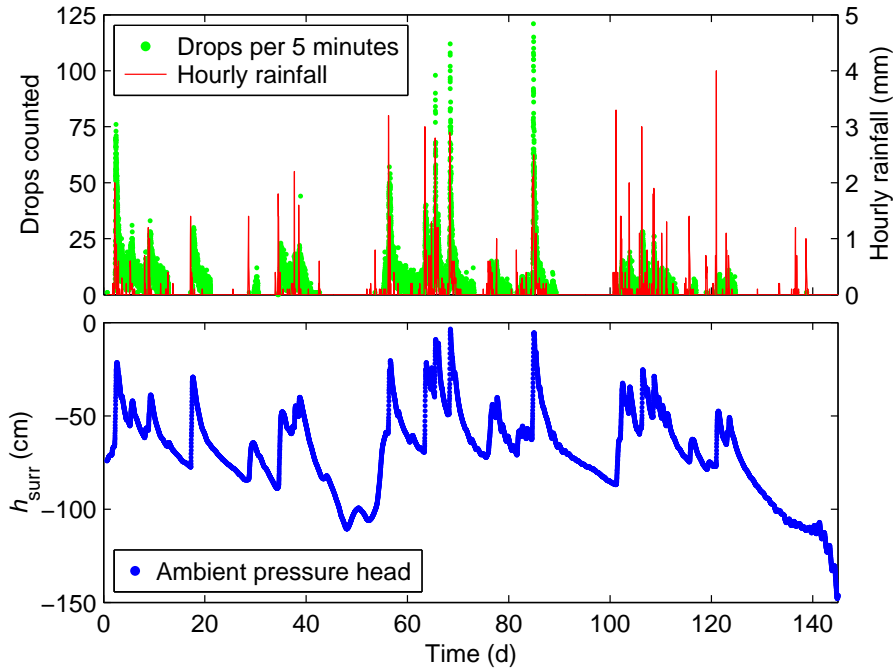
Figure 5.1: Observed accumulated rainfall for 1-hour intervals (right axis) at the field site, pressure head at 0.25 m depth (negative left axis), and number of drops counted in the membrane sampler in 5-minute intervals (positive left axis). Time is zero on 14-12-2007, 0:00. The chloride was applied on day 0.67.

levels on site. Ambient pressure heads < -75 cm only occur for about 50 days in total, often still close to that threshold. The ambient pressure head only drops below -125 cm at the very end of the experiment. Figure 5.2 supports the paucity of matric pressure heads that could generate significant upward flow. We therefore conclude that upward flow, and the disruption caused to this flow by the MCS, were of limited importance during the experiment.

Figures 5.4 and 5.5 show the spatial patterns of drainage and chloride leaching for both samplers. On day 70, some of the cells of the metal sampler overflowed. The excess water was diverted to an overflow collection flask buried alongside the sampler and was extracted from there. This explains the leveled-off appearance of the cells in the back. Throughout the experiment for both samplers the spatial variation of drainage is obvious, and also quite consistent.

Small-scale variations are abundant in the captures amounts of percolate. The captured volumes of adjacent cells can be very different. Nevertheless, the spatial patterns suggest that clusters of high- and low-yielding cells appear in areas of about 5 by 5 cells (16.25 × 16.25 cm). At day 70 large volumes of drainage were captured and several low-yield cells produced relatively large
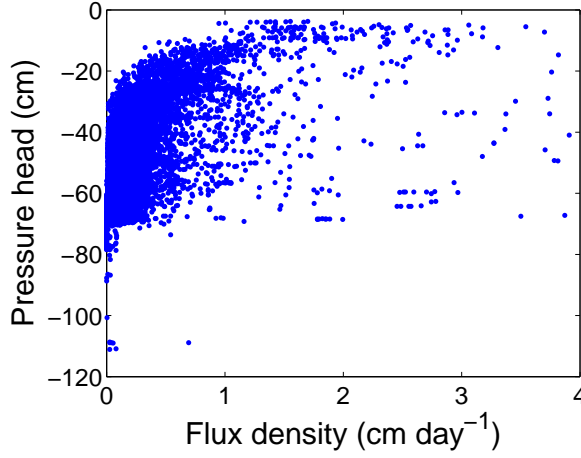
Figure 5.2: : Scatter plot of observed pressure heads at 0.25 m depth and flux densities derived from drop counts in 5-minute intervals for the membrane sampler as a whole (aggregated over all sampling cells).
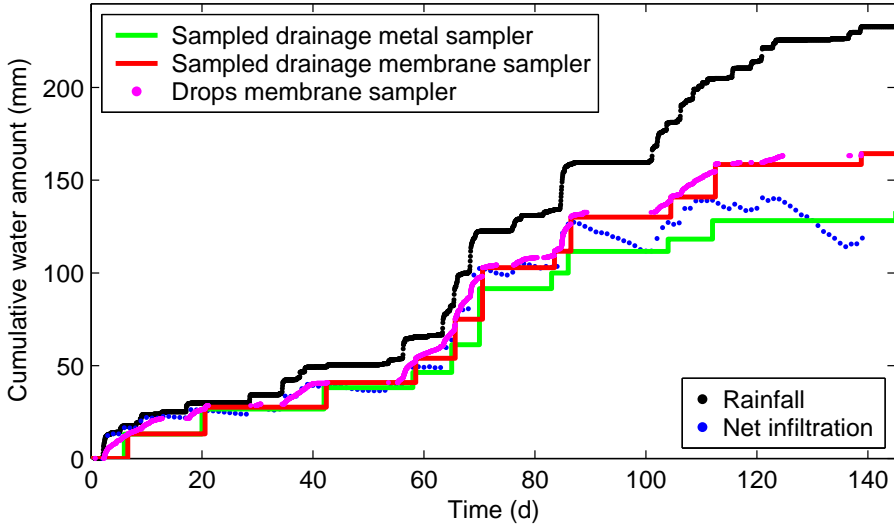
Figure 5.3: Cumulative rainfall and captured percolate during the experimental period for both samplers. For the membrane sampler, percolation between sampling times was derived from 5-minute interval drop counts. Potential evapotranspiration is accounted for to provide the envelope for net infiltration.

Day	Drainage (mm)	Concentration chloride (mg/l)	Mass chloride (mg)
Day 6			
Day 20			
Day 42			
Day 58			
Day 65			
Day 70			
Day 83			
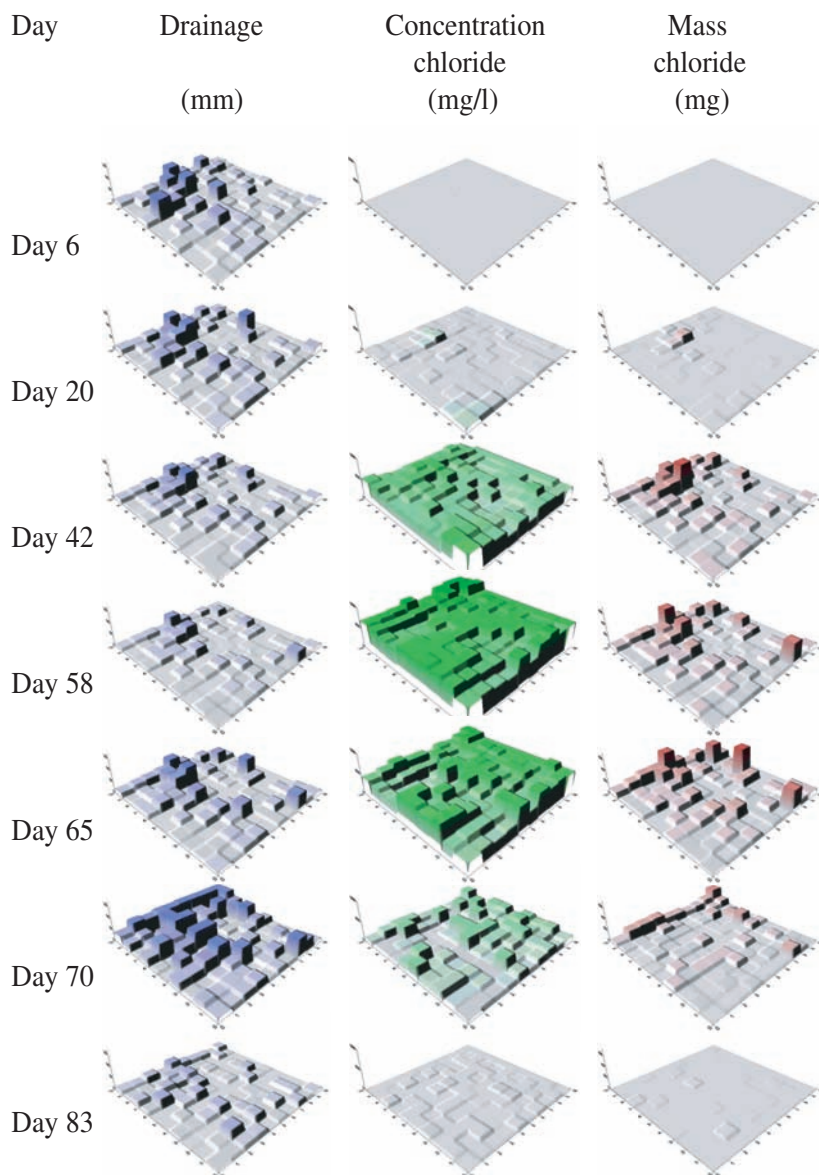
Figure 5.4: Drainage, chloride concentration and amount of chloride for the sampled percolate in the metal sampler of each sampling round (day 6 through day 83). The side of the sampler facing the trench is at the bottom right. On the x-axis the columns and on the y-axis the rows of the sampler are indicated. The z-axes indicate the drainage (0 - 170 mm), the chloride concentration (0 - 10000 mg l^{-1}, and the mass (0 - 700 mg).
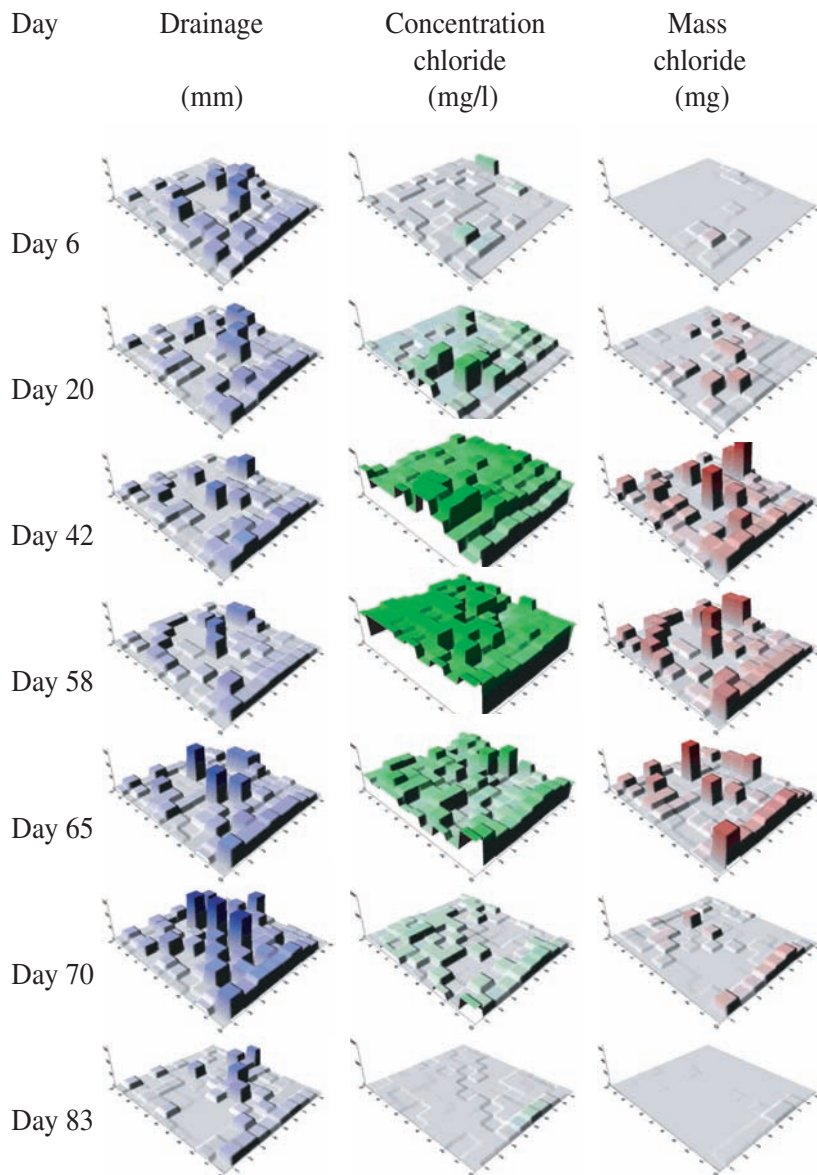
Figure 5.5: Drainage, chloride concentration and amount of chloride for the sampled percolate in the membrane sampler of each sampling round (day 6 through day 83). The side of the sampler facing the trench is at the bottom right. On the x-axis the columns and on the y-axis the rows of the sampler are indicated. The z-axes indicate the drainage (0 - 170 mm), the chloride concentration (0 - 10000 mg l^{-1}, and the mass (0 - 700 mg).
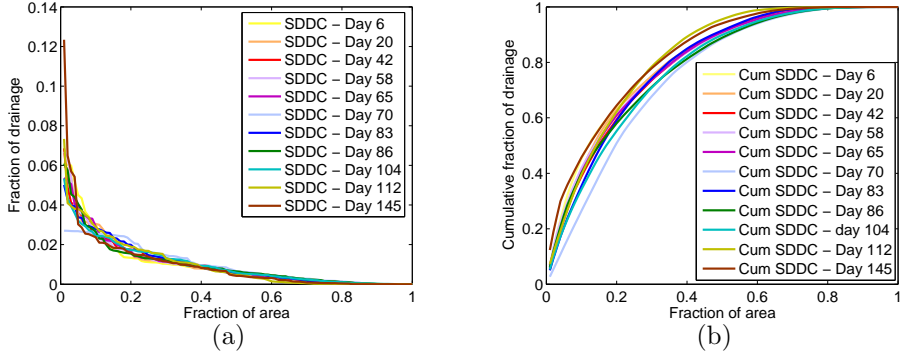
Figure 5.6: Scaled spatial drainage distribution curves (a) and their spatially accumulated equivalents (b) of the metal sampler for each sampling round. The individual compartments are ranked in descending order of captured percolate in a given sampling round (identified by the day number on which the percolate was extracted from the cells). The cumulative curves give the fraction of drainage captured by the cells to the left of the horizontal coordinate. To facilitate comparison, the curves were scaled to make the total captured drainage equal to one for each sampling round.
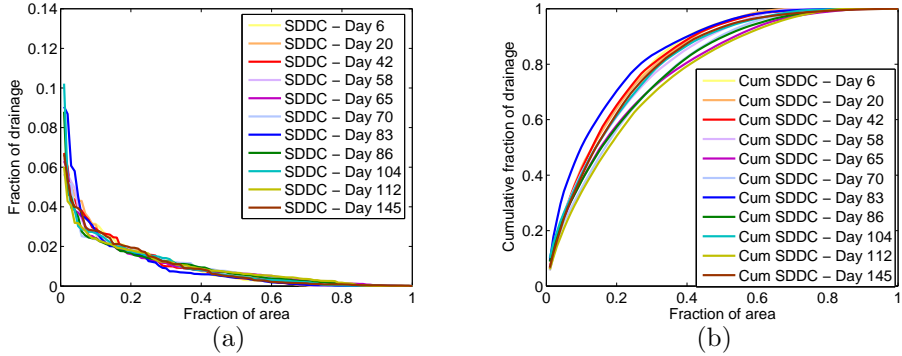
Figure 5.7: Spatial drainage distribution curves (a) and their spatially accumulated equivalents (b) of the membrane sampler for each sampling round. The individual compartments are ranked in descending order of captured percolate in a given sampling round (identified by the day number on which the percolate was extracted from the cells). The cumulative curves give the fraction of drainage captured by the cells to the left of the horizontal coordinate. To facilitate comparison, the curves were scaled to make the total captured drainage equal to one for each sampling round.

amounts of percolation. This indicates that flow routes adapted to handle the increased water supply during the rainy period starting around day 54 (Fig. 5.1).

When the spatial structure was removed by sorting the sampling cells in descending order of percolate captured for each sampling round, the scaled spatial drainage distribution curves (SDDC) (Figs. 5.6 and 5.7) show a smooth transition between cells with high and low percolation rates. The scaled curves for both samplers were very similar, indicating that the different porous materials that captured the percolate were functioning properly. The curve for day 70 is affected by the overflow. When the curves for the various sampling dates are analyzed individually, 25 % of the drainage passed through 6.1 % (metal sampler) or 5.4 % (membrane sampler) of the cross-sectional area on average. If all sampling dates are aggregated these values increase to 8 % and 9 %, respectively (Table 5.5), owing to the small temporal variation of the spatial drainage patterns. The most productive cells generated on average 6.3 (metal sampler) and 7.0 (membrane sampler) times the mean percolation amount per sampling period, indicating a severely converging flow tube.

5.3.2 Chloride experiment

We determined the peak EC-values of all sampling cells during chloride leaching. The smallest peak values (9.5 mS cm^{-1} for the metal sampler and 14.9 mS cm^{-1} for the membrane sampler) were 22 (metal sampler) and 35 (membrane sampler) times larger than the background EC, and we therefore consider the EC (corrected for its background value) an adequate proxy for the tracer flux concentration. In total, the metal sampler captured 67 % of the chloride it should have intercepted if the flow had been perfectly vertical, and the membrane sampler received 87 %. This indicates substantial diverging flow. Whether this is caused by the natural flow pattern above the samplers or is

Table 5.5: The distribution of the total captured percolation and chloride over the porous percolate interception area for both multi-compartment samplers. The fractions of the porous area that intercepted the indicated fractions of the percolate or solute are calculated by considering the most productive sampling cells first.

Fraction captured	Metal sampler		Membrane sampler	
	Percolate	Solute	Percolate	Solute
0.25	0.08	0.06	0.09	0.06
0.50	0.19	0.15	0.20	0.16
0.75	0.38	0.32	0.41	0.34

Fraction of the porous interception area capturing the indicated percolate or solute fraction

related to the level of suction applied cannot be estimated with certainty. The fact that the very thin membrane performed better in this respect than the sintered metal plates does warrant a critical evaluation of the applied suction in case of a significant pressure gradient over the porous cover.

When the actual evapotranspiration is assumed to be nearly potential, the captured drainage indicates slightly diverging (metal sampler) or converging flow (membrane sampler) (Table 5.6). The discrepancy between the outcomes of the tracer and the drainage may reflect changing conditions, with more irregular infiltration early on. Another possibility is that the applied suction was too low during moderate downward flow. A large amount of chloride leached prior to the wet period starting around day 54, as can be assessed from Figs. 5.1, 5.3, and 5.8. This could have led to diverging flow during the period in which most chloride leached. If the applied suction was too high during wet periods, the extra drainage captured then could have compensated for the earlier under sampling.

The dye tracer discussed below indicated absence of diverging flow under relatively dry circumstances. This leaves open the possibility that the under sampling of chloride was not an artefact caused by the samplers, but does indeed reflect the flow pattern.

Table 5.6 also reports values if the samplers solid rim around the interception area is ignored. The large rim together with the sealed half-compartments of the membrane sampler have a large effect. Clearly, if a porous membrane is to be used, its size should be compatible with the sampler. Also, the effect demonstrates the necessity to design buried percolation samplers such that non-conductive areas near the porous interception surface are kept to the absolute minimum, as is the case with the metal sampler.

The maps of percolation and chloride leaching (Figs. 5.4 and 5.5) show

Table 5.6: Amount of percolate (up to day 112) and solute captured for metal and membrane samplers relative to the amounts that would have resulted form vertical, parallel flow tubes. The solute data are based on the electrical conductivity (EC) of the percolate and corrected for the background EC. The background ECs for both samplers were measured prior to the tracer application. The corrected line is based on the rainfall corrected for evapotranspiration.

	Area of interest	Metal sampler	Membrane sampler
		Fraction of captured percolate	
	Sampling area	0.63	0.77
Corrected	Sampling area	0.92	1.14
		Fraction of captured solute	
	Sampling area	0.67	0.87
	Porous area	0.69	1.01
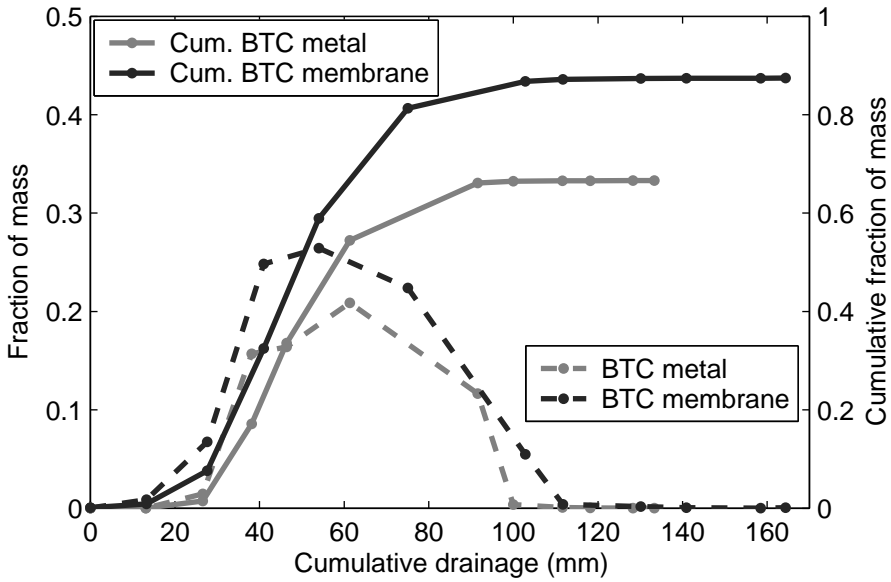
Figure 5.8: Fraction of the amount of chloride applied to the sampling area at the soil surface that was captured in each sampling round for both samplers.

less spatial variation in the chloride flux concentration than in the percolation, reflecting the effect of lateral spreading. Nevertheless, the distribution of chloride mass resembled the percolation pattern. In both samplers, the bulk of the chloride passed between days 42 and 65, but the membrane sampler produced chloride at day 6, and peaked earlier (day 58 vs day 65, Fig. 5.8). Given the shallower depth of the membrane sampler (0.25 vs 0.31 m), this behavior is not surprising.

The percolation (and possibly the chloride concentration after day 58) of the bottom right row of cells of the membrane sampler appear to have been affected by the trench. Possibly, the backfilling was not entirely adequate. The metal sampler shows no boundary effects, except for slightly enhanced drainage in the upper left row of cells.

Figure 5.9 summarizes and aggregates the information of Figs. 5.4 and 5.5 and corroborates the dominant role of the infiltration pattern on the spatial distribution of solute leaching. Interestingly, the maximum chloride concentration is quite independent of the amount of water captured by a sampling cell. Table 5.7 demonstrates that the considerable convergence and divergence of the flow tubes (two to three orders of magnitude variation in amount of captured percolation per cell; four orders of magnitude difference for the amount of chloride) hardly affected the peak concentrations (variation within an order of magnitude). Since the tracer was applied as a pulse with uniform concen-

tration this behavior could in principle be caused by the absence of lateral spreading and by limited longitudinal spreading. However, since the lateral variation of the chloride concentration was relatively limited, even though the flow rates varied massively, a more likely explanation is that of very effective lateral spreading, at least within a few centimeters. This suggests a convective-dispersive rather than stochastic-convective solute transport mechanism in this soil ((*Jury et al.*, 1991), pp 222-255).

The leaching surfaces (Fig. 5.10) support this conclusion: the amount of solute carried at any given time varies massively between cells, but the cells with low flow rates do not peak later than those with high flows, indicating solute transfer between fast and slow domains. This solute transfer leads to much smaller variations in the concentration-based leaching surfaces. Note that the similarity of the concentration BTCs for the low flow cells is an artefact caused by the necessary pooling of small samples to acquire enough liquid for an EC-reading. These results differ considerably from *de Rooij and Stagnitti* (2002a) observations in a hydrophobic soil, where times to peak varied strongly. In their soil, the transport was predominantly stochastic-convective. In our wettable soil, lateral spreading is easier and dispersive transport prevails.

Despite the considerable difference in solute recovery between the samplers, their cumulative SSDCs and SDDCs are reasonably similar (Fig. 5.11). The temporal variation of the percolation pattern gave slightly smoother cumulative SDDCs. The tracer pulse was less affected, because most chloride leached during three of the 11 sampling rounds. This smoothing effect on the variability of cumulative drainage as compared to that of chloride is also noticeable in Table 5.7. Contour plots of the leached masses (Fig. 5.12) illustrate the dominance of a small portion of the soils cross-section for solute transport, even in the absence of fingers caused by hydrophobicity, macropores, or other preferential flow paths not caused by heterogeneity of soil hydraulic properties. The contour plots also show that at any location most leaching occurred within the same 50 mm drainage period.

Table 5.7: Selected descriptive statistics of the captured percolate and chloride for the metal and membrane samplers.

		Total drainage (mm)	Maximum concentration (g l^{-1})	Total amount leached (g)
Metal sampler	Min	0.453	3.41	4.8×10^{-4}
	Max	662.27	9.36	1.25
	CV	0.99	0.17	1.20
Membrane sampler	Min	2.85	5.40	6.2×10^{-4}
	Max	606.83	9.89	1.57
	CV	0.89	0.14	1.13

Metal sampler   Membrane sampler

Total drainage (mm)

Maximum concentration (mg l^{-1})

Total mass (mg)
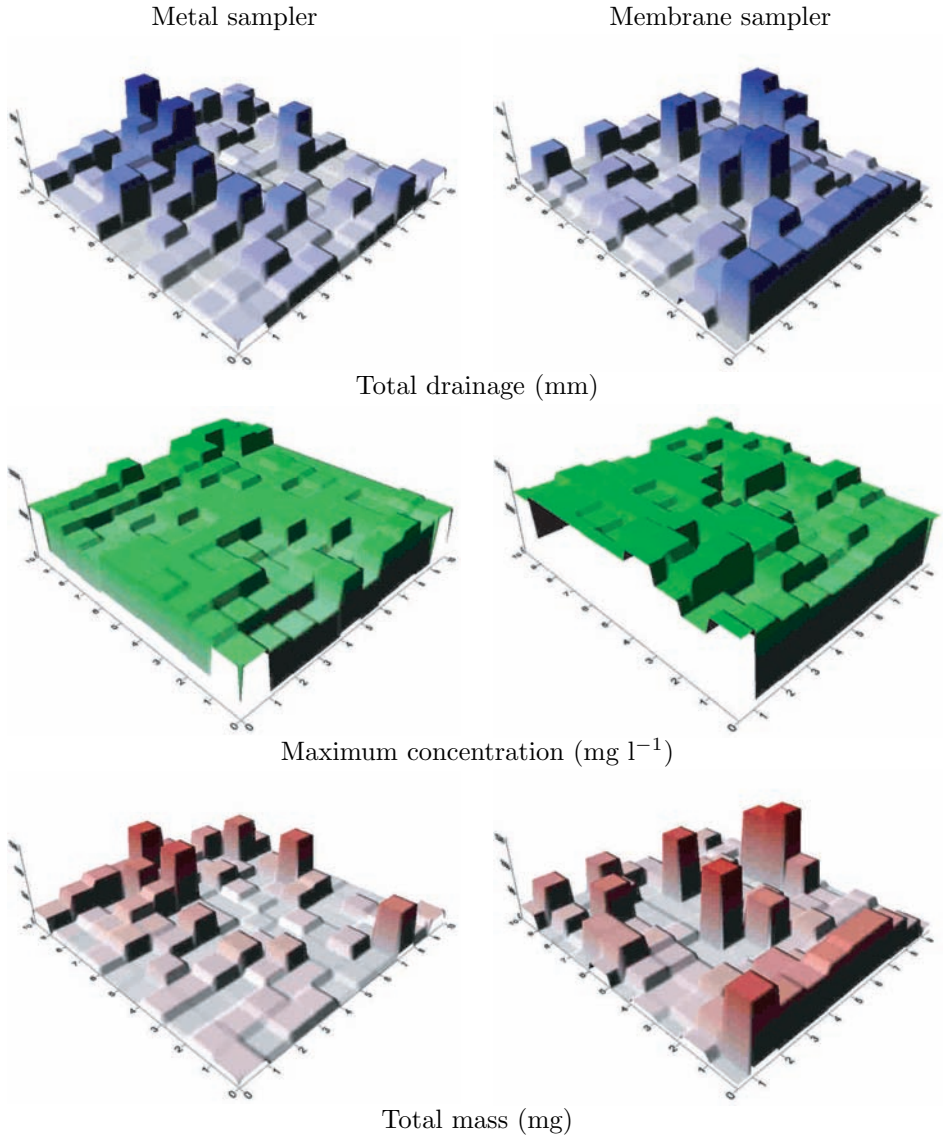
Figure 5.9: Total drainage, maximum measured concentration, and to-
tal captured chloride per cell for the metal (left) and membrane (right)
sampler. The side facing the trench is at the bottom right. On the x-axis
the columns and on the y-axis the rows of the sampler are indicated. The
z-axes indicate the total drainage (0 - 700 mm), the maximum chloride
concentration (0 - 10000 mg l^{-1}, and the total mass (0 - 1600 mg).

Metal sampler   Membrane sampler

(a)   (b)

(c)   (d)

(e)   (f)
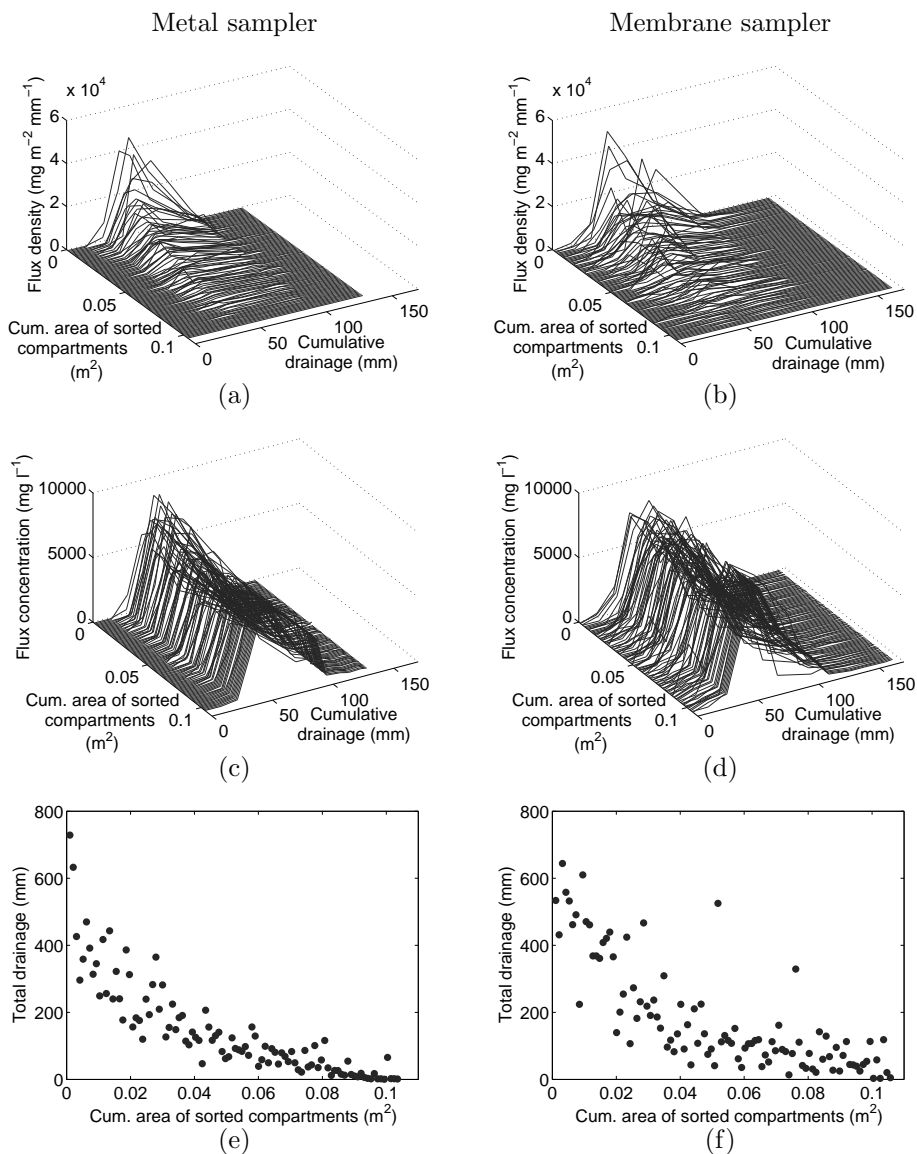
Figure 5.10: Chloride leaching surfaces based on leached amounts (a, b) and flux concentrations (c, d), and relationship between ranking based on total leached amount and amount of captured percolate per cell (e, f). Left: metal sampler; Right: membrane sampler. The drainage on the horizontal axis refers to the drainage captured from the entire sampler, not from individual cells.
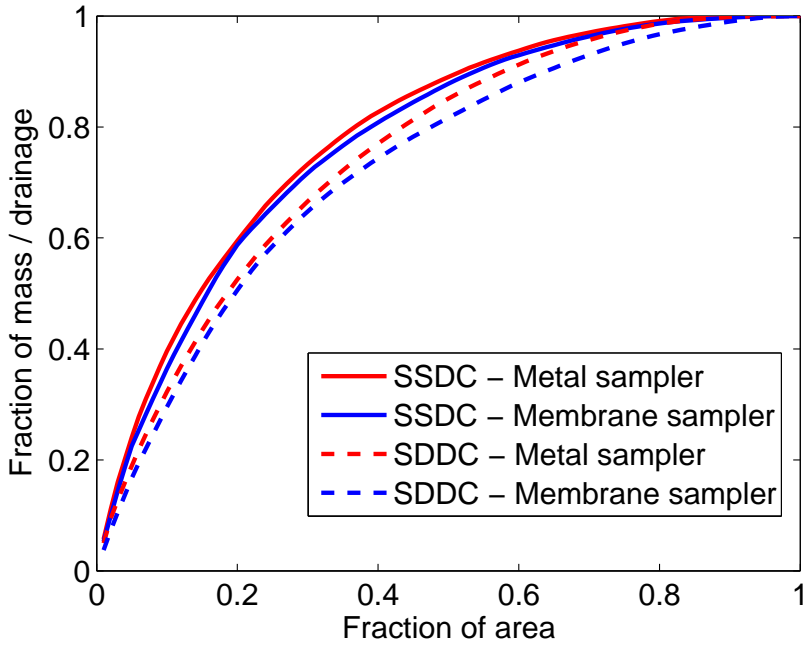
Figure 5.11: Cumulative spatial solute and drainage distribution curves (SSDC and SDDC) for both samplers for the entire experiment. The individual compartments are ranked in descending order of captured solutes. To facilitate comparison, the curves were scaled to make the total captured solutes and drainage equal to one.
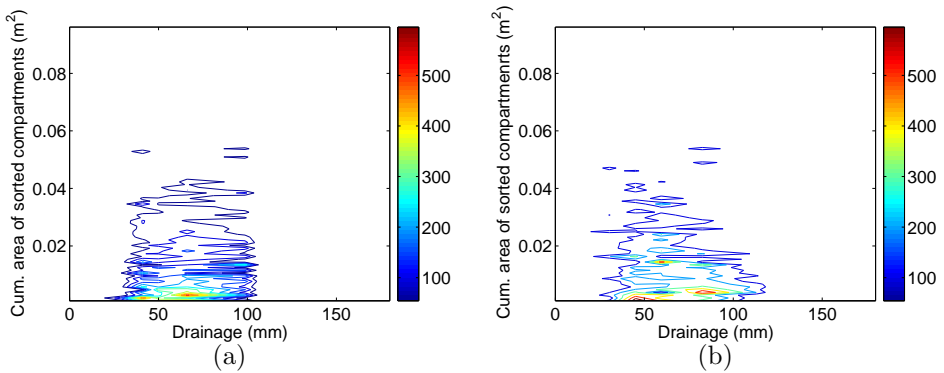
Figure 5.12: Contour plots of the leached masses (mg) for the metal sampler (a) and the membrane sampler (b).

Figure 5.13: The surface of the metal sampler after the Brilliant Blue experiment, with clear dye-staining. The rows of cells discussed in the main text and subsequent figures run from bottom to top. The bottom row was closest to the installation trench. The size of one individual cell is 31.5×31.5 mm.

5.3.3 Brilliant Blue experiment

After excavating and photographing dye-stained profiles above the metal sampler we removed the sampler. The Brilliant Blue left a distinct footprint on the sampling area (Fig. 5.13). The spatial distribution of drainage resembled the dye footprint (Fig. 5.14), but differed considerably from the spatial distribution of the first 51.1 mm of rainfall during the chloride tracer experiment, reflecting the different initial conditions and rainfall regime. The localized percolation area during the Brilliant Blue experiment was also prominent during the chloride experiment. The marked differences in amounts and distribution of percolation and tracer point to the importance of mimicking the natural rainfall regime in artificial rain experiments.

(a)   (b)
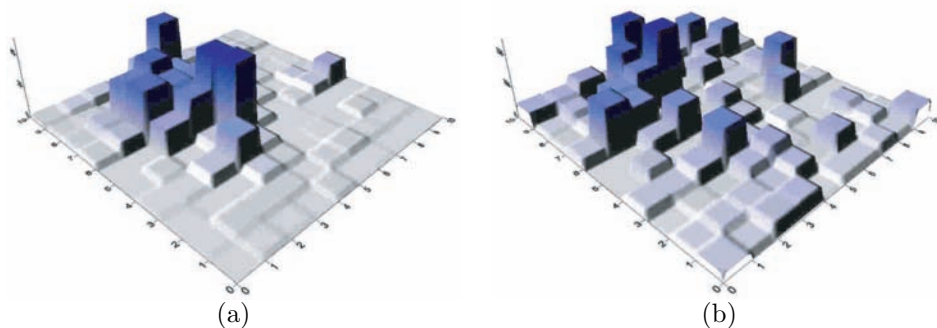
Figure 5.14: Spatial distribution of cumulative drainage of the Brillant Blue experiment (a), and of the chloride experiment after 50.1 mm of rainfall (b) (Table 5.4, day 42; data accumulated over the first three sampling rounds). The z-axis for the Brilliant Blue experiment has a maximum of 50 mm, while the z-axis for the chloride experiment has a maximum of 250 mm. The bottom-right side (row 1) faced the installation trench.

The staining patterns are distinctly irregular, with stained lobes of about 15 cm width as the largest features (Figs. 5.15 and 5.16). The location where the dye stain clearly contacted the sampler corresponds to a region with high percolation and dye concentration (Fig. 5.16 and row 7 in Fig. 5.14). The sharp transition between stained and non-stained soil was more blurred in the percolate, possibly because at the edge of the plume, cells received both stained and unstained water. The staining pattern in the soil and in the percolate suggests that for this soil the sampler size was adequate to register spatial variations within 1 m^2-scale. Also, the staining patterns in the soil showed no effect of the presence of the sampler, which is key to the proper functioning of buried flux samplers.

Figure 5.15: Brilliant Blue staining pattern in a soil profile above the third row of the metal sampler (see Figure 5.13), at 8 cm distance from the trench side of the instrument. The sampler has been replaced by a plate to support the soil during excavation. Light-colored soil on either side of the plate is backfilling material around the sampler to minimize the disturbance of the flow pattern.

Figure 5.16: Brilliant Blue staining pattern in a soil profile above the seventh row of the metal sampler (see Figure 5.13), at 21 cm distance from the trench side of the instrument. The sampler has been replaced by a plate to support the soil during excavation.

5.4   Conclusions

We performed a field solute transport experiment utilizing an anionic tracer amenable to quantitative analysis in combination with a dye tracer on the same soil volume located above a buried multi-compartment sampler. This setting yielded information that widely surpassed the information that can be provided by separate anionic and dye tracer trials, and solute transport monitoring by coring or suction cups.

In this hydrophilic soil without cracks or other obvious causes for preferential flow, the spatial distribution of drainage, the spatio-temporal redistribution of a pulsed tracer, and dye staining consistently indicate markedly non-uniform flow. The spatial scale of the heterogeneities could well be captured by our 32.5 × 32.5 cm samplers.

The limited variation in times to peak, and the small range of total amounts of captured solute per cell compared to the range for captured drainage, indicate effective lateral solute exchange between stream tubes. Despite the small vertical travel distances (0.3 m), this is consistent with a convective-dispersive transport regime. These and other diagnostic characteristics can be readily determined from leaching surfaces and SSDCs/SDDCs, and are very helpful in identifying key solute transport processes in a given soil.

Parameterizing the leaching surface by combining curve-fitting for solute breakthrough and for spatial solute distribution

6.1 Introduction

Solute transport in soils is strongly affected by soil heterogeneity, fingered flow and macropore flow. The heterogeneity affects both water transport and solute transport, but not necessarily to the same extent. Dye tracers such as Brilliant Blue are often used for flow visualization (*Flury et al.*, 1994; *Flury and Wai*, 2003), and increasingly for quantitative analysis (*Persson*, 2005). While dye tracers provides information about spatial spreading, its significant adsorption makes it less suited to determine the travel times of water (*Kasteel et al.*, 2002). Another disadvantage of using dye is that it allows only a single experiment at a given location.

Travel times of water and solutes can be studied efficaciously using column studies where conservative tracers like chloride or bromide are used to measure the temporal response to the injected tracer. In a column experiment, a solute moves downward with the water through a single column. At the bottom, water and solute are collected in a single container covering the entire bottom of the column, and the measurements result in a breakthrough curve (BTC) (*Jury and Roth*, 1990). These single column experiments lack spatial information and the BTC essentially describes one-dimensional solute transport. Field experiments

This chapter is a slightly modified version of the manuscript: Bloem, E., M. de Gee, and G. H. de Rooij, Parameterizing the leaching surface by combining curve-fitting for solute breakthrough and for spatial solute distribution

with single-cell sample collectors also give a single (spatially averaged) BTC, and therefore only give information about solute transport in one direction.

This limitation prompted the ever-increasing deployment of multi-compartment samplers (MCS) that measure solute leaching as a function of space and time (*Wildenschild et al.*, 1994; *Quisenberry et al.*, 1994; *Poletika and Jury*, 1994; *Buchter et al.*, 1995; *Stagnitti et al.*, 1998; *de Rooij and Stagnitti*, 2000; *Strock et al.*, 2001) to assess the fate of salts, nutrients, and pollutants in natural, heterogeneous soils. A multi-compartment sampler can be thought of as a wide column device, where the collector at the bottom of the column is divided into a number of compartments. Each compartment collects the output of a part of the column, which can be represented in a BTC. Therefore, the output of a multi-compartments sampler consists of a family of BTCs.

An individual BTC generally has been interpreted through moment analysis (*Kreft and Zuber*, 1978; *Vanderborght and Vereecken*, 2001; *Brooks and Wise*, 2005) or by means of a solute transport model (model analysis) (*Parker and van Genuchten*, 1984; *Jury and Sposito*, 1985; *Kool et al.*, 1987; *Yamaguchi et al.*, 1989). Moment analysis usually considers the zeroth moment of the distribution of solute with time (recovered tracer mass), the first moment (mean travel time) and the second central moment (variance of the travel time). In model analysis, mathematical equations are used to describe solute transport. The parameters in these equations are matched to the measured response (curve fitting). Thus, the transport properties of the system are represented by the model parameters (*Toride et al.*, 1999). *Fahim and Wakao* (1982), and *Haas et al.* (1997) concluded that curve-fitting in a model analysis is more accurate than moment analysis. Furthermore, model analysis is often preferred, because the model parameters usually have a clear physical interpretation. This, however, may also be a pitfall: the inability of mathematical models to accurately describe the nature of complex systems can be a disadvantage in the model analysis approach (*Brooks and Wise*, 2005).

The most common mathematical model for solute transport in soils is the convection-dispersion equation (CDE). The CDE characterizes solute transport by the velocity and dispersion coefficient. In soil physics the use of the CDE is accepted, even though it is acknowledged that soils have complex pore geometries and heterogeneous structures which are not fully known in detail (*Beven et al.*, 1993). Therefore *Beven et al.* (1993) argue that the CDE may be applicable in a functional sense in which the mean transport velocity reflects the mass flux of water averaged over some unit area in the system, and the 'effective' dispersion coefficient accounts for the complexities of the flow pathways and heterogeneity in local fluid velocities in the direction of the flow. Modifications of the CDE have been made to improve this model. In saturated soils, the dispersion is scale dependent, necessitating the use of a scale dependent coefficient (*Mishra and Parker*, 1989; *Gelhar et al.*, 1992). In unsaturated soils preferential flow exerts a large influence. This can be accounted for by using the mobile-immobile CDE model for example (*Parker and van Genuchten*, 1984; *Beven et al.*, 1993), or by models that include a macropore domain. Many studies have used model analysis for fitting the transport parameters to tracer data

(e.g. *Parker and van Genuchten*, 1984; *Jury and Sposito*, 1985; *Kool et al.*, 1987; *Yamaguchi et al.*, 1989), including the identifiability of the parameter values (e.g. *Mishra and Parker*, 1989). A single BTC can only offer a limited amount of information and certain processes may be taking place outside of its unitary scope. The parameters of the mobile/immobile CDE, for example, may interact in their effect on the predicted outputs, resulting in considerable uncertainty associated with the fitted values (*Beven et al.*, 1993).

Most experiments had a low spatial resolution and used only a single BTC. Therefore, they give poor representations of the heterogeneous transport processes. Tracer experiments with conservative tracers like chloride or bromide, in which multi-compartment samplers are used to measure the response to an injected tracer, are more adequate to characterize solute transport. A new approach to analyze this data has been developed (*de Rooij and Stagnitti*, 2002a,b, 2004), presenting the leaching surface as a tool to analyze the spatially and temporally non-uniform passage of solutes across a monitoring plane. The leaching surface is a curved surface constructed from a population of local-scale BTCs in such a way that the information on the spatial variation in the BTCs is preserved.

Until now, leaching surfaces were merely used to represent data from multi-compartment samplers. In this Chapter we develop a method to quantitatively characterize leaching surfaces. The main objective is to parameterize the leaching surface with a limited number of parameters that can be meaningfully interpreted in terms of the soil's solute transport properties. This is achieved by a separate parameterization of the spatial and temporal aspects of solute leaching. For the temporal aspect, we determine the parameters of the individual BTCs by model analysis. We then detect and parameterize any relationships between the transport velocities and dispersion coefficients of the individual BTCs. The spatial aspect is parameterized using the Beta distribution as outlined by *Stagnitti et al.* (1999); *de Rooij and Stagnitti* (2000, 2004).

The best-fit parameters thus provide a quantitative and objective representation of the leaching surface. This allows a quantitative description of leaching surfaces, providing a means to objectively compare leaching characteristics of different soils, and even of the same soil in different seasons. To test the method, we performed a tracer experiment in the field with a multi-compartment sampler. We constructed a leaching surface from the data and determined its parameters.

6.2 Materials and Methods

6.2.1 Leaching surfaces: spatial and temporal aspects of solute leaching

In a hypothetical experiment, a multi-compartment sampler (MCS) with sample collection area A [L^2] has its sampler cells arranged in a rectangular grid of n $\times$ n cells with positions (x_i, y_j), where x_i and y_j [L] are horizontal cartesian

coordinates of the centers of n^2 individual cells identified by the counters i,j $\epsilon\{1,\ldots,n\}$. Generalization to other geometries or a population of unconnected single-cell samplers is trivial. The sampler is buried in the soil below an undisturbed soil volume. For an experiment at which a solute is applied uniformly as a pulse (Dirac function) to the soil surface of an area much larger than A centered above the sampler, the outflow into the cells is collected at several points t_k [T] in time, with subscript k indicating the kth sampling time since the solute application. Water volume V [L^3] and solute flux concentration C [ML^{-3}] of the samples are measured. For the solute, there are two ways in which to proceed. The first option is to use the measurements of concentration. These concentrations give a solute flux concentration breakthrough curve $BTC_C(x_i, y_i, t)$ for compartment (i,j). The second option is to use solute flux density. Multiplying the measurements of concentration C and volume V results in a derived leached mass measurement. By dividing this mass by the compartment area and by the sampling time interval $t_k - t_{k-1}$ we obtain the solute flux density F [ML^{-2}T^{-1}]

$$F_{i,j,k} = \frac{C_{i,j,k} V_{i,j,k}}{\Delta x_i \Delta y_j (t_k - t_{k-1})} \tag{6.1}$$

For each compartment we can obtain a different breakthrough curve $BTC_F(x_i, y_i, t)$ by plotting F as a function of time. Each of these approaches has its merits and drawbacks. To describe solute transfer through the soil, BTC_F is most valuable. When the concentration is of interest (for instance for substances with non-linear sorption, or for toxic compounds), BTC_C is preferable.

Both functions contain the full spatial information gathered by the multi-compartment device. Since they are functions of three independent variables, it is difficult to analyze them. To facilitate their visualization, the sampling compartments are ranked in decreasing order of their total collected solute over the entire leaching period. Then the corresponding breakthrough functions BTC_F or BTC_C are plotted against the cumulative sampling area s. In this way, the two spatial variables x and y are collapsed into a single pseudo-spatial variable s [L^2]. Using the BTC_F, this leads to the leaching surface as discussed in (*de Rooij and Stagnitti*, 2002a)

$$S(s_{i,j}, t) = F(x_i, y_j, t) \tag{6.2}$$

where $s_{i,j}$ denotes the position of compartment (i,j) on the s-axis.

The leaching surface $S(s, t)$ [M L^{-2} T^{-1}] thus has a horizontal time-axis and a second horizontal axis (s [L^2]) that represents the cumulative area of the compartments into which the control plane is divided. In the ordering, the detailed spatial information is lost, but the variation remains. The leaching surface can be scaled to make the area underneath it equal to one. Suitable cross-sections of the leaching surface parallel to the time-axis or the spatial axis, or integrations along intervals of the space and the time coordinate, can yield a wealth of information about the distribution in space and time of solute

movement. Indeed, at any fixed point s (associated with a location (x_i, y_j), the cross-section of the S parallel to the t-axis returns the breakthrough curve at (x_i, y_j). Integration over t gives the spatial solute distribution curve

$$\text{SSDC}(s) = \int_0^\infty S(s, t) \mathrm{d}t \tag{6.3}$$

By definition, this is a non-negative monotonically decreasing function. It reflects the spatial redistribution of a uniformly applied solute (*Stagnitti et al.*, 1999; *de Rooij and Stagnitti*, 2004).

6.2.2 Parameterizing the temporal aspect of solute leaching

Each BTC_C is scaled to 1 by dividing the concentrations by C_0 [ML^{-3}T] (the area under each BTC_C). We model the scaled BTC_C [T^{-1}] for each cell as the solution of a conventional one-dimensional equilibrium CDE, without modifications (*Toride et al.*, 1999). Thus, the solute transport is characterized by the pore-water velocity v, [LT^{-1}] dispersion coefficient D [L^{2}T^{-1}], retardation factor R [-], and degradation or production parameters μ [T^{-1}] and γ [ML^{-3}T^{-1}]

$$R\frac{\partial C^*}{\partial t} = D\frac{\partial^2 C^*}{\partial z^2} - v\frac{\partial C^*}{\partial z} - \mu C^* + \gamma(z) \tag{6.4}$$

with z denoting depth below the soil surface [L], and C^* the scaled flux concentration [L^{-3}].

In our experiment we used a conservative tracer, thus $R = 1$, $\mu = 0$, and $\gamma = 0$. For input we used the Dirac delta pulse. Furthermore, we measured flux-averaged concentrations. To allow an analytical solution we assumed steady-state flow. We used a boundary value problem condition consistent with our flux concentration observations. The specific solution for this problem is given by (*Toride et al.*, 1999)

$$C^*(t) = \left(\frac{L^2}{4\pi D t^3}\right)^{\frac{1}{2}} \exp\left(\frac{(L - vt)^2}{4Dt}\right) \tag{6.5}$$

with L denoting the depth at the sampling area [L].

As *Toride et al.* (1999) stated, this solution is sometimes referred to as the travel time probability density function (pdf) for the equilibrium CDE (*Jury and Roth*, 1990). The parameters v and D were fitted using CXTFIT (*Toride et al.*, 1999). For our hypothetical experiment, we obtain n^2 BTC$_C$s, each with its own v and D. To have a workable number of parameters we adopted simple functional relationships between v and D on one hand and s on the other

$$v(s) = a_v s^{b_v} + c_v \tag{6.6}$$

$$D(s) = a_D s^{b_D} + c_D \tag{6.7}$$

where a_v, a_D, b_v, b_D, c_v, and c_D are fitting parameters. The chosen functions allow both linear and power law fits but can of course be replaced by any desired relationship. Also, constraints linking some of the parameters can be added to reduce the number of fitting parameters. As a starting point we defined a reference fit by setting c_v and c_D to the mean fitted pore water velocity and dispersion coefficient, respectively, with the remaining fitting parameters set to zero.

6.2.3 Parameterizing the spatial aspect of solute leaching

The various single-cell BTCs produced by an MCS differ because of soil spatial variation and possibly preferential flow. It is desirable to characterize the effect of soil heterogeneity on solute leaching directly (i.e., not through numerical simulations in which the soil hydraulic properties vary between nodes). When MCS data are available, a simple yet descriptive way of doing so is through the SSDC, which is obtained by ranking the sampling compartments in decreasing order of amount of total captured solute and plotting the fraction of captured solute as a function of the cumulative area of the ordered compartments (*Quisenberry et al.*, 1994; *Stagnitti et al.*, 1999). Thus, the SSDC only contains information about the spatial redistribution of solutes. If lateral dispersion is of minor importance, *de Rooij and Stagnitti* (2000) showed that the SSDC describes the geometry of the flow paths in terms of flow constriction and divergence. The SSDC can be parameterized by fitting the Beta distribution (*Stagnitti et al.*, 1999)

$$p(x, \alpha, \zeta) = B(\alpha, \zeta)x^{\alpha-1}(1-x)^{\zeta-1}, \qquad 0 \leq x \leq 1 \tag{6.8}$$

where p is the probability of the Beta variate as a function of coordinate x,

$$B(\alpha, \zeta) = \frac{\Gamma(\alpha + \zeta)}{\Gamma(\alpha)\Gamma(\zeta)} \tag{6.9}$$

is the Beta function, and α and ζ are positive shape parameters (*Nadarajah and Gupta*, 2004). The mean, variance and coefficient of variation CV of the Beta distribution are (*Gupta and Nadarajah*, 2004)

$$\mu(\alpha, \zeta) = \frac{\alpha}{\alpha + \zeta} \tag{6.10}$$

$$\sigma^2(\alpha, \zeta) = \frac{\alpha\zeta}{(\alpha + \zeta)^2(\alpha + \zeta + 1)} \tag{6.11}$$

$$\mathrm{CV}(\alpha, \zeta) = \sqrt{\frac{\zeta}{\alpha(\alpha + \zeta + 1)}} \tag{6.12}$$

Note that the uniform distribution arises by setting $\alpha = \zeta = 1$, with a coefficient of variation $3^{-1/2}$.

We needed to transform the fitted BTC_C for each compartment (i,j) to a BTC_F in order to be able to produce a leaching surface based on solute

flux density. We approximated the flux concentration during the kth sampling interval by

$$C_{i,j,k} \approx C_{0,i,j} C_{i,j}^*(t_k) \tag{6.13}$$

i.e. based on the fitted scaled concentration at the end of the sampling interval. With Eq. (6.1), this gives

$$F_{i,j,k} \approx \frac{C_{0,i,j} C_{i,j}^*(t_k) V_{i,j,k}}{\Delta x_i \Delta y_j \left(t_k - t_{k-1}\right)} \tag{6.14}$$

The group $V_{i,j,k} \left[\Delta x_i \Delta y_j \left(t_k - t_{k-1}\right)\right]^{-1}$ is the water flux density for compartment (i,j) during sampling interval k [L T^{-1}]. We recall we ranked the n^2 compartments in order of total captured solute, so that each compartment (i,j) has a unique rank number, which we denote w : w $\epsilon\{1,\ldots,n^2\}$. If we denote the total number of sampling rounds m, we have k $\epsilon\{1,\ldots,m\}$. With these, we can create a flux density matrix $\underline{\underline{q}}$ with n^2 rows and m columns in which each of the entries is given by the water flux density of the compartment corresponding to the row number (ranking along the s-axis) at the sampling round indicated by the column. By summing over the columns the vector $\underline{q}_s$ [L T^{-1}]

$$q_{s,i} = \sum_{k=1}^{m} q_{i,k} \tag{6.15}$$

By summing over the rows we obtain the vector $\underline{q}_t$ [L T^{-1}]

$$q_{t,k} = \sum_{i=1}^{n^2} q_{i,k} \tag{6.16}$$

We now approximate the solute flux density in the compartment with rank number i at sampling interval k as

$$F_{i,k} \approx C_{0,i} C_{i,k}^* q_{s,i} \frac{q_{t,k}}{\sum\limits_{k=1}^{m} q_{t,k}} \tag{6.17}$$

Here, $C_{0,i} q_{s,i}$ approximates the total amount of solutes leached from the compartment with rank number i. It is a function of i, and this function can be parameterized by the Beta distribution in analogy with the SSDC.

The Beta distribution fitted on $C_{0,i} q_{s,i}$ gives the fraction of the total leached solute passing through a particular region associated with an interval ds. This provides a scale factor to adjust the scaled breakthrough curve BTC$_F$ with $v(s)$ and $D(s)$ for that location.

6.2.4   Leaching experiment in the field

We used a variable-suction multi-compartment sampler of the type developed in Chapter 3 with metal porous plates (metal sampler). The sampler consisted

of 10×10 compartments (n = 10), each with a sampling area of 10.35 cm^2. The sampler was installed in the field (Vreedepeel, the Netherlands) at 31 cm depth as described Chapter 5. On the 14th of December 2005 we cut the grass in the 0.70×0.70 m area above the sampler to 3 cm and applied 4.5 mm of a 1 M CaCl$_2$*2H$_2$O solution. To eliminate the side effects of both converging and diverging streamlines of the chloride concentration, the tracer solution was applied on the entire 0.70×0.70 m plot. To do this, we covered the application area with a 21×21 cell PVC grid, with a syringe holder in the center of each cell. We filled 441 medical 10 ml syringes with 5 ml tracer solution (CV = 0.7 %), and placed these in the syringe holders. We then emptied all syringes within two minutes to achieve a spatially uniform tracer pulse application. The soil surface directly above the sampling area of the sampler received 33.0 g Cl$^-$.

After each rainfall event (usually a cluster of small rain showers), the collected leachate was extracted from the sampling cells while leaving the sampler buried *in situ*. The collected volumes were determined and the solute concentrations were derived from the EC as measured with an EC meter (Cond 315i and TetraCon325 from WTW; individually calibrated). After 145 days (11 sampling rounds; $k \in 1,..,11$), nearly all tracer had passed the sampling depth. The mass collected during the final sampling round was less than 0.01 % of the applied mass over the sampling area.

6.2.5 Data analysis

Rainfall during the experimental period was erratic. We therefore replaced the time coordinate [T] by a cumulative drainage coordinate [L], with the cumulative drainage at each sampling round calculated as the average cumulative drainage of all 100 sampling cells since the solute application. This coordinate transformation eliminates most of the irregularities arising from dry periods between rainfall events (*van Ommen et al.*, 1989; *Jury et al.*, 1991). We determined BTC$_C$ and BTC$_F$ for each compartment and constructed leaching surfaces from both sets of curves. Each leaching surface comprised 1100 data points. To fit the BTC$_C$s of all compartments we ran CXTFIT. Before doing so we scaled every curve by the area underneath it (C_0 [mass per volume times cumulative drainage; M L^{-3} L; note the separate length dimension emerging from the coordinate transformation outlined above]), and then fitted v and D to the scaled curves. The flux concentration for a given cell at a given time can be approximated by multiplying the fitted concentration by C_0 of that cell.

The final ten velocities give a biased result, as these BTCs were constructed from average concentrations. The samples which did not contain enough water were pooled during the analysis. We did not take these values into account for the further construction of the leaching surface.

We fitted the leaching surface as described above, with $v(s)$ and $D(s)$ equal to their average values for all s. In fitting the Beta distribution to approximate total amounts of leaching, we fitted the non-cumulative form of the distribution. We found this significantly improved the goodness of fit as compared to fitting the cumulative Beta distribution according to *de Rooij and Stagnitti* (2000).

Of course, the fitted leaching surface is smooth. To reproduce some of the detailed features of the observed leaching surface we replaced the average values of v and D by randomly generated values from Gaussian distributions with mean and standard deviation given by the populations of fitted v and D. We subdivided s in equidistant intervals and assigned one set of the random values to each interval (qualitative approach).

For comparison we also constructed the leaching surface based on flux concentration directly from the 100 fitted values of v and D. Thus, the only difference with the observed leaching surface based on flux concentration is the fact that the individual BTCs were now fitted, isolating the effect of CXTFIT. Conversely, we scaled the observed BTC_Cs according to the fitted instead of the observed approximated SSDC to see how the Beta distribution affected $S(s,t)$.

For each BTC within the leaching surface we calculated the normalized root mean square error (RMSE)

$$\text{RMSE}_\text{n} = \frac{\sqrt{\sum\limits_{\text{k}=1}^{m}(F_O(\text{i,k}) - F_P(\text{i,k})^2)}}{\sum\limits_{\text{k}=1}^{m} F_O(\text{i,k})} \cdot 100\% \tag{6.18}$$

with subscript O denoting observed solute flux densities, and subscript P indicated their calculated counterparts.

We also calculated the normalized mean RMSE between the observed and fitted leaching surface

$$\text{RMSE}_\text{nm} = \frac{\sum\limits_{\text{i}=1}^{w}\sqrt{\sum\limits_{\text{k}=1}^{m}(F_O(\text{i,k}) - F_P(\text{i,k})^2)}}{\sum\limits_{\text{i}=1}^{w}\sum\limits_{\text{k}=1}^{m} F_O(\text{i,k})} \cdot 100\% \tag{6.19}$$

The same equation is used to calculate the error of the flux concentration C (i.e. F is replaced by C in Eqs. (6.18) and (6.19)).

6.3 Results and discussion

Figure 6.1 presents the observed leaching surfaces. The leaching surface based on solute flux density shows more variation than the leaching surface based on flux concentration because the variations in concentration and in amount of drainage are both represented in this graph. This figure shows the importance of the drainage in solute movement, as most of the mass is displaced within the cells with the highest fluxes, whereas the concentration is divided more or less equally over the whole sampling area. The area under each BTC_C based on flux concentration was determined (Fig. 6.2a), as well as the approximated SSDC (Fig. 6.2b). Figure 6.2b shows the Beta distribution fitted through the approximated SSDC. The fitted parameter values are in Table 6.1.
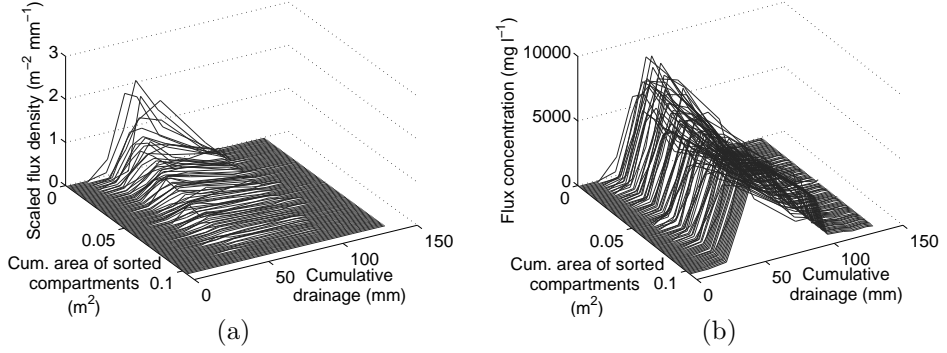
Figure 6.1: Leaching surfaces for the tracer experiment based on scaled flux density (a) and based on flux concentration (b).
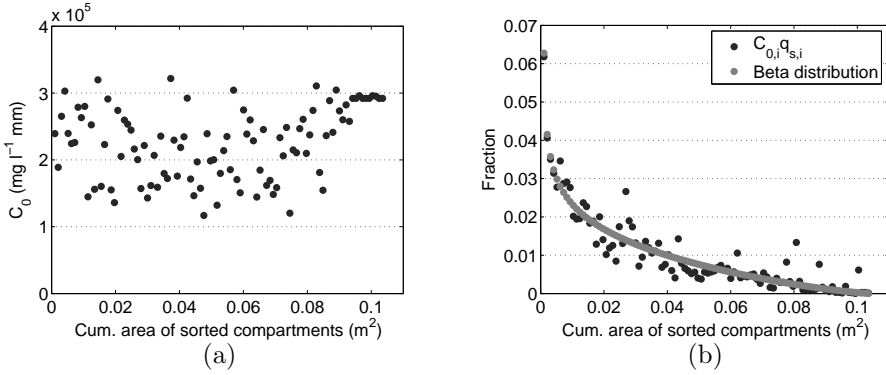

Figure 6.2: C_0 is the area under each breakthrough curve based on flux concentration BTC_C (a), used to scale each BTC_C to unity. In order to obtain the scaled flux density the scaled flux concentration BTC_C must be multiplied by $C_{0,i}q_{s,i}$. The fraction of this function is fitted by the Beta distribution (b).

The results of the CXTFIT runs are given in Table 6.1 and Figure 6.3. The error between the observed and fitted BTC_Cs is acceptable given the low noise that is evident in Figs. 6.3, 6.4a,b and Table 6.2. The fitted velocities v are fairly uniform, but seem to slightly decrease with s. The fits for D are much more erratic without a clear trend. The velocities and dispersion coefficients are parameterized by one average velocity and one average dispersion coefficient as given in Table 6.1. This results in Figure 6.4c, the error is slightly increased by 6 % due to this operation. Applying the Beta distribution results in the final parameterized leaching surface S (Fig. 6.5c).

Figure 6.6b shows the leaching surface obtained when the observed BTCs were scaled according to the fitted Beta distribution, and thus solely reflects
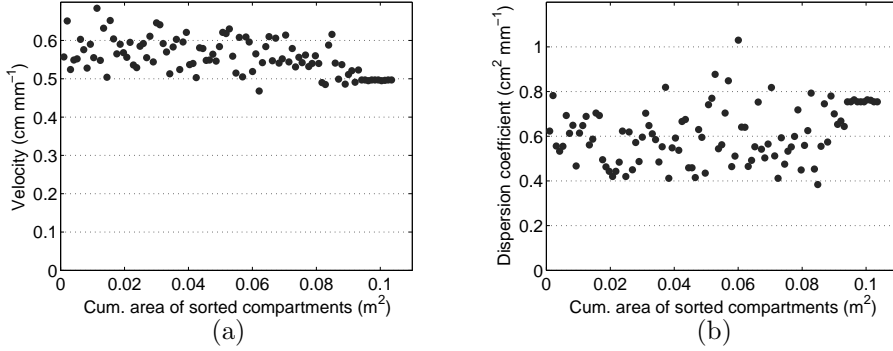
Figure 6.3: CXTFIT curve fitting results for the velocity v (a) and dispersion coefficient D (b) of the 100 sorted scaled BTC$_C$s based on flux concentration.

the effect of replacing the observed SSDC by its fitted counterpart. The errors of CXTFIT for the fitted BTC$_C$ are 12.7 %. The error of the Beta distribution is 16.9 %.

Because trends in $v(s)$ and $D(s)$ are small or absent, we only applied the reference fit (with v and D equal to their mean for all s). This reduced the parameters describing the leaching surface to the four given in the top row of Table 6.1. The resulting leaching surface is shown in Fig. 6.5c. A comparison with the observed leaching surface (Fig. 6.5a) shows that the noise has been stripped to reveal the main features. The absence of a trend in v and D leads to a crest parallel to the s-axis and equally wide BTCs. The error for this leaching surface compared to the observed leaching surface is 20.7 %.

For visualisation we also used a qualitative approach, in which we sampled velocity and dispersion values from a normal distribution about the averaged velocity and averaged dispersion coefficient. These v and D values lead to scaled flux concentrations as presented in Fig. 6.4d. Visually the results for the scaled flux concentrations show a good resemblance for observed scaled

Table 6.1: The fitted parameters velocity v, dispersion coefficient D from the model output of CXTFIT (Fig. 6.3), and α and ζ from the Beta distribution (Fig. 6.2) for a quantitative description of the leaching surface based on flux density.

	v (cm mm^{-1})	D (cm^2 mm^{-1})	α	ζ
Mean	0.564	0.592	0.740	2.250
STDEV	0.043	0.123		
CV (%)	7.69	20.73		
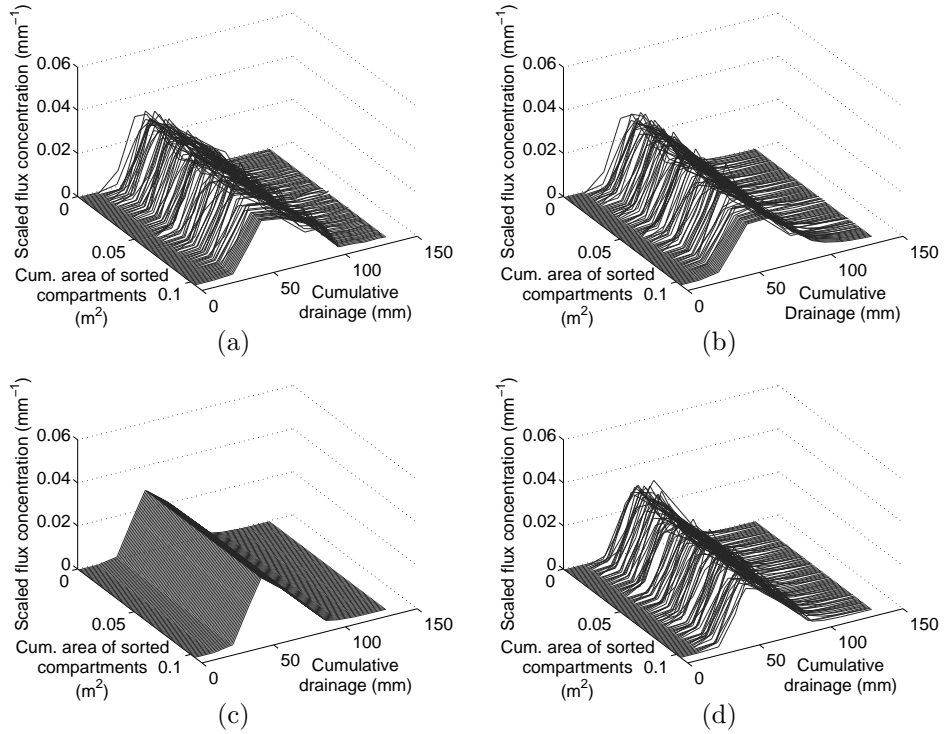
Figure 6.4: The observed scaled leaching surface based on flux concentration (a), the scaled leaching surface based on flux concentration for the calculated v and D per BTC_C, fitted with CXTFIT (b), the scaled leaching surface based on flux concentration with the average v and average D as given in Table 6.1 (c), and the scaled leaching surface based on flux concentration with a qualitative approach (d).

flux concentrations (Fig. 6.4a and d). Applying the Beta distribution give the qualitative leaching surface (Fig. 6.5d). In comparison with the smoothed leaching surface of Figure 6.5c, the qualitative leaching surface gives a better visual result.

Figure 6.5: The observed scaled leaching surface based on flux density (a) and parameterizations: scaled leaching surfaces based on flux density are constructed on the calculated v and D per BTC$_C$ together with the fitted Beta distribution (b), the average v and D (Table 6.1) with the fitted Beta distribution (c), and a qualitative fit of v and D together with the fitted Beta distribution (d).

6.4   Conclusions

We developed a parameterization of the leaching surface that requires four to eight parameters. The parameterization was used to fit an observed leaching surface and found to represent the main features rather well. This opens up the prospect of a quantitative comparison of leaching surfaces from different soils or obtained in different seasons. Possibly, leaching surface parameters can be used to characterize a local soil or field in terms of its leaching behavior. This would be a more direct characterization than the currently used method of identifying soil hydraulic and transport properties to feed a numerical model that calculates leaching scenarios. Furthermore, a parametric fit of a leaching surface allows the trend to be subtracted from the observations, thereby isolating the noise to allow an analysis of residuals.
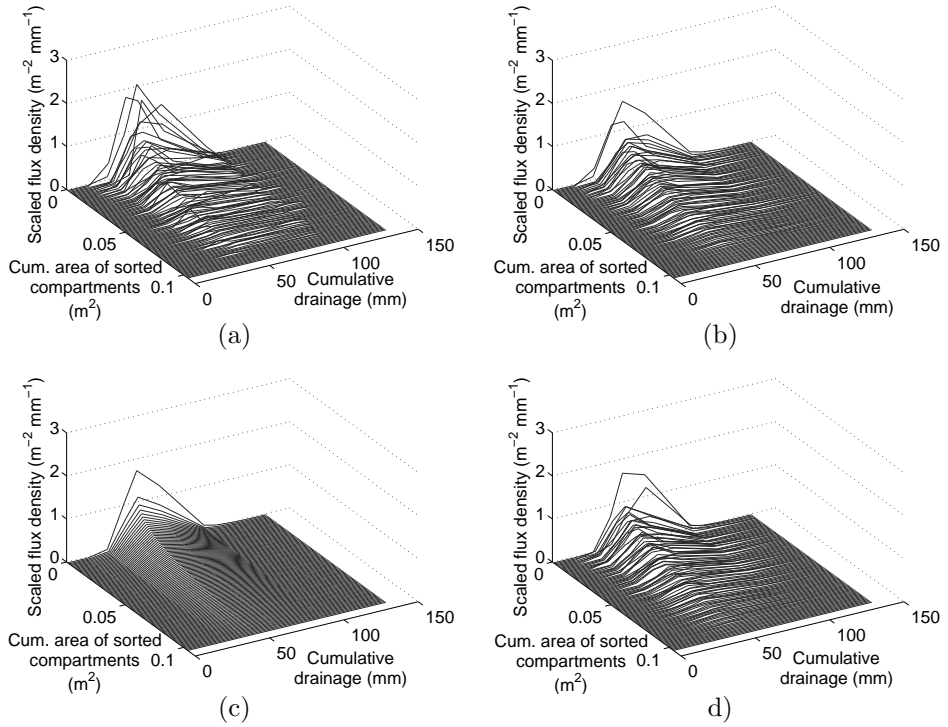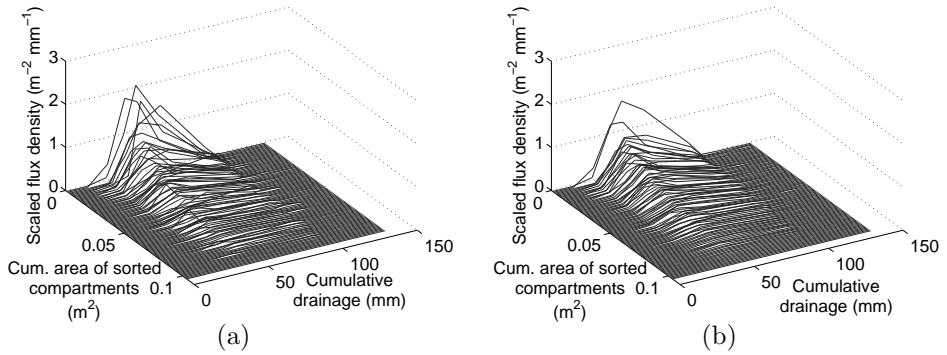
Figure 6.6: The observed scaled leaching surface based on flux density (a) and the parameterization: scaled leaching surface based on flux density constructed using the the observed scaled BTC_C together with the fitted Beta distribution (b).

Table 6.2: The normalized mean root mean square error (RMSE) (%) between the observed and parameterized leaching surfaces based on flux concentration (BTC_C) and between the observed and parameterized leaching surfaces based on flux density (BTC_F). For the leaching surfaces based on flux concentrations the errors have been calculated for the fitted v and D, and for the averaged v and D. For the scaled leaching surface based on flux density we calculated the error for the fit if the Beta distribution has been applied directly on the observed BTC_F, applied on the fitted v and D, and applied on the averaged v and D.

	Fit	normalized mean RMSE (%)
BTC_C	Direct	0
	v and D calculated	6.7
	v and D averaged	12.7
BTC_F	Direct	16.9
	v and D calculated	17.9
	v and D averaged	20.7

An alternative fitting procedure for the leaching
surface parameters

7.1   Introduction

To understand soil and groundwater contamination, both spatial and tempo-
ral aspects of solute leaching are important. Soil heterogeneity for example
affects both travel time and spatial distribution of the solute transport. One
observational method that captures both aspects is the multi-compartment
sampler, either installed underneath a soil column in the laboratory (*Quisen-
berry et al.*, 1994; *Poletika and Jury*, 1994; *Buchter et al.*, 1995; *Stagnitti et al.*,
1998; *de Rooij and Stagnitti*, 2000; *Strock et al.*, 2001) or *in situ*(*Boll et al.*,
1997).

   Multi-compartment samplers provide large amounts of temporal and spatial
solute transport data. The breakthrough curve (BTC) captures the temporal
aspect of solute leaching, which describes the travel time of solutes at a given
depth (*Jury and Roth*, 1990). The spatial aspect can be described by the
spatial solute distribution curve (SSDC) (*Stagnitti et al.*, 1999; *de Rooij and
Stagnitti*, 2000). Both aspects are combined in the leaching surface (*de Rooij
and Stagnitti*, 2002a,b, 2004).

   In order to compare leaching surfaces from different experiments and from
different soils a quantitative analysis of the leaching surface is important. In
Chapter 6 we introduced a method to quantify the leaching surface in four to

---

This chapter is a slightly modified version of the manuscript: Bloem, E., M. de
Gee, and G. H. de Rooij, An alternative fitting procedure for the leaching surface
parameters

eight parameters. The parameterization requires the BTCs of the individual compartments of a multi-compartment sampler, scaled to have a unit area underneath the curve. These BTCs give the flux concentration as a function of time or cumulative drainage (BTC$_C$s), and are parameterized by a pore water velocity and a dispersion coefficient. The scaled BTC$_C$s are transformed into fitted BTCs based on flux densities (BTC$_F$s) by multiplying each by a scaling factor derived from the Beta distribution fitted to an approximated SSDC. The ensemble of BTC$_F$s thus obtained comprises the leaching surface if plotted adjacent to one another in order of decreasing area underneath the curve. The approximation is not always optimal, partly because water flux densities were summed over time and space.

Therefore, in this chapter, we parameterize solute flux densities directly from BTCs of the solute flux density (BTC$_F$s), thereby bypassing the approximation. We develop a method to quantitatively characterize leaching surfaces in analogy of the method presented in Chapter 6. This is achieved by a separate parameterization of the spatial and temporal aspects of solute leaching. For the temporal aspect, we determine the parameters of the individual BTC$_F$s by model analysis. We then detect and parameterize any relationships between the transport velocities and dispersion coefficients of the individual BTC$_F$s. The spatial aspect is parameterized using the Beta distribution as outlined by *Stagnitti et al.* (1999); *de Rooij and Stagnitti* (2000, 2004).

The best-fit parameters thus provide a quantitative and objective representation of the leaching surface. This allows a quantitative description of leaching surfaces, providing a means to objectively compare leaching characteristics of different soils, and even of the same soil in different seasons. We present the theory and apply this method to the three leaching surfaces discussed in Chapters 4 and 5.

7.2 Materials and Methods

7.2.1 Field experiment with metal and membrane samplers

We used two variable-suction multi-compartment samplers of the type developed in Chapter 3, one with metal porous plates (metal sampler) and one with a porous membrane (membrane sampler), both with 10 × 10 sampling compartments. The metal sampler compartments each had a sampling area of 10.35 cm^2. This sampler was installed in the field (Vreedepeel, the Netherlands) at 31 cm depth as described in Chapter 5. The membrane sampler had compartments of 10.57 cm^2. This sampler was installed in the same field at 25 cm depth as described in Chapter 5.

On the 14th of December 2005 we cut the grass in the 0.70 × 0.70 m area above each sampler to 3 cm and applied 4.5 mm of a 1 M CaCl$_2$*2H$_2$O solution. To eliminate the side effects of converging and diverging streamlines of the chloride concentration, the tracer solution was applied on 0.70 × 0.70 m

plots. To do this, we covered each application area with a 21 × 21 cell PVC grid, with a syringe holder in the center of each cell. For each plot, we filled 441 medical 10 ml syringes with 5 ml tracer solution (C.V. = 0.7 %), and placed these in the syringe holders. We then emptied all syringes within two minutes to achieve a spatially uniform tracer pulse application.

After each rainfall event, usually a cluster of small rain showers (of which 11 occurred during the experiment), the collected leachate was extracted from the sampling compartments while leaving the samplers buried in-situ. The collected volumes were determined and the solute concentrations were derived from the EC as measured with an EC meter (Cond 315i and TetraCon325 from WTW; individually calibrated). After 145 days (11 sampling rounds), nearly all tracer had passed the sampling depth. The mass collected during the final sampling round was less than 0.01 % of the applied mass over the sampling areas. The results of this experiment are described in Chapter 5.

7.2.2   Laboratory experiment with nylon sampler

We used a variable-suction multi-compartment sampler of the type developed in Chapter 3 with a nylon cover (nylon sampler). The nylon sampler consisted of 10×10 compartments, each with a sampling area of 10.35 m^2. A soil monolith (length 43 cm × width 43 cm × height 29 cm) was placed on top of the nylon sampler as described in Chapter 4. With this set-up, a leaching experiment was performed. We uniformly applied a pulse of 8 mm of 3.699 g l^{-1} NaBr solution above the sampler over an area of 35 × 35 cm. The pulse was leached out by artificial rain showers of 71 mm each (rainfall rate: 8 mm h^{-1}).

During and after each water application event, we collected leachate samples as often as required to prevent individual sample collection compartments from overflowing. The collected volumes were measured and the solute concentration was determined by ion chromatography (US EPA method 300). After 400 mm of drainage, nearly all tracer had passed the sampling depth. The results of this experiment are described in Chapter 4.

7.3   Modified fitting procedure

The outflow area of a multi-compartment sampler is divided into small compartments with the positions of their centers indicated by Cartesian coordinates (x_i, y_j) [L]. The effluent into these compartments is collected at several points t_k [T] in time, and each time the volume V [L^3] of collected drainage and its solute concentration C [ML^{-3}] are measured. Their product gives the collected solute mass. By dividing the mass by the compartment area and by the sampling time interval $t_k - t_{k-1}$, the solute flux density is found. The results per compartment with respect to time give the solute flux density breakthrough curves BTC$_F$s.

The leaching surface is obtained by ranking the sampling compartments in decreasing order of their total collected solute over the entire leaching period,

and then plotting the corresponding breakthrough functions BTC_F against the cumulative sampling area s. In this way, the two spatial coordinates x and y are collapsed into a single pseudo-spatial variable s.

de Rooij and Stagnitti (2002a) proposed to scale the solute flux densities by dividing them by the total amount of solute captured to facilitate comparison. The resulting variable $S(s,t)$ has dimensions $[\mathrm{L}^{-2}\mathrm{T}^{-1}]$.

The BTCs conveyed the temporal aspect of the leaching surface. To characterize the solute flux density BTC of a single compartment, we used CXTFIT (*Toride et al.*, 1999). In doing so we disregarded the fact that CXTFIT expects normalized flux concentrations on input to estimate the pore water velocity and the dispersion coefficient from a solution to the convection-dispersion equation. The fitted pore water velocity should be interpreted as an average solute velocity, and the fitted dispersion coefficient as a descriptor of the spreading of this solute velocity around its mean. We model the scaled BTC_F (area underneath the curve equal to one) for each compartment as the solution of a conventional one-dimensional equilibrium CDE, without modifications (*Toride et al.*, 1999). In our experiments we used a conservative tracer, and therefore set the retardation factor R to 1 and the degradation and production coefficients to zero. The solute application was modeled as a Dirac delta pulse. We used the solution for flux-averaged concentrations (*Toride et al.*, 1999).

$$C^*(t) = \left(\frac{L^2}{4\pi D t^3} \right)^{\frac{1}{2}} \exp \left(\frac{(L - vt)^2}{4Dt} \right) \tag{7.1}$$

with L denoting the depth of the sampling area [L] and C^* the scaled concentration. In our case we use in Eq. (7.1) the scaled solute flux density instead of the scaled concentration.

The area under each observed BTC_F is represented by C_0. CXTFIT returned the velocity v and dispersion coefficient D as additional parameters to describe the observed BTC_F.

With our 100-compartment samplers, that leaves us with 300 parameters. We reduced that number by fitting flexible expressions that related v and D to s:

$$v(s) = a_v s^{b_v} + c_v \tag{7.2}$$
$$D(s) = a_D s^{b_D} + c_D \tag{7.3}$$

where a_v, a_D, b_v, b_D, c_v, and c_D are fitting parameters. We now have at most six parameters to describe the temporal redistribution of solutes, but still have 100 values of C_0 that describe the spatial distribution of the leached solute.

By integrating the leaching surface with respect to t we obtain the spatial solute distribution curve (*Stagnitti et al.*, 1999; *de Rooij and Stagnitti*, 2000)

$$\mathrm{SSDC}(s) = \int_0^\infty S(s,t)\mathrm{d}t \tag{7.4}$$

This function represents the spatial aspect of the leaching surface. For each compartment, SSDC(s) is the integral of the corresponding BTC$_F$. Owing to the ranking of compartments that led to the creation of the coordinate s, SSDC is a non-negative monotonously decreasing function of s. For $S(s,t)$ scaled as indicated above, SSDC integrates to unity over the full range of s, and the value of SSDC and C_0 for any particular s differ only by a constant. Therefore, SSDC(s) can be used equally well as the set of observed C_0 to capture the spatial redistribution of solutes (see *de Rooij and Stagnitti* (2000), for a detailed discussion). This is a major advantage over the analysis based on flux concentration BTCs in Chapter 6.

The scaled SSDC(s) can often be fitted very well by a Beta distribution (*Stagnitti et al.*, 1999; *de Rooij and Stagnitti*, 2004)

$$p(x, \alpha, \zeta) = B(\alpha, \zeta) x^{\alpha-1} (1-x)^{\zeta-1}, \qquad 0 \le x \le 1 \tag{7.5}$$

where p is the probability of the Beta variate as a function of coordinate x,

$$B(\alpha, \zeta) = \frac{\Gamma(\alpha+\zeta)}{\Gamma(\alpha)\Gamma(\zeta)} \tag{7.6}$$

is the Beta function, and α and ζ are positive shape parameters (*de Rooij and Stagnitti*, 2004; *Nadarajah and Gupta*, 2004). The mean, variance and coefficient of variation CV of the Beta distribution are (*Gupta and Nadarajah*, 2004)

$$\mu(\alpha, \zeta) = \frac{\alpha}{\alpha+\zeta} \tag{7.7}$$

$$\sigma^2(\alpha, \zeta) = \frac{\alpha\zeta}{(\alpha+\zeta)^2(\alpha+\zeta+1)} \tag{7.8}$$

$$\mathrm{CV}(\alpha, \zeta) = \sqrt{\frac{\zeta}{\alpha(\alpha+\zeta+1)}} \tag{7.9}$$

Note that the uniform distribution arises by setting $\alpha = \zeta = 1$, with a coefficient of variation $3^{-1/2}$.

Note that the coordinate x is obtained by scaling s to run from zero to one. We scaled s accordingly, scaled the C_0 values to ensure they added up to one, and then fitted the Beta distribution to describe the scaled C_0 as a function of s. Thus, we found two parameters for capturing the spatial aspect of the leaching surface.

The combination of the six breakthrough-related parameters and the two spatial parameters yields a quantitative description of the leaching surface.

The parametric expression for Eq. (7.1), using the scaled solute flux densities F^* is given by

$$F^*(s,t) = \left(\frac{L^2}{4\pi \left(a_D s^{b_D} + c_D\right) t^3} \right)^{\frac{1}{2}} \exp\left(\frac{\left(L - \left(a_v s^{b_v} + c_v\right) t\right)^2}{4 \left(a_D s^{b_D} + c_D\right) t} \right) \tag{7.10}$$

The parametric expression for the leaching surface based on solute flux density (F) combines Eq. (7.10), the temporal aspect of solute leaching with Eq. (7.5), the spatial aspect of solute leaching

$$
\begin{aligned}
F(s,t) = & B(\alpha, \zeta) \left(\frac{s}{s_{\max}} \right)^{\alpha-1} \left(1 - \frac{s}{s_{\max}} \right)^{\zeta-1} \cdot \\
& \left(\frac{L^2}{4\pi \left(a_D s^{b_D} + c_D \right) t^3} \right)^{\frac{1}{2}} \exp \left(\frac{\left(L - \left(a_v s^{b_v} + c_v \right) t \right)^2}{4 \left(a_D s^{b_D} + c_D \right) t} \right)
\end{aligned}
\tag{7.11}
$$

To reduce irregularities caused by the non-steady input of water, we substituted the time-axis [T] by the cumulative drainage axis [L], measured over the entire sampling area (*van Ommen et al.*, 1989; *Jury et al.*, 1991).

We fitted the leaching surfaces of the three samplers as outlined above. For comparison we also constructed the leaching surface based on flux density directly from the 100 fitted values of v and D, using the observed values of C_0 to scale the fitted BTCs. Hereby we can see how well the CXTFIT program fitted the BTCs. We also constructed the leaching surface by applying the fitted Beta distribution directly to the observed flux density BTCs to see how well the Beta distribution fitted our data.

For the membrane sampler at the Dutch field site, some of the BTCs did not converge with CXTFIT, therefore this resulted in a zero velocity. These eight BTCs have not been taken into account when calculating the average velocity and dispersion coefficient. The same holds for a few BTCs of the nylon sampler under the Australian soil.

We calculated the normalized mean root mean square error (RMSE) between the observed and fitted leaching surface by

$$
\text{RMSE}_{\text{nm}} = \frac{\sum\limits_{i=1}^{w} \sqrt{\sum\limits_{k=1}^{m} \left(F_O(i, k) - F_P(i, k)^2 \right)}}{\sum\limits_{i=1}^{w} \sum\limits_{k=1}^{m} F_O(i, k)} \cdot 100\%
\tag{7.12}
$$

with subscript O denoting observed solute flux densities, and subscript P indicated their calculated counterparts of the sorted compartments, with w denoting the number of compartments. Counter k gives the number of the sampling rounds. The total number of sampling rounds is m.

7.4   Results and discussion

In Fig. 7.1 the leaching surfaces for all three experiments are presented. The leaching surfaces from the two samplers at the Dutch field site with a sandy, fairly moist, hydrophyllic soil are quite similar (Fig. 7.1 a and b), but very different from those of the Australian soil (poorly sorted, clayey, with some
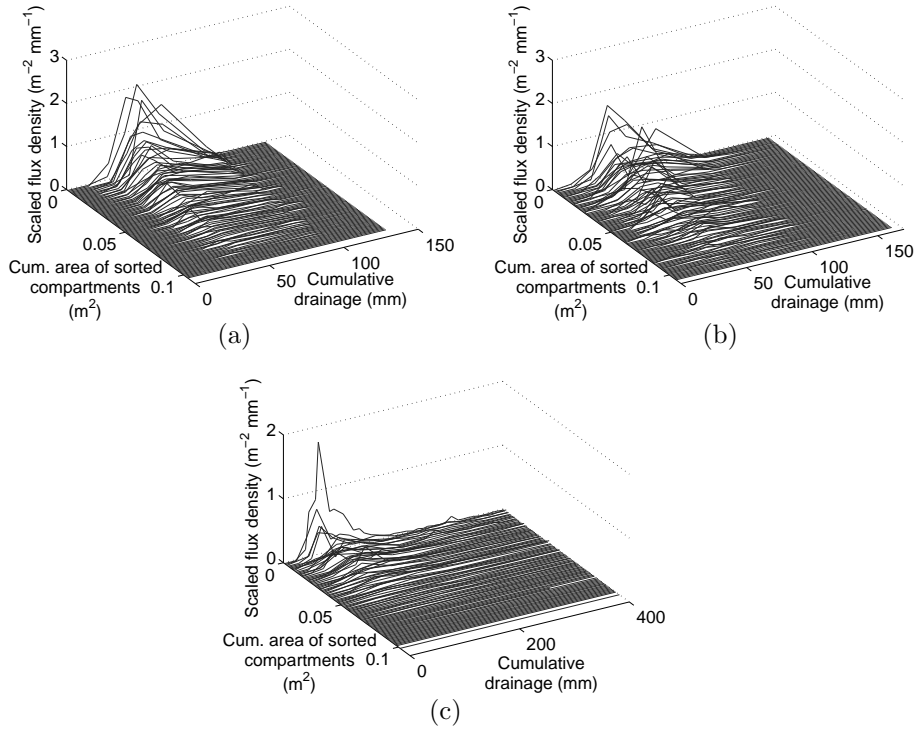
Figure 7.1: Leaching surfaces based on scaled flux density for the metal sampler experiment (a), the membrane sampler experiment (b), and the nylon sampler experiment (c).

stones) (Fig. 7.1c). One individual compartment was dominant in the Australian soil, suggesting the possibility of macropore flow. The Australian soil also required much more drainage to leach the tracer from the soil, pointing at the presence of areas of low flow or zones with immobile water (*van Genuchten and Wierenga*, 1976).

The SSDCs of the Dutch and the Australian soil again are different (Fig. 7.2; Table 7.1) but not as dramatically as the leaching surface. The Beta distribution produced an excellent fit in all cases, even for the Australian soil with one dominating compartment.

The fitted pore water velocities v $[LT^{-1}]$ and dispersion coefficients D $[L^2T^{-1}]$ are given in Figure 7.3 and Table 7.1. Pore water velocities appear fairly uniform at the Dutch field site at the scale of the sampling area, but vary between the two samplers. Tracer tests at the end of the experiment revealed no anomalies in the vertical flow above the sampler, and we therefore consider it probable that the difference between the samplers was caused by soil spatial variation at the scale of a few meters. The dispersion coefficients seem to have no convincing trend either within or between samplers, but differ considerably

113
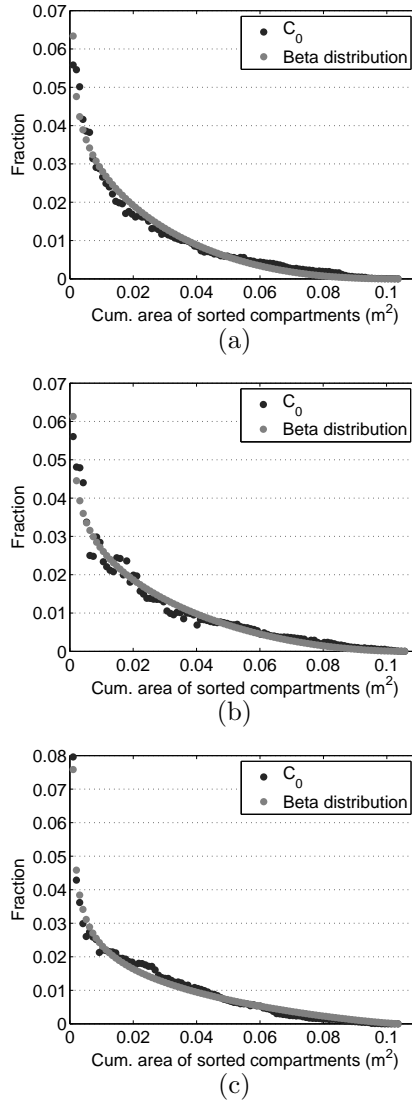
Figure 7.2: Observed areas under the flux density breakthrough curves (C_0) for the ranked compartments of the various multi-compartment samplers, as well as the fitted Beta distribution (see Table 7.1 for parameter values). Results for the metal sampler experiment (a), the membrane sampler experiment (b), and the nylon sampler experiment (c).

Figure 7.3: CXTFIT curve fitting results for the velocity v (a, b, e) and dispersion coefficient D (b, d, f) of the 100 sorted scaled BTC_Fs based on flux density. Results for the metal sampler experiment (a and b), the membrane sampler experiment (c and d), and the nylon sampler experiment (e and f).

within the samplers, resulting in a high CV. In the Australian soil, both the pore water velocity and the dispersion decrease with increasing s. Here also the variation around the trend for the dispersion coefficient is high. The BTC_Fs of individua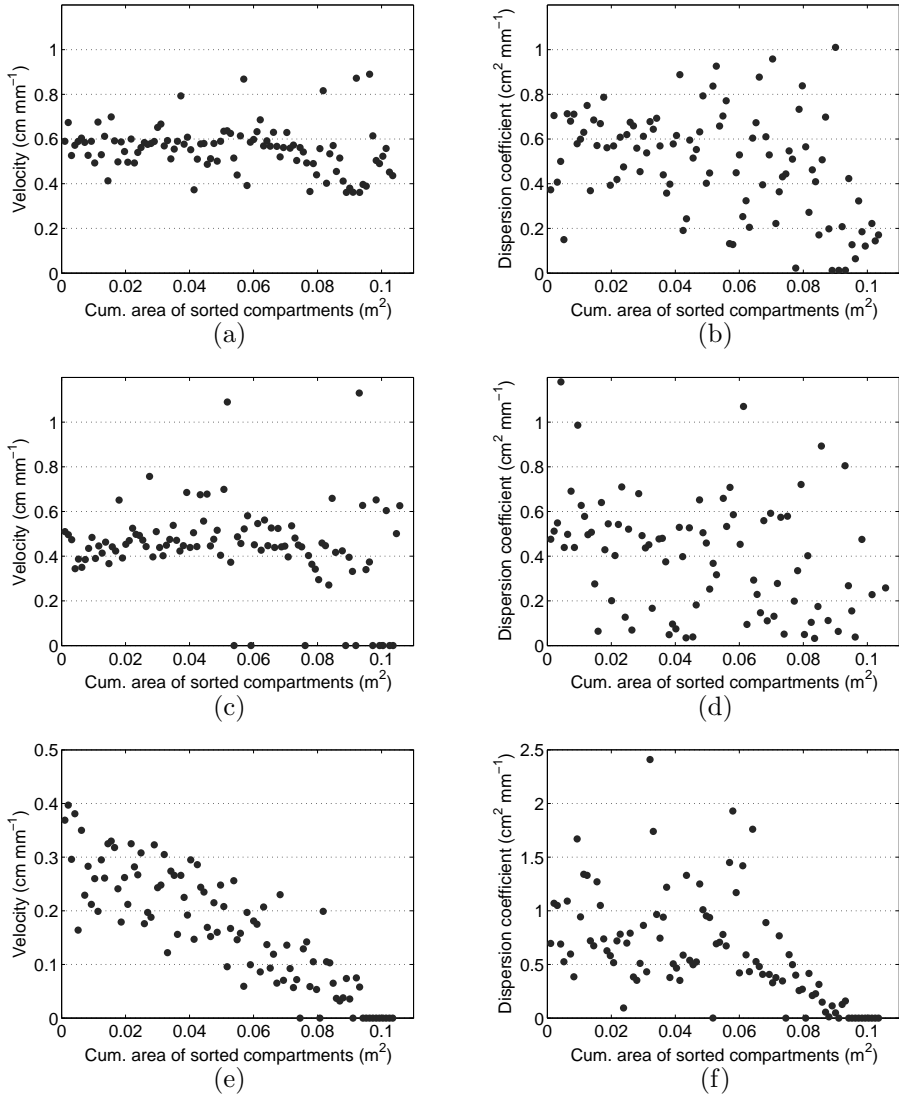l cells were fitted well by CXTFIT (small errors in Table 7.2) and the Figures 7.4a and b, 7.4e and f, and 7.4i and j show a good resemblance with the original scaled BTC_Fs.

The absence of a trend for the Dutch soil allowed us to replace $v(s)$ and $D(s)$ of the metal and membrane samplers by their respective mean values for all s. The lack of a trend is consistent with efficient lateral mixing, which is considered to be reflecting a convective-dispersive transport mechanism (*Flühler et al.*, 1996). Replacing the actual measurements by smooth breakthrough curves calculated from fitted v and D increased the normalized mean RMSE for the scaled BTC_Fs significantly. The averaged results (Figs. 7.4c and g) produce less peaky leaching surfaces than those observed at the Dutch field site (Figs. 7.4a and e); this feature is well preserved when the CXTFIT approximations for each compartment are used, as can be seen in Figs. 7.4b and f.

In the qualitative approach, we sampled velocity and dispersion values from a normal distribution about the averaged velocity and averaged dispersion coefficient. When we use these parameter values to construct a leaching surface that looks similar to the observed leaching surface, we see that the results for the scaled flux densities show a good resemblance for the metal sampler in the Dutch soil (Fig. 7.4d). For the membrane experiment, however, the large standard deviation of D and, to a lesser extent, v, generated some excessively large values in the reproduced leaching surface (Fig. 7.4h).

Replacing the actual measurements by smooth breakthrough curves calculated from fitted v and D and scaled by the value of the fit to the SSDC for the value of s corresponding to each BTC gave somewhat smoother but still accurate leaching surfaces of the flux densities (Figs. 7.5b, f, j). We completed

Table 7.1: Statistics of the population of fitted parameters (v and D for the metal and membrane samplers), the fitted parameter values if only a single fit was required (α and ζ), and the fitted relationship between v and s, and between D and s (nylon sampler).

Sampler		v (cm mm^{-1})	D (cm^2 mm^{-1})	α	ζ
Metal	Mean	0.559	0.516	0.824	3.374
	STDEV	0.099	0.223		
	CV (%)	17.67	43.26		
Membrane	Mean	0.484	0.470	0.800	2.916
	STDEV	0.134	0.402		
	CV (%)	27.81	85.37		
Nylon	Mean	$-2.8663s + 0.3211$	$-7.0388s + 1.0234$	0.689	2.214

116

the parametric fit of the leaching surfaces by replacing the individual values of v and D by their mean values for the samplers in the Dutch field site (Figs. 7.4c and g). Applying the Beta distribution to the averaged results does not alter the data any further (Figs. 7.5c and g). The normalized mean RMSE even improved slightly to 19 % for the metal sampler and 30 % for the membrane sampler.

The qualitative results (Figs. 7.5d and h) show here a better similarity to the real leaching surfaces (Figs. 7.5a and e), although the highest peak is still much larger for the simulated leaching surfaces than in reality.

The Beta distribution fit the data very well (Figs. 7.5a and b). Applying the Beta distribution directly to the observed scaled flux densities resulted in Figs. 7.6b and f. The normalized mean RMSE related to this fit is 7 % for the metal sampler and 8 % for the membrane sampler.

The Australian soil exhibited clear trends of v and D with s (Fig. 7.3); we replaced the individual values $v(s)$ and $D(s)$ by their linear regression fit to produce Fig. 7.4k.

By applying the Beta distribution to the scaled flux densities for the nylon experiment we obtained the scaled parametric leaching surface based on flux density (Fig. 7.5k). The smooth fitted leaching surface missed the peak and the narrow BTC of the first dominant compartment, stressing its deviation of that compartment from the average behavior as reflected by the fitted surface, which generally represents the observed leaching surface rather well. The normalized mean RMSE here is of the same order as that of the metal sampler (Table 7.2).

Applying the Beta function directly to the observed scaled flux densities leads to an error of 4 %. The resulting leaching surface (Fig. 7.6f) does show

Table 7.2: The normalized mean root mean square error (RMSE) (%) between the observed and parameterized leaching surfaces based on flux density scaled per BTC and between the observed and parameterized scaled leaching surface based on flux density. For the leaching surfaces scaled by each BTC_F the errors have been calculated for the fitted v and D, for the averaged v and D. For the scaled leaching surface based on flux density we calculated the error for the fit if the Beta distribution has been applied directly on the observed BTC_F, and after the fitted v and D, and the averaged v and D.

	Fit	Metal	Membrane	Nylon
		normalized mean RMSE (%)		
scaled	Direct	0	0	0
per BTC	v and D fitted	10.0	16.3	10.9
BTC_F	v and D averaged	26.6	40.1	23.4
scaled	Direct	6.8	7.9	3.8
BTC_F	v and D fitted	10.3	14.1	12.1
	v and D averaged	19.6	30.3	20.1
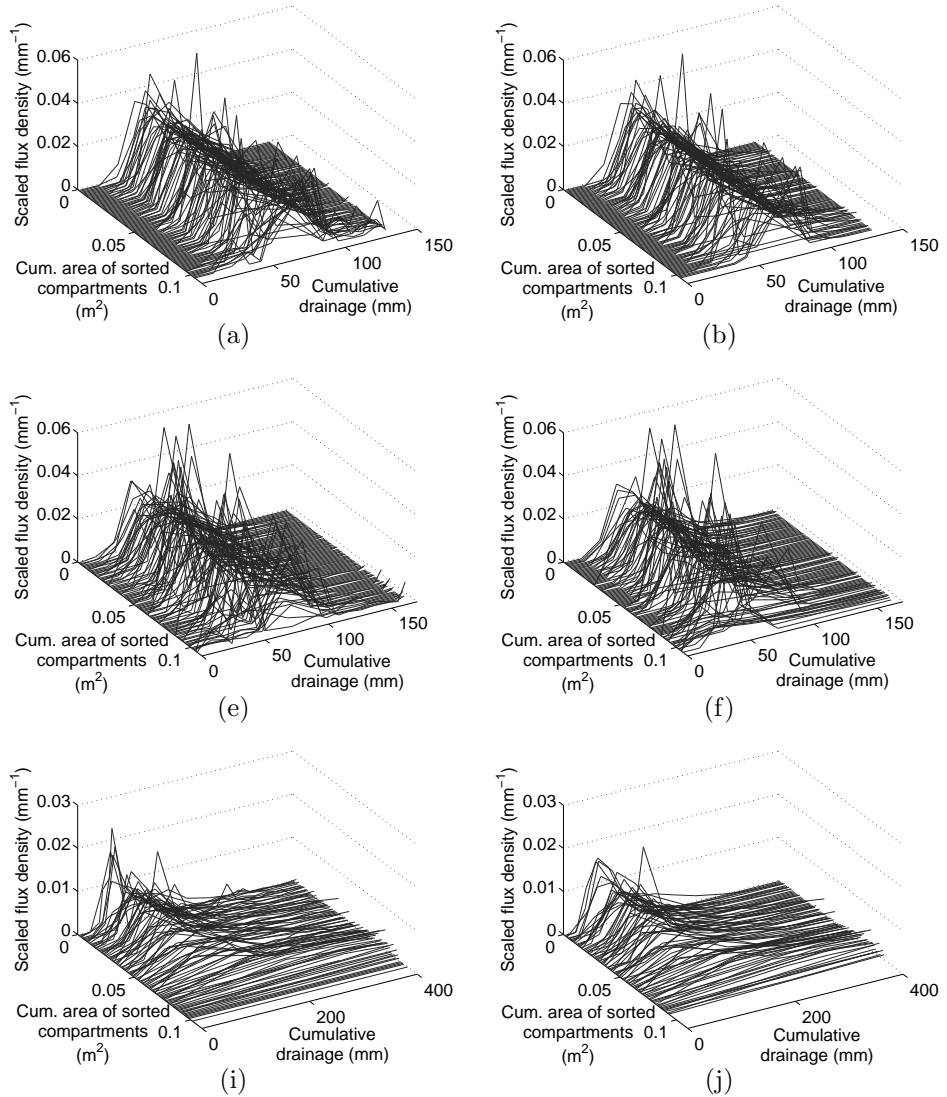
Figure 7.4: The observed scaled leaching surface based on flux density (a, e, i), with all individual breakthrough curves scaled to integrate to unity. The scaled leaching surface based on flux density for the calculated v and D per BTC_F, fitted with CXTFIT (b, f, j), the scaled leaching surface based on flux density with the average v and average D as given in Table 7.1 (c, g, k), and the scaled leaching surface based on flux density with a qualitative approach (d, h). Results for the metal sampler experiment (a, b, c, and d), the membrane sampler experiment (e, f, g and h), and the nylon sampler experiment (i, j, and k) (continued on p. 119).

118

(c)

(d)

(g)

(h)

(k)

Figure 7.4: Continued from p. 118.

Figure 7.5: The observed scaled leaching surface based on flux density (a, e, i) and parameterizations: scaled leaching surfaces based on flux density are constructed on the calculated v and D per BTC_F together with the fitted Beta distribution (b, f, j), the average v and D (Table 7.1) with the fitted Beta distribution (c, g, k), and a qualitative fit of v and D together with the fitted Beta distribution (d, h). Results for the metal sampler experiment (a, b, c, and d), the membrane sampler experiment (e, f, g and h), and the nylon sampler experiment (i, j, and k)

120

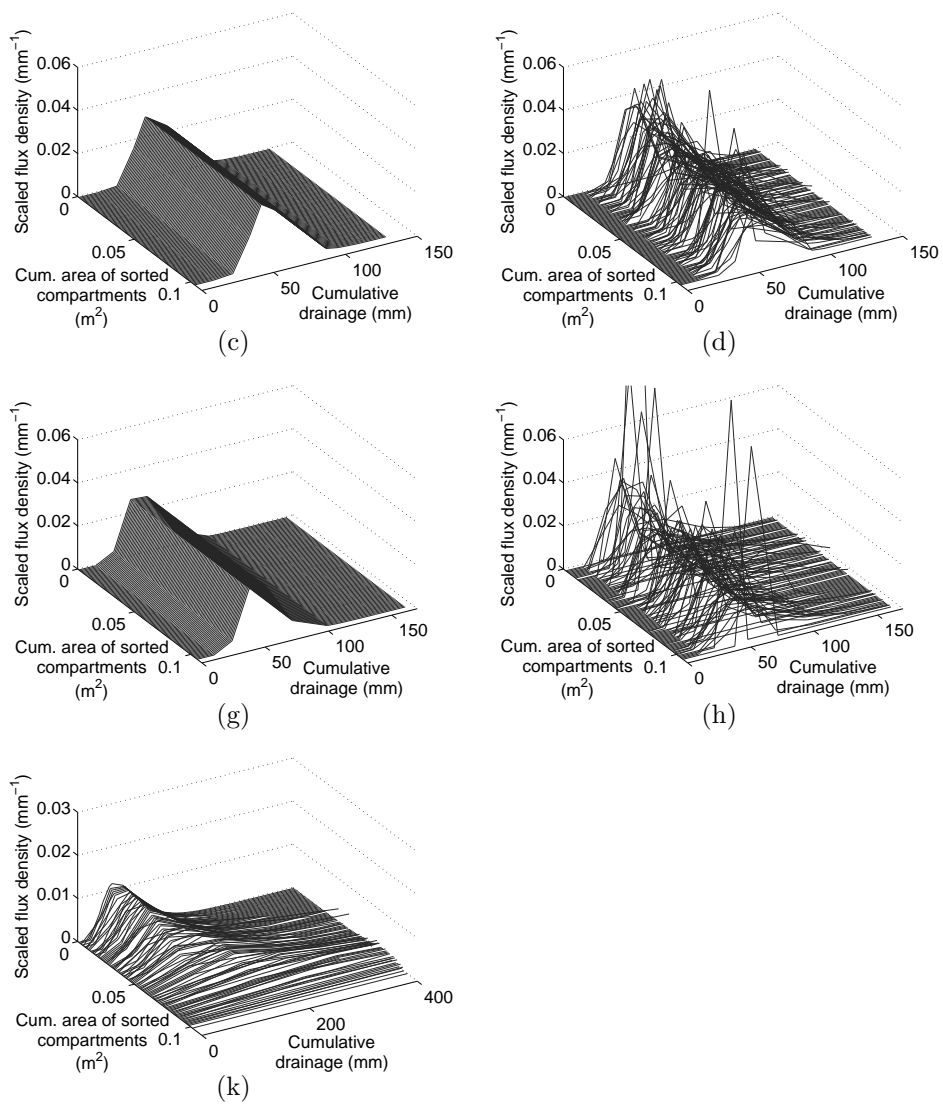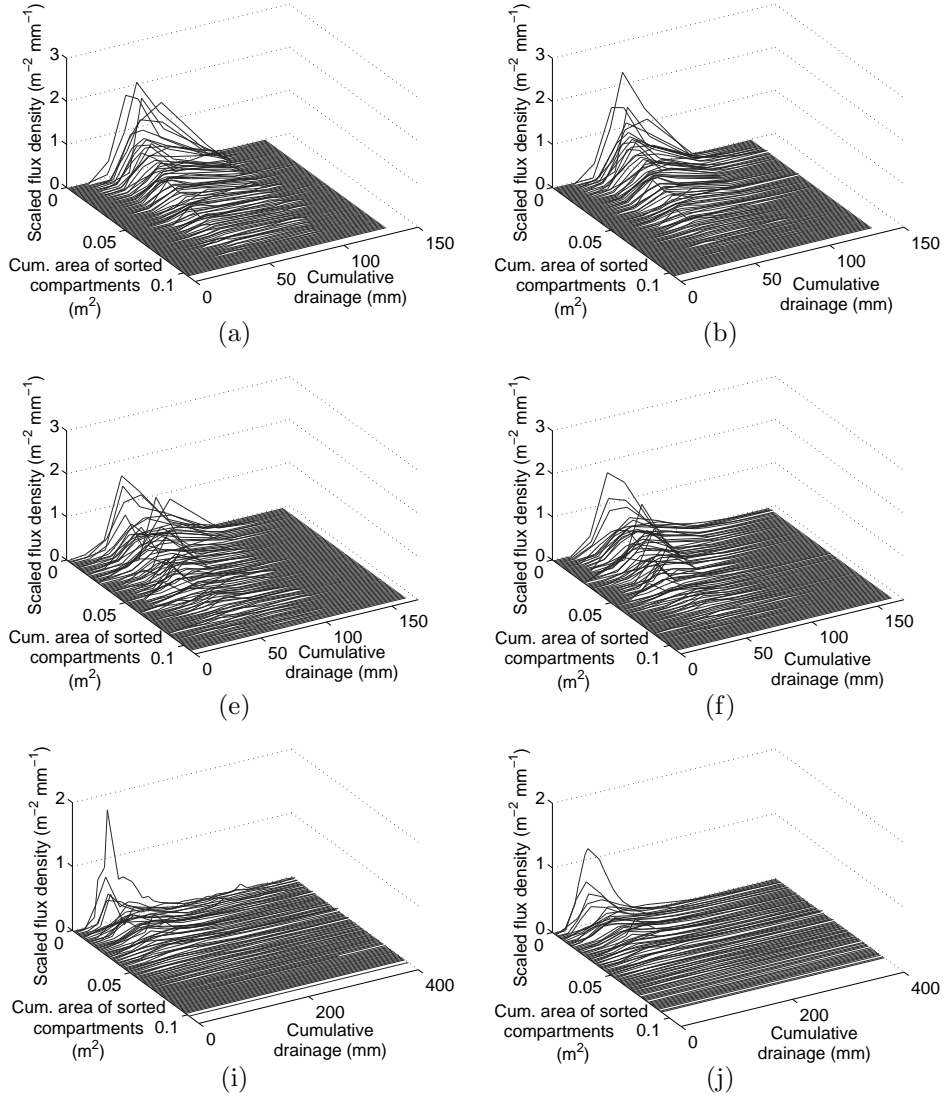**Figure 7.5:** Continued from p. 120.
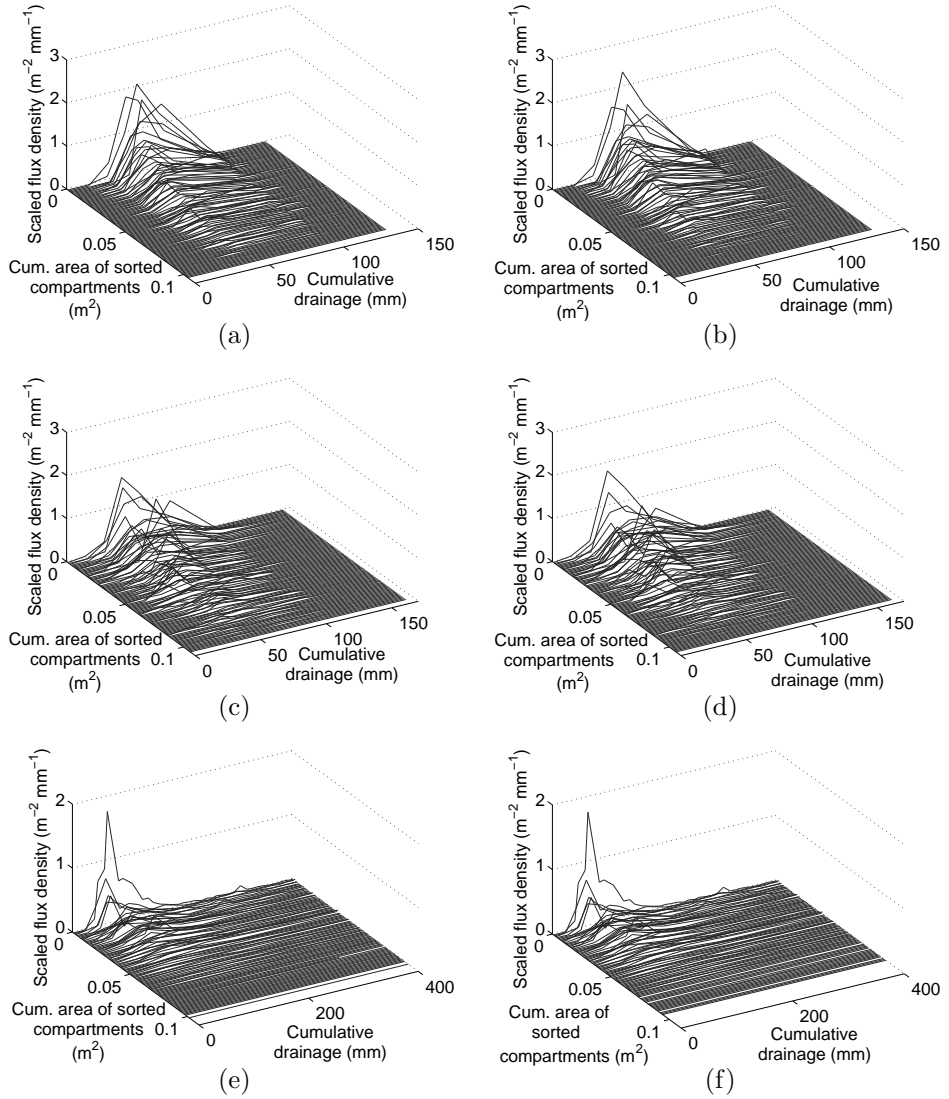
Figure 7.6: The observed scaled leaching surface based on flux density (a, c, e) and the parameterizations: scaled leaching surface based on flux density constructed on the observed scaled BTC_F together with the fitted Beta distribution (b, d, f). Results for the metal sampler experiment (a, b), the membrane sampler experiment (c, d), and the nylon sampler experiment (e, f).

the first peak of the BTC very well. Also the pattern is identical to the observed leaching surface.

Despite the fact that the Australian fit required five parameters and the Dutch fits only four, the goodness-of-fits (RMSE) were not significantly different (Table 7.2), reflecting the different natures of the observed leaching surface. Still, all fitted leaching surfaces appeared to capture the main pattern of the observed leaching surfaces rather well.

7.5 Conclusions

We developed a method to approximate the leaching surface S using only a few parameters. This method is based on the flux density BTCs directly. The resulting approximation showed to have a good resemblance to the real leaching surface. The quantitative approach showed its advantages. The quantitative method showed that it is possible with only four to eight parameters to parameterize the leaching surface.

CHAPTER 8

Summary and conclusions

8.1 Summary and conclusions

The experimental and theoretical work reported in this thesis improves our the
ability to observe subsurface solute transport and increases the understanding
of solute redistribution as it travels through the subsurface with the flowing
water.

The numerical aquifer study (Chapter 2) showed the differences between the
use of resident and flux concentrations. Although these differences are theoreti-
cally well understood, the practical difficulties of measuring flux concentrations
still lead to measurement protocols that generate resident concentrations, or
a concentration somewhere between a resident and a flux concentration. It
was demonstrated that assessing solute movement from resident concentra-
tions should be done with care. Only if the local concentrations vary weakly
within the pore space, resident concentrations will give reliable results. This
conclusion implies that to reduce local concentration gradients, diffusion and
dispersion must have had sufficient time. The numerical study showed that to
acquire the necessary degree of local mixing for a realistic degree of heterogene-
ity, travel distances of 70 m are still insufficient.

In the range where resident and flux concentrations have not yet converged,
moment analysis can help to improve the results obtained from resident concen-
tration observations. Moment analysis works well if solute transport is analyzed
over an entire cross-section of the aquifer, but performs poorly on the scale of
individual numerical grid cells, mainly because it approximates local pore wa-
ter velocities by averages over the entire trajectory upstream of the location of
interest.

It is likely that the difference between resident and flux concentrations in-

creases with increasing aquifer heterogeneity and with increasing connectivity of conductive areas. The degree of heterogeneity in this study was by no means extreme. For aquifers with a more pronounced variation and / or high flow regions, the conclusions drawn above become even more pertinent. It is therefore desirable to develop methodologies for measuring flux concentrations.

The massive amount of solute transport data described in Chapter 2 has been organized in leaching surfaces for the analysis. This helped to pinpoint and clearly show the weak points of using resident concentrations.

While the measurement of flux concentrations in aquifers will probably remain very difficult for years to come, there is much more promise in unsaturated zone research. Inspiration was taken from progress made by different groups in developing sophisticated soil solution samplers to design and construct a new variable-suction multi-compartment sampler (Chapter 3). The sampler contained 100 compartments, each with a size of 31.5 × 31.5 mm, closed with a porous cover. The sampler had a sample collection chamber in which a variable suction could be maintained. With this set-up, high suction can be maintained in a sampler that is much shorter than a wick sampler, making the instrument excellently suited for areas with shallow groundwater tables. In view of the desire to be able to sample various reactive compounds, three separate prototypes with different porous covers were constructed: one with a polyamide fiber nylon mesh 'nylon sampler', another with sintered porous stainless steel 316 metal plates 'metal sampler', and one with a polyamide membrane 'membrane sampler'. To resemble ambient conditions, a pump kept the pressure head within the sampler, if necessary with a correction factor for pressure head loss over the porous cover, at the same level as the ambient pressure head at the same depth. Drop counters accurately registered the percolation for each compartment with an unprecedented 5-minute temporal resolution.

In laboratory and field trials we established operating conditions for the various porous covers. Not surprisingly, there appeared to be a trade-off between conductivity and the air-entry value. The selection of the porous cover for a particular application should take into account the ambient pressure head regime at the experimental site, the speed with which the various covers dry out during prolonged dry periods, and the desired sturdiness of the cover. Rewetting upon the arrival of a wetting front did not pose major problems for those covers that were subjected to dry conditions. The support for the membrane cover however is less suitable for long dry periods during which the support dries out and deformation occurs. Therefore it is desirable to construct a new support for the membrane cover.

During flow the suction control ideally should take into account the pressure drop over the porous cover. Because the flux densities vary greatly between compartments but the applied suction within the sampler does not, we suggest to keep on the safe side by correcting for the pressure drop during fairly high percolation rates. This was only an issue for the metal sampler though; the other samplers had such thin porous covers that the pressure drop over them was negligible. All things considered, the membrane sampler performed best,

while the metal sampler is also recommendable.

The experiments with the samplers gave a wealth of new information. For instance, the 5-minute drop counter readings allowed us to monitor in detail the response to individual rain showers. The heterogeneity of the drainage patterns during a field experiment as captured with the samplers indicated that the size of the samplers was adequate.

The samplers' long-term performance under harsh field conditions was very convincing. This makes them suitable for a wide range of applications. The drop counters allow detailed studies of a soil's response to rainfall at any desired depth above the phreatic level, which is e.g. useful for water management purposes. For agricultural research the instrument can prove its value by showing intricate details of solute movement in soils not accessible for observation before. This can be of great value in cases where small amounts of leaching are important (e.g. for pesticides and phosphate) or where the uniformity of the distribution in the soil is relevant (e.g. nematicides).

The nylon sampler has been used in the laboratory for a wastewater application project in Australia (Chapter 4). It helped to monitor the leaching from a soil monolith of a vineyard clay loam soil under an irrigation regime which in summer augments the amount of rainfall with application of treated sewage water, while during winter completely relies on rainfall. We noted that the chloride in the wastewater kept leaching through the winter, with the average outflow concentration reduced to 3 % of the input concentration (less than 1 % for the high-flow compartments) at the end of the winter. This showed that the summer irrigation of wastewater causes a year-round pollution of the groundwater with chloride, associated with high EC levels in the soil during the growing season and posing a threat to the scarce fresh groundwater below.

The experiment also involved a pulse application of bromide, which produced a leaching surface comparable to that of the chloride. The main difference was the elevated chloride content of drainage water from cells that produced only small volumes. The bromide pulse resided in the soil too shortly to be able to reach the less mobile water. This was corroborated by large differences in bromide concentrations in the percolate, while the chloride concentrations became fairly uniform as time progressed, apparently caused by diffusion-dominated slow lateral spreading.

To quantitatively analyze solute leaching in a sandy soil, the metal and membrane multi-compartment samplers were installed 2 m apart in a field experiment under natural circumstances in Vredepeel, the Netherlands (Chapter 5). In addition to a chloride tracer, a dye tracer was applied at the end of the experiment. This method yielded information that widely surpassed the information that can be provided by separate anionic and dye tracer trials, or by solute monitoring by coring or suction cups.

The spatial distribution of the dye tracer was similar to that of the chloride in the metal sampler. The spatial solute distribution curves (SSDCs) of the chloride tracers measured by the two samplers showed high similarities. The

leaching surfaces differed somewhat, mainly in the different volumes of drainage collected by the samplers.

In this hydrophilic soil without cracks or other obvious causes for preferential flow, the spatial distribution of drainage, the spatio-temporal redistribution of a pulsed tracer, and dye staining consistently indicated markedly non-uniform flow. The spatial scale of the heterogeneities could well be captured by the 32.5×32.5 cm samplers. The limited variation in times to peak, and the small range of total amounts of captured solute per cell compared to the range for captured drainage, indicated effective lateral solute exchange between stream tubes. Despite the small vertical travel distances (0.3 m), this exchange is consistent with a convective-dispersive transport regime. These and other diagnostic characteristics can be readily determined from leaching surfaces and from SSDCs and their equivalents for the spatial distribution of drainage. They are very helpful in identifying key solute transport processes in a given soil.

While the leaching surfaces proved their value, a method to describe them in quantitative terms would further enhance their use by facilitating comparison between different leaching surfaces. In Chapter 6 a procedure has been developed to capture the leaching surface in four to eight parameters. The procedure starts by fitting a pore water velocity (v) and a dispersion coefficient (D) for the breakthrough curve (BTC) of each compartment. The values of v and D are then expressed as a function of the pseudo-spatial coordinate of the leaching surface, that indicates the rank order in the sorted line up of the sampling compartments. This reduces the 100 values of v and D to two to six parameters, depending on the selected functional relationships. Finally, the spatial distribution of total leaching is approximated by a fit of the Beta distribution, adding another two parameters.

In Chapter 7 the fitting procedure has been modified to make it directly applicable to solute flux densities instead of flux concentrations, and a concise functional expression for the leaching surface is presented.

The parameter values of the two Dutch and one Australian leaching surface clearly reflected the similarity between the Dutch leaching surfaces that were consistent with convective-dispersive transport regime, and the contrast with the Australian leaching surface, which showed clear evidence of preferential flow and poor lateral mixing. The parameterization proved to be sufficiently flexible to capture both types of leaching surface quite well.

The leaching surfaces resulting from the fitting procedures in Chapter 6 and in Chapter 7 differed little. The parameters of the fits based on flux concentrations (Chapter 6) have a better defined physical meaning, while the parameterization based on solute flux densities (Chapter 7) is more direct and captures the leaching surface in a single equation.

One difference we observed between the two different methods is that the velocities and dispersion coefficients calculated with the program CXTFIT based

128

on the flux concentration show lower variations than those calculated on the basis of the solute flux densities. Therefore the averaging of the velocity and dispersion coefficient for the BTCs based on flux concentration gave a lower root mean square error than these for the BTCs of the solute flux density. But the flux concentration fits need to be transformed to solute flux densities. This step requires additional operations that turned out to increase the root mean square error of the fitted leaching surface to be similar to that of the directly parameterized BTCs based on solute flux density.

8.2   Opportunities for further research

Although the multi-compartment sampler served its task well during our experiments, improvements are still possible. One of the main points of attention is the rim surrounding the sampling area of the membrane sampler, which might cause boundary effects. Although no significant deviations were noticed during the performed experiments, the effects of this can be reduced in follow-up designs by minimizing its width. Further the support for the membrane cover needs to be improved to prevent deformation during dry periods. A few practical aspects can also be improved: at the moment the instrument is working on batteries, which is a practical disadvantage for long term projects, but can easily be improved. The sample retrieval is now done manually and could be automated, for instance with a pumping system and a manifold. This would drastically reduce the labor demand.

During our field experiment in Vredepeel, the Netherlands (Chapter 5) we have collected all the information about rainfall, ambient pressure head, pressure head inside the sampler, measured concentrations and volumes, and the properties of the soil. Besides this the properties of the porous covers are known. With this information the water and solute transport of the experiment can be simulated with a program like Hydrus2D (*Simúnek et al.*, 1999). As we have measured the actual fluxes during the experiment, a comparison can be made between the simulated results and our measured results. After calibrating the computational model, the leaching processes can be simulated and presented in an easier and more visible way, stimulating policy making on and practical use of the results.

For the quantitative parameterization of the leaching surface (Chapters 6 and 7) we only used four to six parameters to describe a complex system. This resulted in a 'smooth' model. Further research may focus on the scale and significance of the 'noise' (i.e. the measured minus parameterized leaching surfaces). The fitted leaching surface allows us to quantify the 'noise', paving the way for techniques such as residual analysis.

During this study we focused on the solute transport of conservative trac-

ers. The samplers we developed are also suitable for reactive transport. Experiments focusing on a wide variety of transport may further broaden our view on the transport of solutes in the soil.

APPENDIX A

Flux and resident concentrations

In a soil with water and solutes moving through the pore space we can define a water content field, a concentration field (both scalar fields), and a flux density field (vector field):

$$
\begin{aligned}
&\theta(x_1, x_2, x_3, t) \\
&C(x_1, x_2, x_3, t) \\
&q_1(x_1, x_2, x_3, t) \\
&q_2(x_1, x_2, x_3, t) \\
&q_3(x_1, x_2, x_3, t)
\end{aligned}
\tag{A.1}
$$

where θ denotes the volumetric water content, C [ML^{-3}] the point solute concentration, q_a [LT^{-1}] the flux density in principal direction a, x_a [L] the spatial coordinate in principal direction a, and t [T] time. In defining C as a point concentration, we imply that the scale of analysis is well beyond the molecular scale. For scales approaching the pore scale, the water content field becomes an indicator field that takes the value of 1 wherever liquid water is present, and equals 0 in the solid and gas phases. The other fields are only defined where the indicator field equals 1, and the flux density field is identical to the flow velocity field. For the scale of the representative elementary volume (REV), q represents the Darcian flux density, and θ is continuous but can have a (spatially variable) residual value below which flow cannot occur. All components of the flux density field are zero if θ is at its residual value.

Note that, even at this scale, q and θ are considered heterogeneous within the REV. Therefore, hydrodynamic dispersion is assumed to be captured by the variation of the flux density field and does not need to be described by a dispersion tensor. Molecular diffusion is the only spreading mechanism not accounted for the flux density field, and is neglected here.

The resident concentration within a given (incremental) soil volume can be calculated by weighting the concentrations in that volume by the volumes of water having these concentrations:

$$C^r(x_1, x_2, x_3, t) =$$

$$\lim_{\substack{\Delta x_1^* \downarrow 0 \\ \Delta x_2^* \downarrow 0 \\ \Delta x_3^* \downarrow 0}} \frac{\displaystyle\int_{x_1-\frac{1}{2}\Delta x_1^*}^{x_1+\frac{1}{2}\Delta x_1^*} \int_{x_2-\frac{1}{2}\Delta x_2^*}^{x_2+\frac{1}{2}\Delta x_2^*} \int_{x_3-\frac{1}{2}\Delta x_3^*}^{x_3+\frac{1}{2}\Delta x_3^*} \theta(\xi_1, \xi_2, \xi_3, t) C(\xi_1, \xi_2, \xi_3, t) \mathrm{d}\xi_3 \mathrm{d}\xi_2 \mathrm{d}\xi_1}{\displaystyle\int_{x_1-\frac{1}{2}\Delta x_1^*}^{x_1+\frac{1}{2}\Delta x_1^*} \int_{x_2-\frac{1}{2}\Delta x_2^*}^{x_2+\frac{1}{2}\Delta x_2^*} \int_{x_3-\frac{1}{2}\Delta x_3^*}^{x_3+\frac{1}{2}\Delta x_3^*} \theta(\xi_1, \xi_2, \xi_3, t) \mathrm{d}\xi_3 \mathrm{d}\xi_2 \mathrm{d}\xi_1}$$

$$(A.2)$$

where the superscript r denotes a resident concentration, and ξ_a [L] is an integration variable in direction a. The superscript * serves to distinguish the grid-scale length intervals from the larger scale travel distances elsewhere in the paper. Analogously, we define the flux concentration at an incremental area of a plane defined by a constant value of one of the principal components (we choose x_2 here) during an incremental time interval as the amount of solute passing through the area during the time interval divided by the volume of water passing through:

$$C^f(x_1, x_3, t, x_2) =$$

$$\lim_{\substack{\Delta x_1^* \downarrow 0 \\ \Delta x_3^* \downarrow 0 \\ \Delta t \downarrow 0}} \frac{\displaystyle\int_{x_1-\frac{1}{2}\Delta x_1^*}^{x_1+\frac{1}{2}\Delta x_1^*} \int_{x_3-\frac{1}{2}\Delta x_3^*}^{x_3+\frac{1}{2}\Delta x_3^*} \int_{t-\frac{1}{2}\Delta t}^{t+\frac{1}{2}\Delta t} q_2(\xi_1, \xi_3, \chi, x_2) C(\xi_1, \xi_3, \chi, x_2) \mathrm{d}\chi \mathrm{d}\xi_3 \mathrm{d}\xi_1}{\displaystyle\int_{x_1-\frac{1}{2}\Delta x_1^*}^{x_1+\frac{1}{2}\Delta x_1^*} \int_{x_3-\frac{1}{2}\Delta x_3^*}^{x_3+\frac{1}{2}\Delta x_3^*} \int_{t-\frac{1}{2}\Delta t}^{t+\frac{1}{2}\Delta t} q_2(\xi_1, \xi_3, \chi, x_2) \mathrm{d}\chi \mathrm{d}\xi_3 \mathrm{d}\xi_1}$$

$$(A.3)$$

where the superscript f denotes a flux concentration, and χ [T] is an integration variable. In the definition of flux concentrations in Eq. A.3, we neglected the solute flux due to local scale dispersion so that the local resident and flux concentrations are assumed to be equal, which follows from Eqs. A.2 and A.3 when the integrating interval goes to 0. This assumption implies that the local dispersive flux, which depends on the local scale dispersion coefficient, can be neglected compared with the advective flux. This condition is fulfilled when the local scale Peclet number, which is a measure for the ratio of the advective to dispersive fluxes and is defined as $\Delta x_2/\lambda_L$ (with Δx_2 the lateral travel distance), is sufficiently large.

132

Both equations are valid for the pore, REV, and macroscopic scales, provided that the θ -field is treated as an indicator field at the pore scale, as discussed above.

In the limit as the integration intervals go to zero, both equations refer to the same parcel of water centered around (x_1, x_2, x_3) at time t, and the resident and flux concentrations become identical. However, for non-zero integration intervals, as will occur with every sensor and every sampling protocol, the volume of water residing in the vicinity of (x_1, x_2, x_3) at time t will be different from the volume passing through a plane around (x_1, x_2, x_3) during a time interval centered at t, and the values of C^r and C^f will diverge. The most obvious case is that of a small fraction of highly mobile water and a large fraction of immobile water with a non-uniform concentration in the water phase. The resident concentration is dominated by the immobile water, because it contributes heavily to the integration over the water content field in Eq. A.2, while the small fraction of mobile water contributes only little. In contrast, the immobile water has no effect whatsoever on the flux concentration because its q_a is zero.

Bibliography

Adams, E. E., and L. W. Gelhar (1992), Field study of dispersion in a heterogeneous aquifer. 2. Spatial moments analysis, *Water Resources Research*, *28*(12), 3293–3307.

Andersen, M. K., K. Raulund-Rasmussen, B. W. Strobel, and H. C. B. Hansen (2002), Adsorption of cadmium, copper, nickel, and zinc to a poly(tetrafluorethene) porous soil solution sampler, *Journal of Environmental Quality*, *31*, 168–175.

Anderson, M. P. (1987), Field studies in groundwater hydrology – A new era, *Reviews of Geophysics*, *25*(2), 141–147.

APHA (1999), *Standard methods for the examination of water and wastewater. 20th edition*, American Public Health Association, Americal Water Works Association, and Water Environment Federation, Washington, DC.

Aris, R. (1956), On the dispersion of a solute in a fluid flowing through a tube, *Proceedings of the Royal Society of London. Series A. Mathematical and Physical Sciences*, *235*, 67–78.

Ayers, R. S., and D. W. Westcot (1994), *Water quality for agriculture. FAO irrigation and drainage paper*, vol. 29, FAO, Rome, 174pp.

Badawy, N. S. (1982), *Soils of the vineyards of the Great Western district*, Research Project Series No 133, Division of Agricultural Chemistry, Department of Agriculture, Victoria.

Bear, J. (1972), *Dynamics of fluid in porous media*, Elsevier, New York.

Beier, C., K. Hansen, P. Gundersen, B. R. Andersen, and L. Rasmussen (1992), Long-term field comparison of ceramic and poly(tetrafluoroethene) porous cup soil water samplers, *Environmental Science and Technology*, *26*, 2005–2011.

Bellin, A., and Y. Rubin (2004), On the use of peak concentration arrival times

for the inference of hydrogeological parameters, *Water Resources Research*, *40*, W07404, doi:10.1029/2003WR002179.

Bennett, A. J. (2000), Environmental consequences of increasing production: some current perspectives, *Agriculture, Ecosystems and Environment*, *82*, 89–95.

Beven, K., and P. Germann (1982), Macropores and water flow in soils, *Water Resources Research*, *18*(5), 1311–1325.

Beven, K. J., D. E. Henderson, and A. D. Reeves (1993), Dispersion parameters for undisturbed partially saturated soil, *Journal of Hydrology*, *143*, 19–43.

Biggar, J. W., and D. R. Nielsen (1976), Spatial variability of the leaching characteristics of a field soil, *Water Resources Research*, *12*(1), 78–84.

Binnie, C., M. Kimber, and G. Smethurst (2002), *Basic water treatment*, third ed., Thomas Telford Publishing.

Boggs, J. M., S. C. Young, L. M. Beard, L. W. Gelhar, K. R. Rehfeldt, and E. E. Adams (1992), Field study of dispersion in a heterogeneous aquifer. 1. Overview and site description, *Water Resources Research*, *28*(12), 3281–3291.

Boll, J., T. S. Steenhuis, and J. S. Selker (1992), Fiberglass wicks for sampling of water and solutes in the vadose zone, *Soil Science Society of America Journal*, *56*, 701–707.

Boll, J., J. S. Selker, G. Shalit, and T. S. Steenhuis (1997), Frequency distribution of water and solute transport properties derived from pan sampler data, *Water Resources Research*, *33*(12), 2655–2664.

Bolt, G. H. (1982), Movement of solutes in soil: principles of adsorption / exchange chromatography, in *Soil chemistry. B. Physio-chemical models*, edited by G. H. Bolt, pp. 285–348, Elsevier, Amsterdam. 527 pp.

Bottcher, A. B., L. W. Miller, , and K. L. Campbell (1984), Phosphorus adsorption in various soil-water extraction cup materials: Effect of acid wash, *Soil Science*, *137*(4), 239–244.

Brooks, M. C., and W. R. Wise (2005), Quantifying uncertainty due to random errors for moment analyses of breakthrough curves, *Journal of Hydrology*, *303*, 165–175.

Brye, K. R., J. M. Norman, L. G. Bundy, and S. T. Gower (1999), An equilibrium tension lysimeter for measuring drainage through soil, *Soil Science Society of America Journal*, *63*, 536–543.

Buchter, B., C. Hinz, M. Flury, and H. Flühler (1995), Heterogeneous flow and solute transport in an unsaturated stony soil monolith, *Soil Science Society of America Journal*, *59*(1), 14–21.

Butters, G. L., W. A. Jury, and F. F. Ernst (1989), Field scale transport of bromide in an unsaturated soil. 1. Experimental methodology and results, *Water Resources Research*, *25*(7), 1575–1581.

Candela, L., S. Fabregat, A. Josa, J. Suriol, N. Vigúes, and J. Mas (2007), Assessment of soil and groundwater impacts by treated urban wastewater

reuse. A case study: Application in a golf course (Girona, Spain), *Science of the Total Environment*, *374*, 26–35.

Cary, J. W. (1968), An instrument for *in situ* measurements of soil moisture flow and suction, *Soil Science Society of America Proceedings*, *32*, 3–5.

Cary, J. W. (1970), Measuring unsaturated soil moisture flow with a meter, *Soil Science Society of America Proceedings*, *34*, 24–27.

Cho, H., and G. H. de Rooij (2002), Pressure head distribution during unstable flow in relation to the formation and dissipation of fingers, *Hydrology and Earth System Sciences*, *6*(4), 763–771.

Cole, D. W. (1958), Alundum tension lysimeter, *Soil Science*, *85*(6), 293–296.

Cole, D. W. (1968), A system for measuring conductivity, acidity, and rate of water flow in a forest soil, *Water Resources Research*, *4*(5), 1127–1136.

Coleman, D. C., and D. A. Crossley (1996), *Fundamentals of soil ecology*, Academic Press, London.

Coppola, A., A. Santini, P. Botti, S. Vacca, V. Comegna, and G. Severino (2004), Methodological approach for evaluating the response of soil hydrological behavior to irrigation with treated municipal wastewater, *Journal of Hydrology*, *292*, 114–134.

Corwin, D. L. (2002), Measurement of solute concentration using soil water extraction. Suction cups, in *Methods of soil analysis. Part 4. Physical methods*, edited by J. H. Dane and G. C. Topp, Soil Science Society of America Book Series No. 5, pp. 1261–1266, Soil Science Society of America, Inc., Madison, Wisconsin, U.S.A.

Corwin, D. L., J. Hopmans, and G. H. de Rooij (2006), From field- to landscape-scale vadose zone processes: scale issues, modeling, and monitoring, *Vadose Zone Journal*, *5*, 129–139, doi:10.2136/vzj2006.0004.

Dagan, G. (1993), Towards pore-scale analysis of preferential flow and chemical transport, in *Water flow and solute transport in soils: development and applications*, edited by R. J. Luxmoore et al., pp. 45–60, Springer-Verlag GmbH & Co. KG, Berlin.

Dagan, G., V. Cvetkovic, and A. Shapiro (1992), A solute flux approach to transport in heterogeneous formations. 1. The general framework, *Water Resources Research*, *28*(5), 1369–1376.

Dagan, G., P. Indelman, and G. Moltyaner (1997), Stochastic analysis of concentration measurements in the transport experiment at Twin Lake site, *Water Resources Research*, *33*(4), 559–567.

de Rooij, G. H. (1996), Preferential flow in water-repellent sandy soils - Model development and lysimeter experiments, Ph.D. thesis, Wageningen Agricultural University, The Netherlands.

de Rooij, G. H. (2000), Modeling fingered flow of water in soils owing to wetting front instability: a review, *Journal of Hydrology*, *231-232*, 277–294.

de Rooij, G. H., and F. Stagnitti (2000), Spatial variability of solute leach-

ing: experimental validation of a quantitative parameterization, *Soil Science Society of America Journal*, *64*(2), 499–504.

de Rooij, G. H., and F. Stagnitti (2002a), Spatial and temporal distribution of solute leaching in heterogeneous soils: analysis and application to multisampler lysimeter data, *Journal of Contaminant Hydrology*, *54*, 329–346.

de Rooij, G. H., and F. Stagnitti (2002b), The solute leaching surface as a tool to assess the performance of multidimensional unsaturated solute transport models., in *Pre-conference proceedings of the International Conference on Computational Methods in Water Resources, Delft, The Netherlands*, edited by S. M. Hassanizadeh, R. J. Schotting, W. G. Gray, and G. F. Pinder, pp. 639–646, Elsevier, Amsterdam, The Netherlands.

de Rooij, G. H., and F. Stagnitti (2004), Applications of the beta distribution in soil science, in *Handbook of Beta distribution and its applications*, edited by A. K. Gupta and S. Nadarajah, pp. 535–550, Marcel Dekker, Inc., New York.

de Rooij, G. H., O. A. Cirpka, F. Stagnitti, S. H. Vuurens, and J. Boll (2006), Quantifying minimum monolith size and solute dilution from multicompartment percolation sampler data, *Vadose Zone Journal*, *5*, 1086–1092.

DeBano, L. F. (1981), Water repellent soils: a state-of-the-art, *Tech. rep.*, General Technical Report PSW-46, Pacific Southwest Forest and Range Experiment Station, U.S. Department of Agriculture, Berkeley, California, U.S.A., 21 pp.

DeBano, L. F. (2000), Water repellency in soils: a historical overview, *Journal of Hydrology*, *231-232*, 4–32.

Dirksen, C. (1974), Field test of soil water flux meters, *Transactions of the American Society of Agricultural Engineers*, *17*, 1038–1042.

Duke, H. R., and H. R. Haise (1973), Vacuum extractors to assess deep percolation losses and chemical constituents of soil water, *Soil Science Society of America Proceedings*, *37*, 963–964.

EPA (2000), *A guide to the sampling and analysis of waters, wastewaters, soils and wastes*, 7th ed., Environment Protection Authority, Victoria, Puclication 441.

Epstein, L., and S. Bassein (2001), Pesticide applications of copper on perenial crops in California, 1993 to 1998, *Journal of Environmental Quality*, *30*, 1844–1847.

Fahim, M. A., and N. Wakao (1982), Parameter estimation from tracer response measurements, *The Chemical Engineering Journal*, *25*, 1–8.

Flemming, C. A., and J. T. Trevors (1989), Copper toxicity and chemistry in the environment: A review., *Water, Air and Soil Pollution*, *44*, 143–158.

Flühler, H., W. Durner, and M. Flury (1996), Lateral solute mixing processes - A key for understanding field-scale transport of water and solutes, *Geoderma*, *70*, 165–183.

Flury, M., and H. Flühler (1994), Brilliant Blue FCF as a dye tracer for so-

lute transport studies - a toxicological overview, *Journal of Environmental Quality*, *23*(5), 1108–1112.

Flury, M., and H. Flühler (1995), Tracer characteristics of Brilliant Blue FCF, *Soil Science Society of America Journal*, *59*, 22–27.

Flury, M., and N. N. Wai (2003), Dyes as tracers for vadose zone hydrology, *Reviews of Geophysics*, *41*(1), 2.1–2.37, 1002, doi:10.1029/2001RG000109.

Flury, M., H. Flühler, W. A. Jury, and J. Leuenberger (1994), Susceptibility of soils to preferential flow of water: A field study, *Water Resources Research*, *30*(7), 1945–1954.

Flury, M., M. V. Yates, and W. A. Jury (1999), Numerical analysis of the effect of the lower boundary condition on solute transport in lysimeters, *Soil Science Society of America Journal*, *63*, 1493–1499.

Forrer, I., R. Kasteel, M. Flury, and H. Flühler (1999), Longitudinal and lateral dispersion in an unsaturated field soil, *Water Resources Research*, *35*(10), 3049–3060.

Freyberg, D. L. (1986), A natural gradient experiment on solute transport in a sand aquifer. 2. Spatial moments and the advection and dispersion of nonreactive tracers, *Water Resources Research*, *22*(13), 2031–2046.

Garabedian, S. P., D. R. LeBlanc, L. W. Gelhar, and M. A. Celia (1991), Large-scale natural gradient tracer test in sand and gravel, Cape Cod, Massachusetts. 2. Analysis of spatial moments for a nonreactive tracer, *Water Resources Research*, *27*(5), 911–924.

Gelhar, L. W., C. Welty, and K. R. Rehfeldt (1992), A critical review of data on field-scale dispersion in aquifers, *Water Resources Research*, *28*(7), 1955–1974.

Germann, P. F. (1988), Approaches to rapid and far-reaching hydrologic processes in the vadose zone, *Journal of Contaminant Hydrology*, *3*, 115–127.

Glass, R. J., T. S. Steenhuis, and J.-Y. Parlange (1989), Mechanism for finger persistence in homogeneous, unsaturated, porous media: Theory and verification, *Soil Science*, *148*(1), 60–70.

Grossmann, J., and P. Udluft (1991), The extraction of soil water by the suction-cup method: a review, *Journal of Soil Science*, *42*, 83–93.

Grover, B. L., and R. E. Lamborn (1970), Preparation of porous ceramic cups to be used for extraction of soil water having low solute concentrations, *Soil Science Society of America Proceedings*, *34*, 706–708.

Gupta, A. K., and S. Nadarajah (2004), Mathematical properties of the beta distribution, in *Handbook of Beta distribution and its applications*, edited by A. K. Gupta and S. Nadarajah, pp. 33–53, Marcel Dekker, Inc., New York.

Haas, C. N., J. Joffe, M. S. Heath, and J. Jacangelo (1997), Continuous flow residence time distribution function characterization, *Journal of Environmental Engineering*, *123*(2), 1121–1123.

Hamilton, A. J., F. Stagnitti, X. Xiong, S. L. Kreidl, K. K. Benke, and P. Maher

(2007), Wastewater irrigation: The state of play, *Vadose Zone Journal*, *6*(4), 823 – 840.

Hansen, E. A., and A. R. Harris (1975), Validity of soil-water samples collected with porous ceramic cups, *Soil Science of America Proceedings*, *39*, 528–536.

Hespanhol, I. (1997), Wastewater as a resource, in *Water pollution control - A guide to the use of water quality management principles*, edited by R. Helmer and I. Hespanhol, pp. 91–124, Published by E. and F. N. Spon, London on behalf of WHO/UNEP.

Hess, K. M., S. H. Wolf, and M. A. Celia (1992), Large-scale natural gradient tracer test in sand and gravel, Cape Cod, Massachusetts. 3. Hydraulic conductivity variability and calculated macrodispersivities, *Water Resources Research*, *28*(8), 2011–2027.

Hillel, D. (1998), *Environmental soil physics*, Academic Press, San Diego, California, U.S.A.

Hillel, D., and R. S. Baker (1988), A descriptive theory of fingering during infiltration into layered soils, *Soil Science*, *146*(1), 51–56.

Holder, M., K. W. Brown, J. C. Thomas, D. Zabcik, and H. E. Murray (1991), Capillary-wick unsaturated zone soil pore water sampler, *Soil Science Society of America Journal*, *55*(5), 1195–1202.

Hughes, S., and B. Reynolds (1988), Cation exchange properties of porous ceramic cups: Implications for field use, *Plant and Soil*, *109*, 141–144.

IMT (1996), *Reconnaissance soil survey report Arrawatta block Great Western, Victoria for Southcorp Wines Pty Ltd*, Irrigation Management Technology Pty Ltd.

Isbell, R. F., W. S. McDonald, and L. J. Ashton (1997), *Concepts and rationale of the Australian soil classification*, CSIRO Australia.

Ivie, J. O., and L. A. Richards (1937), A meter for recording slow liquid flow, *Rev. Sci. instr.*, *8*, 86–89.

Jemison, J. M., and R. H. Fox (1994), Nitrate leaching from nitrogen-fertilized and manured corn measured with zero-tension pan lysimeters, *Journal of Environmental Quality*, *23*, 337–343.

Jury, W. A., and H. Flühler (1992), Transport of chemicals through soil: mechanisms, models, and field applications, *Advances in Agronomy*, *47*, 141–201.

Jury, W. A., and K. Roth (1990), *Transfer functions and solute movement through soil*, Birkhauser Verlag, Basel, 226 pp.

Jury, W. A., and D. R. Scotter (1994), A unified approach to stochastic-convective transport problems, *Soil Science Society of America Journal*, *58*, 1327–1336.

Jury, W. A., and G. Sposito (1985), Field calibration and validation of solute transport models for the unsaturated zone, *Soil Science Society of America Journal*, *49*, 1331–1341.

Jury, W. A., W. R. Gardner, and W. H. Gardner (1991), *Soil Physics*, 5th ed., John Wiley and sons, Inc., New York, U.S.A.

140

Kasteel, R., H.-J. Vogel, and K. Roth (2002), Effect of non-linear adsorption on the transport behaviour of brilliant blue in a field soil, *European Journal of Soil Science*, *53*, 231–240.

Keremane, G. B., and J. McKay (2007), Successful wastewater reuse scheme and sustainable development: a case study in Adelaide, *Water and Environment Journal*, *21*, 83–91.

Khan, A. U.-H., and W. A. Jury (1990), A laboratory study of the dispersion scale effect in column outflow experiments., *Journal of Contaminant Hydrology*, *5*, 119–131.

Killey, R. W. D., and G. L. Moltyaner (1988), Twin Lake tracer tests: setting, methodology, and hydraulic conductivity distribution, *Water Resources Research*, *24*(10), 1585–1612.

Knutson, J. H., and J. S. Selker (1994), Unsaturated hydraulic conductivities of fiberglass wicks and designing capillary wick pore-water samplers, *Soil Science Society of America Journal*, *58*, 721–729.

Kool, J. B., J. C. Parker, and M. Th. van Genuchten (1987), Parameter estimation for unsaturated flow and transport models - a review, *Journal of Hydrology*, *91*, 255–293.

Kosugi, K., and M. Katsuyama (2004), Controlled-suction period lysimeter for measuring vertical water flux and convective chemical fluxes, *Soil Science Society of America Journal*, *68*, 371–382.

Kraichnan, R. H. (1970), Diffusion by a random velocity field, *The physics of fluids*, *13*, 22–31.

Kreft, A., and A. Zuber (1978), On the physical meaning of the dispersion equation and its solutions for different initial and boundary conditions, *Chemical Engineering Science*, *33*, 1471–1480.

Krejsl, J., R. Harrison, C. Henry, N. Turner, and D. Tone (1994), Comparison of lysimeter types in collecting microbial constituents from sewage effluent, *Soil Science Society of America Journal*, *58*, 131–133.

Kung, K.-J. S. (1993), Laboratory observation of funnel flow meachanism and its influence on solute transport, *Journal of Environmental Quality*, *22*, 91–102.

LeBlanc, D. R., S. P. Garabedian, K. M. Hess, L. W. Gelhar, R. D. Quadri, K. G. Stollenwerk, and W. W. Wood (1991), Large-scale natural gradient tracer test in sand and gravel, Cape Cod, Massachusetts. 1. Experimental design and observed tracer movement, *Water Resources Research*, *27*(5), 895–910.

Leistra, M., and J. J. T. I. Boesten (1994), Pesticide contamination of groundwater in Western Europe, *Agriculture, Ecosystems and Environment*, *26*, 369–389.

Levin, M. J., and D. R. Jackson (1977), A comparison of in situ extractors for sampling soil water, *Soil Science Society of America Journal*, *41*, 535–536.

Long, F. L. (1978), A glass filter soil solution sampler, *Soil Science Society of America Journal*, *42*, 834–835.

Mackay, D. M., D. L. Freyberg, P. V. Roberts, and J. A. Cherry (1986), A natural gradient experiment on solute transport in a sand aquifer. 1. Approach and overview of plume movement, *Water Resources Research*, *22*(13), 2017–2029.

Maher, P. M., K. M. Hermon, G. Allinson, F. Stagnitti, and R. Armstrong (2005), Variability of soil chemistry following irrigation with municipal effluent: A Great Western vineyard study, *Water Resources Management III, WIT Transactions on Ecology and the Environment*, *80*, 655–675, ISBN: 1–84,564–007–1.

Martínez-Beltrán, J. (1999), Irrigation with saline water: benefits and environmental impact, *Agricultural Water Management*, *40*, 183–194.

McGuire, P. E., B. Lowery, and P. A. Helmke (1992), Potential sampling error: trace metal adsorption on vacuum porous cup samplers, *Soil Science Society of America Journal*, *56*, 74–82.

Miller, E. E., and A. Salehzadeh (1993), Stripper for bubble-free tensiometry, *Soil Science Society of America Journal*, *57*, 1470–1473.

Mishra, S., and J. C. Parker (1989), Parameter estimation for coupled unsaturated flow and transport, *Water Resources Research*, *25*(3), 385 – 396.

Moltyaner, G. L., and R. W. D. Killey (1988), Twin Lake tracer tests: longitudinal dispersion, *Water Resources Research*, *24*(10), 1613–1627.

Morrison, R. D. (1982), A modified vacuum-pressure lysimeter for soil water sampling, *Soil Science*, *134*(3), 206–210.

Nadarajah, S., and A. K. Gupta (2004), Beta funtion and the incomplete beta function, in *Handbook of Beta distribution and its applications*, edited by A. K. Gupta and S. Nadarajah, pp. 1–31, Marcel Dekker, Inc., New York.

Nagpal, N. K. (1982), Comparison among and evaluation of ceramic porous cup soil water samplers for nutrient transport studies, *Canadian Journal of Soil Science*, *62*, 685–694.

Nannipieri, P., and L. Badalucco (2003), Biological processes, in *Processes in the soil-plant system: modelling concepts and applications*, edited by D. Bembi and R. Nieder, The Haworth Press: Binghamton, NY.

Neuendorf, O. (1997), Numerische 3D-simulation des stofftransports in einem heterogenen aquifer, *Tech. rep.*, Berichte des Forschungszentrums Jülich, Forschungszentrum Jülich GmbH, Germany.

Nielsen, D. R., M. Th. van Genuchten, and J. W. Bigger (1986), Water flow and solute transport processes in the unsaturated zone, *Water Resources Research*, *26*, 89S–108S.

Parker, J. C., and M. Th. van Genuchten (1984), Flux-averaged and volume-averaged concentrations in continuum approaches to solute transport, *Water Resources Research*, *20*(7), 866–872.

Persson, M. (2005), Accurate dye tracer concentration estimations using image analysis, *Soil Science Society of America Journal*, *69*(4), 967–975.

Pimentel, D., O. Bailey, P. Kim, E. Mullaney, J. Calabrese, L. Walman, F. Nelson, and X. Yao (1999), Will limits of the earth's resources control human numbers?, *Environment, Development and Sustainability*, *1*, 19–39.

Poletika, N. N., and W. A. Jury (1994), Effects of soil surface management on water flow distribution and solute dispersion, *Soil Science Society of America Journal*, *58*(4), 999–1006.

Ptak, T., and G. Schmid (1996), Dual-tracer transport experiments in a physically and chemically heterogeneous porous aquifer: effective transport parameters and spatial variability, *Journal of Hydrology*, *183*, 117–138.

Ptak, T., and G. Teutsch (1994), Forced and natural gradient tracer tests in a highly heterogeneous aquifer: instrumentation and measurements, *Journal of Hydrology*, *159*, 79–104.

Qadir, M., Th. M. Boers, S. Schubert, A. Ghafoor, and G. Murtaza (2003), Agricultural water management in water-starved countries: challanges and opportunities, *Agricultural Water Management*, *62*, 165–185.

Quisenberry, V. L., R. E. Phillips, and J. M. Zeleznik (1994), Spatial distribution of water and chloride macropore flow in a well-structured soil, *Soil Science Society of America Journal*, *58*(5), 1294–1300.

Raats, P. A. C. (1973), Unstable wetting fronts in uniform and nonuniform soils, *Soil Science Society of America Proceedings*, *37*, 681–685.

Rehfeldt, K. R., J. M. Boggs, and L. W. Gelhar (1992), Field study of dispersion in a heterogeneous aquifer. 3. Geostatistical analysis of hydraulic conductivity, *Water Resources Research*, *28*(12), 3309–3324.

Richards, L. A., M. B. Russell, and O. R. Neal (1937), Further developments on apparatus for field moisture studies, *Soil Science Society Proceedings*, *2*, 55–64.

Rimmer, A., T. S. Steenhuis, and J. S. Selker (1995), One-dimensional model to evaluate the performance of wick samplers in soils, *Soil Science Society of America Journal*, *59*, 88–92.

Ritsema, C. J., and L. W. Dekker (1994), How water moves in a water repellent sandy soil. 2. Dynamics of fingered flow, *Water Resources Research*, *30*(9), 2519–2531.

Ritsema, C. J., L. W. Dekker, J. M. H. Hendrickx, and W. Hamminga (1993), Preferential flow mechanism in a water repellent sandy soil, *Water Resources Research*, *29*(7), 2183–2193.

Roth, K., W. A. Jury, H. Flühler, and W. Attinger (1991), Transport of chloride through an unsaturated field soil, *Water Resources Research*, *27*(10), 2533–2541.

Rubin, Y., and S. Ezzedine (1997), The travel times of solutes at the Cape Cod tracer experiment: Data analysis, modeling, and structural parameters inference, *Water Resources Research*, *33*(7), 1537–1547.

Siemens, J., and M. Kaupenjohann (2003), Dissolved organic carbon is released from sealings and glues of pore-water samplers, *Soil Science Society of America Journal*, *67*, 795–797.

Siemens, J., and M. Kaupenjohann (2004), Comparison of three methods for field measurement of solute leaching in a sandy soil, *Soil Science Society of America Journal*, *68*, 1191–1196.

Simmons, C. T., M. L. Pierini, and J. L. Hutson (2002), Laboratory investigation of variable-density flow and solute transport in unsaturated-saturated porous media, *Transport in porous media*, *47*, 215–244.

Simúnek, J., M. Šejna, and M. Th. van Genuchten (1999), *Hydrus-2D/Meshgen-2D*, International Groundwater Modeling Center, Colorado School of Mines, Golden, CO 80401, USA, 2.0 ed.

Soil Survey Staff (1988), *A basic system of soil classification for making and interpreting soil surveys*, U.S. Department of Agriculture, Soil Conservation Service. Robert E. Krieger Pubishing Company, Malabar, Florida.

Stagnitti, F., J. Sherwood, G. Allinson, L. Evans, M. Allinson, L. Li, and I. Phillips (1998), An investigation of localised soil heterogeneities on solute transport using a multisegment percolation system, *New Zealand Journal of Agricultural Research*, *41*, 603–612.

Stagnitti, F., L. Li, G. Allinson, I. Phillips, D. Lockington, A. Zeiliguer, M. Allinson, J. Lloyd-Smith, and M. Xie (1999), A mathematical model for estimating the extent of solute- and water-flux heterogeneity in multiple sample percolation experiments, *Journal of Hydrology*, *215*, 59–69.

Stevens, D. (2006), *Growing crops with reclaimed wastewater*, CSIRO Publishing, Melbourne.

Strock, J. S., D. K. Cassel, and M. L. Gumpertz (2001), Spatial variability of water and bromide transport through variably saturated soil blocks, *Soil Science Society of America Journal*, *65*(6), 1607–1617.

Sudicky, E. A. (1986), A natural gradient experiment on solute transport in a sand aquifer: spatial variability of hydraulic conductivity and its role in the dispersion process, *Water Resources Research*, *22*(13), 2069–2082.

Sudicky, E. A., J. A. Cherry, and E. O. Frind (1983), Migration of contaminants in groundwater at a landfill: a case study. 4. A natural-gradient dispersion test, *Journal of Hydrology*, *63*, 81–108.

Tarchitzky, J., Y. Golobati, R. Keren, and Y. Chen (1999), Wastewater effects on montmorillonite suspensions and hydraulic properties of sandy soils, *Soil Science Society of America Journal*, *63*, 554–560.

Toride, N., F. J. Leij, and M. Th. van Genuchten (1999), The CXTFIT code for estimating transport parameters from laboratory or field tracer experiments. Version 2.1, *Tech. Rep. Research Report No. 137*, U. S. Salinity Laboratory, Agricultual Research Service, U. S. Department of Agriculture, Riverside, California, United States.

USEPA (1993), *The determination of inorganic anions in water by ion chro-*

matography, U.S. Environment Protection Agency, Method 300.0, Cincinnati, Ohio.

van Es, H. M. (2002), Soil sampling and statistical procedures: Soil variability, in *Methods of soil analysis. Part 4. Physical methods*, edited by J. H. Dane and G. C. Topp, pp. 1–13, Soil Science Society of America Book Series No. 5, Soil Science Society of America, Inc., Madison, Wisconsin, U.S.A.

van Genuchten, M. Th., and P. J. Wierenga (1976), Mass transfer studies in sorbing porous media. I. Analytical solutions, *Soil Science Society of America Journal*, *40*(4), 473–480.

van Grinsven, J. J. M., H. W. G. Booltink, C. Dirksen, N. van Breemen, N. Bongers, and N. Waringa (1988), Automated in stitu measurement of unsaturated soil water flux, *Soil Science Society of America Journal*, *52*, 1215–1218.

van Ommen, H. C., M. T. van Genuchten, W. H. van der Molen, R. Dijksma, and J. Hulshof (1989), Experimental and theoretical analysis of solute transport from a diffuse source of pollution, *Journal of Hydrology*, *105*, 225–251.

van Wesenbeeck, I. J., and R. G. Kachanoski (1991), Spatial scale dependence of in situ solute transport, *Soil Science Society of America Journal*, *55*, 3–7.

van Wesenbeeck, I. J., and R. G. Kachanoski (1994), Effect of variable horizon thickness on solute transport, *Soil Science Society of America Journal*, *58*, 1307–1316.

Vanderborght, J., and H. Vereecken (2001), Analyses of locally measured bromide breakthrough curves from a natural gradient tracer experiment at Krauthausen, *Journal of Contaminant Hydrology*, *48*, 23–43.

Vanderborght, J., A. Kemna, H. Hardelauf, and H. Vereecken (2005), Potential of electrical resistivity tomography to infer aquifer transport characteristics from tracer studies: A synthetic case study, *Water Resources Research*, *41*, w06013, doi:10.1029/2004WR003774.

Vandevivere, P., and P. Baveye (1992), Saturated hydraulic conductivity reduction caused by aerobic bacteria in sand columns, *Soil Science Society of America Journal*, *56*, 1–13.

Vereecken, H., G. Lindenmayr, O. Neuendorf, U. Döring, and R. Seidemann (1994), TRACE, a mathematical model for reactive transport in 3D variable saturated porous media., *Tech. rep.*, KFA, ICG-4 Internal Report No. 501494, Forschungszentrum Jülich GmbH, Germany.

Vereecken, H., U. Döring, H. Hardelauf, U. Jaekel, U. Hashagen, O. Neuendorf, H. Schwarze, and R. Seidemann (2000), Analysis of solute transport in a heterogeneous aquifer: the Krauthausen field experiment, *Journal of Contaminant Hydrology*, *45*, 329–358.

Vinten, A. J. A., U. Mingelgrin, and B. Yaron (1983), The effect of suspended solids in wastewater on soil hydraulic conductivity: II. Vertical distribution of suspended solids, *Soil Science Society of America Journal*, *47*, 408–412.

Wagenet, R. J. (1990), Quantitative prediction of the leaching of organic and inorganic solutes in soil, *Phil. Trans. R. Soc. Lond. B.*, *329*, 321–330.

Wagner, G. H. (1962), Use of porous ceramic cups to sample soil water within the profile, *Soil Science*, *94*, 379–386.

Wang, Z., J. Feyen, and C. J. Ritsema (1998a), Susceptibility and predictability of conditions for preferential flow, *Water Resources Research*, *34*(9), 2169–2182.

Wang, Z., J. Feyen, M. Th. van Genuchten, and D. R. Nielsen (1998b), Air entrapment effects on infiltration rate and flow instability, *Water Resources Research*, *34*(2), 213–222.

Weihermüller, L., J. Siemens, M. Deurer, S. Knoblauch, H. Rupp, A. Göttlein, and T. Pütz (2007), In situ soil water extraction: A review, *Journal of Environmental Quality*, *36*, 1735–1748.

Wendroth, O., W. Pohl, S. Koszinski, H. Rogasik, C. J. Ritsema, and D. R. Nielsen (1999), Spatio-temporal patterns and covariance structures of soil water status in two Northeast-German field sites, *Journal of Hydrology*, *215*, 38–58.

Wenzel, W. W., and G. Wieshammer (1995), Suction cup materials and their potential to bias trace metal analyses of soil solutions: A review, *International Journal of Environmental Analytical Chemistry*, *59*, 277–290.

Wessel-Bothe, S., S. Pätzold, C. Klein, G. Behre, and G. Welp (2000), Sorption of pesticides and doc on glass and ceramic suction cups. (in German with English abstract)., *Journal of Plant Nutrition and Soil Science*, *163*, 53–56.

WHO (1989), *Guidelines for the safe use of wastewater and excreta in agriculture and aquaculture*, edited by S. Cairncross and D. Mara, Geneva, Switserland: World Health Organisation, 194 pp.

Wildenschild, D., K. H. Jensen, K. Villholth, and T. H. Illangasekare (1994), A laboratory analysis of the effect of macropores on solute transport, *Ground Water*, *32*(3), 381–389.

Woodbury, A. D., and Y. Rubin (2000), A full-Bayesian approach to parameter inference from tracer travel time moments and investigation of scale effects at the Cape Cod experimental site, *Water Resources Research*, *36*(1), 159–171.

Yamaguchi, T., P. Moldrup, and S. Yokosi (1989), Using breakthrough curves for parameter estimation in the convection-dispersion model of solute transport, *Soil Science Society of America Journal*, *53*, 1635 – 1641.

146

Samenvatting en conclusies

Samenvatting en conclusies

Het experimentele en theoretische onderzoek gepresenteerd in dit proefschrift heeft geleid tot een verbetering van de mogelijkheden om stoffentransport in de ondergrond d.w.z. beneden een onverzadigde bodem(volume) te observeren. Ook heeft dit onderzoek geleid tot een beter inzicht in de herverdeling van stoffen zowel in de onverzadigde- als verzadigde zone.

De numerieke grondwater studie (Hoofdstuk 2) laat zien dat er verschillen bestaan tussen het gebruik van residentconcentraties dan wel fluxconcentraties. Hoewel deze verschillen theoretisch goed worden begrepen, leiden praktische problemen om fluxconcentraties te meten nog steeds tot meetprotocollen waarbij residentconcentraties worden gemeten. Aangetoond werd dat zorgvuldig moet worden gedaan met het vaststellen van de verplaatsing van stoffen met behulp van residentconcentraties. Alleen als de variatie van de lokale concentraties binnen de poriënruimte laag is, zullen residentconcentraties betrouwbare resultaten geven. Deze conclusie houdt in dat om de lokale concentratie gradiënten te reduceren, diffusie en dispersie voldoende tijd gehad moeten hebben. De numerieke studie laat zien dat in deze watervoerende laag, met een realistische heterogeniteit, voor het verwerven van de benodigde mate van lokale menging, een afgelegde afstand van 70 m onvoldoende is.

In het gebied waar resident- en flux-concentraties nog niet geconvergeerd zijn, kan analyse van momenten helpen om de resultaten verkregen uit de observaties van residentconcentraties te verbeteren. Deze analyse werkt goed als het transport van stoffen wordt geanalyseerd over de gehele doorsnede van de watervoerende laag. Ze werkt echter minder goed op de schaal van de individuele numerieke rastercellen. De reden hiervoor is dat de lokale water snelheden binnen de poriën worden benaderd door de gemiddelde snelheden over het totale afgelegde traject.

Het is aannemelijk dat het verschil tussen resident- en flux-concentraties

wordt vergroot bij een grotere heterogeniteit van de watervoerende laag en een grotere doorlatendheid. De mate van heterogeniteit in deze studie was niet extreem. Voor watervoerende lagen met meer uitgesproken variaties en/of gebieden met een grotere stromingssnelheid, worden nog grotere verschillen verwacht. Het is daarom wenselijk om methoden te ontwikkelen die fluxconcentraties kunnen meten.

In Hoofdstuk 2 is de analyse van het grote aantal stoffentransport data uitgevoerd met behulp van leaching surfaces. Deze analyse laat duidelijk de zwakte van het gebruik van residentconcentraties zien.

Terwijl het meten van fluxconcentraties in watervoerende lagen de komende jaren waarschijnlijk moeilijk zal blijven, bestaan voor metingen in de onverzadigde zone meer mogelijkheden. In Hoofdstuk 3 zijn voor het eerst de ontwikkelingen op het gebied van drukhoogte regeling en een instrument dat uit meerdere compartimenten bestaat, gecombineerd. De variabele drukhoogte 'multi-compartment sampler' (MCS) bestaat uit 100 compartimenten, elk compartiment met een oppervlak van 31,5 mm × 31,5 mm, afgedekt met een poreus medium. De sampler heeft een bemonsteringskamer waarbinnen de variërende drukhoogte kan worden gehandhaafd. Met deze set-up kunnen lage drukhoogtes worden gehandhaafd met een instrument welke veel korter is dan de zo genaamde 'wick'-instrumenten. Dit maakt deze 'multi-compartment sampler' uitstekend geschikt voor gebieden met een ondiepe grondwaterspiegel. Met het oog op de wens om reactieve stoffen te kunnen bemonsteren zijn drie aparte prototypes met verschillende poreuze afdichtingen gebouwd: één met een polyamide fiber nylon mesh (='nylon instrument'), één met gesinterd poreus roestvrij staal 316 metaal plaatjes (='metalen instrument'), en één met een polyamide membraan (='membraan instrument'). Om in evenwicht met de natuurlijke omgeving te komen regelt een pomp dat de drukhoogte binnen de sampler op hetzelfde niveau blijft als de omringende drukhoogte. Indien nodig kan dit met een correctiefactor voor het drukhoogteverlies over de poreuze afdichting gebeuren. Druppeltellers registreren voor elk compartiment nauwkeurig het percolerende vocht met een tot nu toe ongekende temporele resolutie van 5 minuten.

In laboratorium- en veldproeven zijn de eigenschappen van de verschillende poreuze afdichtingen vastgesteld. Niet verrassend bleek er een relatie te bestaan tussen de doorlatendheid van de poreuze afdichtingen en de luchtintreewaarde. Voor de selectie van de poreuze afdichting moet rekening worden gehouden met het natuurlijke drukhoogteregime van de experimentele locatie, de snelheid waarmee de verschillende afdichtingen uitdrogen, en de gewenste stijfheid van de afdichting. Voor de poreuze afdichtingen die onderworpen werden aan droge condities leverde het herbevochtigen tijdens het arriveren van een vochtfront geen onoverkomelijke problemen op. De ondersteuning voor de membraan afdichting is voor langdurige droge periodes echter minder geschikt. Bij uitdroging vervormt deze. Daarvoor zou een nieuwe ondersteuning dienen te worden ontwikkeld.

De regeling van de drukhoogte zou idealiter rekening moeten houden met

het drukhoogteverlies over de poreuze afdichtingen. Omdat de fluxen tussen de compartimenten erg variëren, maar de opgelegde drukhoogte in de sampler niet, wordt voorgesteld om bij hoge drainage snelheden voor wat betreft het corrigeren voor het drukhoogteverlies, aan de veilige kant te blijven. Dit was echter alleen het geval voor het metalen instrument. De andere samplers hadden zodanig dunne afdichtingen dat het drukhoogteverlies hierover verwaarloosbaar was. Alles in overweging nemende, presteerde het membraan instrument het beste, met het metalen instrument als goede tweede.

De experimenten met de nieuwe 'multi-compartiment samplers' leverden een overvloed aan nieuwe informatie op. De 5 minuten waarnemingen met de druppeltellers stelden ons bijvoorbeeld in staat om in detail de reacties van individuele regenbuien te bestuderen. De heterogeniteit van de gedurende een veldexperiment door de samplers gemeten drainagepatronen gaven aan dat de grootte van de samplers voldoende was.

De lange termijn prestaties van de nieuwe 'multi-compartiment samplers' onder de ruwe omstandigheden van het open veld waren overtuigend. De samplers bleken hiermee geschikt voor een grote verscheidenheid aan toepassingen. Met de druppeltellers kunnen gedetailleerde studies naar de reactie op neerslag op elke gewenste diepte in de bodem boven het freatisch vlak worden uitgevoerd. Dit is nuttig voor waterbeheerdoeleinden. Voor landbouwkundig onderzoek kan de sampler zijn waarde bewijzen door het inzichtelijk maken van ingewikkelde details van stoffentransport in bodems. Dit kan van grote waarde zijn voor het geval dat kleine hoeveelheden uitspoeling belangrijk zijn (b.v. bij pesticiden en fosfaten) of wanneer de uniformiteit van de verdeling in de bodem relevant is (b.v. bij nematiciden).

Het nylon instrument werd gebruikt in het laboratorium voor een irrigatieproject met afvalwater in Australië (Hoofdstuk 4). Het instrument was in staat om de uitspoeling van het afvalwater uit een bodemmonoliet van een wijngaard leem-bodem vast te leggen onder een irrigatieregime waarbij in de zomer de hoeveelheid neerslag aangevuld wordt met behandeld afvalwater, terwijl er in de winter alleen neerslag valt. We vonden dat de chloride in het afvalwater bleef uitspoelen gedurende de winter, met uitstroomconcentraties van gemiddeld 3 % van de geïrrigeerde concentraties aan het eind van de winter (minder dan 1 % voor de hoge-flux compartimenten). Het afvalwater dat in de zomer wordt geïrrigeerd vervuilt dus het hele jaar door het grondwater met chloride. Dit vormt een bedreiging voor het schaarse zoete grondwater. Dit wordt ook geassocieerd met hoge EC-niveaus in de bodem tijdens het groeiseizoen.

Het experiment bevatte ook een puls-toepassing van bromide, welke een leaching surface produceerde vergelijkbaar met die van de chloride. Het grote verschil tussen de bromide puls en chloride irrigatie was de verhoogde chlorideconcentraties in het water van compartimenten die alleen maar kleine volumes draineerden. De bromide puls verbleef te kort in de bodem om het minder mobiele water te kunnen bereiken. Dit werd bevestigd door de grote verschillen in bromideconcentraties in het gedraineerde water. De chlorideconcentraties in het gedraineerde water werden tamelijk uniform naarmate de tijd vorderde

waarschijnlijk door langzame laterale spreiding als gevolg van diffusie.

Om uitspoeling van de stoffen te kunnen kwantificeren in een zandige bodem, werden de metalen en membraan 'multi-compartiment samplers' 2 m uit elkaar geïnstalleerd in een veldexperiment in Vredepeel, Nederland (Hoofdstuk 5). Als aanvulling op een chloride tracer, werd aan het einde van het experiment een kleurstof tracer toegediend. Deze methode leverde informatie op welke duidelijk de informatie overtrof die wordt geleverd bij afzonderlijk anion en kleurstof tracer testen, het meten van stoffen door bemonstering, dan wel bij het meten met suction cups.

De ruimtelijke distributie van de kleurstoftracer in het metalen instrument was vergelijkbaar met dat van de chloride. De ruimtelijk stoffendistributie-curven (SSDCs) van de chloride tracers in beide samplers toonden grote overeenkomsten. De leaching surfaces verschilden iets, hoofdzakelijk door de verschillende drainage volumes verzameld door de samplers.

In deze niet waterafstotende bodem, en zonder scheuren of andere oorzaken voor preferente stroming, gaven de ruimtelijke distributie van drainage, de ruimtelijke en temporele herverdeling van een tracer puls, en het kleurstof patroon allen een opvallend niet-uniforme stroming aan. De ruimtelijke schaal van de heterogeniteit kon goed worden weergegeven met de $32,5 \times 32,5$ cm samplers. De beperkte variatie in tijd die nodig is om de maximale concentratie te bereiken, en de smalle bandbreedte van de totale hoeveelheid bemonsterde stoffen per compartiment vergeleken met de bandbreedte voor bemonsterde drainage, gaven effectieve laterale stoffenuitwisseling aan tussen de stroombanen. Ondanks de smalle verticale afstanden (0,3 m), is dit consistent met een convectief-dispersief transport regime. Deze en andere karakteristieke diagnoses kunnen direct bepaald worden uit de leaching surfaces en de SSDCs en hun equivalenten voor de ruimtelijke distributie van drainage. Ze zijn erg nuttig voor het kwalificeren van de stoffentransport-processen in een gegeven bodem.

Terwijl de leaching surfaces hun waarde hebben bewezen, zou een methode die deze oppervlaktes op een kwantitatieve manier kan beschrijven hun waarde verder verhogen. Dit zou een vergelijking tussen verschillende leaching surfaces vergemakkelijken. In Hoofdstuk 6 is een procedure ontwikkeld waarbij een leaching surface beschreven wordt met vier tot acht parameters. De procedure start met het fitten van een poriewater snelheid (v) en een dispersiecoëfficiënt (D) voor de doorbraak curve (BTC) van elk compartiment. Vervolgens worden de waarden van v en D uitgedrukt als een functie van het pseudo-ruimtelijke coördinaat van de leaching surface, welke de rangorde aangeeft van de gesorteerde volgorde van de bemonsterde compartimenten. Dit reduceert de 100 waarden van zowel v als D naar twee tot zes parameters, afhankelijk van de geselecteerde relaties. Uiteindelijk wordt de ruimtelijke distributie van de totaal uitgespoelde stoffen benaderd door een fit van de Beta distributie, welke twee parameters toevoegt.

150

In Hoofdstuk 7 wordt de parameterisatie-procedure gewijzigd om deze direct toepasbaar te maken op de fluxdichtheden in plaats van op de fluxconcentraties, en levert een functionele uitdrukking op voor de leaching surface. De leaching surfaces uit de eerdere experimenten van de Hoofdstukken 4 en 5 zijn op deze wijze geparameteriseerd. De parameter waarden voor de twee 'Nederlandse' leaching surfaces reflecteren duidelijk de overeenkomsten tussen de leaching surfaces welke samengaan met een convectief-dispersief transport regime. Ook is er een duidelijk contrast met de 'Australische' leaching surface. Deze laat een duidelijk bewijs van preferente stroming en slechte laterale mixen zien. De parameterisatie bleek voldoende flexibel te zijn om beide types leaching surfaces goed te kunnen beschrijven.

De twee verschillende parameterisatie procedures beschreven in respectievelijk Hoofdstuk 6 en 7, leverden geparameteriseerde leaching surfaces op, waarvan het eindresultaat weinig van elkaar verschilde. De parameter waarden zijn echter wel verschillend. De parameters van de fits gebaseerd op fluxconcentraties (Hoofdstuk 6) hebben een beter gedefinieerde fysische betekenis. Daarentegen is de parameterisatie gebaseerd op fluxdichtheden (Hoofdstuk 7) directer en beschrijft de leaching surface met een vergelijking.

Een verschil tussen de twee verschillende methoden beschreven in de Hoofdstukken 6 en 7 is dat de berekende snelheden (v) en dispersiecoëfficiënten (D) gebaseerd op de fluxconcentraties een lagere variatie lieten zien dan deze berekend op basis van de stoffen fluxdichtheden. Het middelen van de snelheden en de dispersiecoëfficiënten voor de doorbraakcurven (BTCs) gebaseerd op fluxconcentraties geeft daardoor een lagere RMSE (root mean square error) dan deze voor de doorbraakcurven gebaseerd op de stoffen fluxdichtheden. De fluxconcentratie fit moet echter getransformeerd worden naar stoffen fluxdichtheden. Deze stap vereist een extra operatie welke een verhoging van de RMSE geeft van de gefitte leaching surface.

Kansen voor verder onderzoek

Ondanks het feit dat de 'multi-compartment sampler' goed functioneerde gedurende de experimenten, zijn verbeteringen mogelijk. Een van de belangrijkste punten van aandacht is de rand rondom het membraan instrument. Hoewel tijdens de experimenten geen randeffecten werden waargenomen, zou het risico van eventuele randeffecten in nieuwe samplers verminderd kunnen worden door de rand van de sampler te verkleinen. Daarnaast zou een stijvere ondersteuning van het membraan instrument wenselijk zijn om vervorming hiervan bij langdurige droge periodes te voorkomen. Ook een paar praktische aspecten kunnen nog worden verbeterd. Op dit moment werkt de sampler op accu's, wat voor lange termijn projecten een praktisch bezwaar vormt. Dit kan makkelijk verbeterd worden. Het bemonsteren van de compartimenten gebeurt nu met de hand en kan worden geautomatiseerd, bijvoorbeeld met een pompsysteem en

een opvangbak. Dit zal tot een aanzienlijke vermindering van de arbeidstijd leiden.

Tijdens ons veldexperiment in Vredepeel, Nederland (Hoofdstuk 5) hebben we gedurende een half jaar informatie verzameld over de natuurlijke neerslag, de drukhoogtes in het veld, de drukhoogtes in de samplers, de gemeten concentraties en volumes, en de eigenschappen van de bodem. Daarnaast zijn de eigenschappen van de metaal en membraan afdichtingen bekend. Met deze unieke dataset kan het water en stoffentransport van het experiment gesimuleerd worden met behulp van een programma zoals Hydrus2D (*Simúnek et al.*, 1999). Omdat de actuele fluxen zijn gemeten tijdens dit experiment kan een vergelijking gemaakt worden tussen de gesimuleerde en de gemeten resultaten. Na calibratie van het simulatieprogramma kan een nog duidelijker inzicht in de uitspoelingsprocessen worden verkregen. Presentatie kan hierbij op een begrijpelijke visuele manier plaatsvinden, zodat er ten behoeve van de sturing van het beleid en praktisch gebruik van gemaakt kan worden.

Voor een kwantitatieve parameterisatie van de leaching surfaces (Hoofdstukken 6 en 7) hebben we slechts vier tot zes parameters gebruikt voor het beschrijven van een complex model. Dit resulteerde in een 'glad' model. Verder onderzoek kan zich richten op de schaal en de betekenis van de hierbij voorkomende 'ruis' (i.e. de gemeten minus de geparameteriseerde leaching surfaces). De geparameteriseerde leaching surfaces geven de mogelijkheid om de 'ruis' te kwantificeren, en maakt het mogelijk om technieken zoals residue analyses te gebruiken.

Deze studie was gericht op het transport van niet reagerende tracers. De 'samplers' zijn echter eveneens geschikt voor het meten van reactieve stoffen. Experimenten gericht op een grote variatie van transport zou onze horizon op stoffentransport in de bodem verder kunnen verbreden.

Curriculum Vitae

Esther Bloem, 19 May 1977, Schagen

1989 – 1995
    Secondary school, Openbare Scholengemeenschap Schagen

1995 – 2002
    Ir. Mining and Petroleum Engineering
    Engineering Geology and Applied Geophysics (cum laude)
    Delft University of Technology

1997 – 2000
    Propaedeutic Law, Leiden University

2003 – 2008
    Doctoral research project (2003 – 2007) and Post-doctoral research
    project (2007 – 2008) at the Soil Physics, Ecohydrology and
    Groundwater Management Group, Wageningen University

May 2008
    Certificate Netherlands Research School for the Socio-Economic and
    Natural Sciences of the Environment (SENSE)
    Activities included among others:
    Course 5th *Summerschool of Environmental Physics, Part Soil* (Heidelberg, 2003)
    Course *Uncertainty modelling and analysis* (Wageningen, 2004)
    Course *Advanced Soil Physics* (Wageningen, 2004)
    Organization of *Public and media activities in Dutch Science Week on 'Energy in*
    Soil, Water and Air: the Water Cycle' (Wageningen, 2006)